RL-TR-97-198
In-House Report
March 1998

PASSIVELY MODE-LOCKED ERBIUM-DOPED FIBER LASERS USING MULTIPLE QUANTUM WELL SATURABLE ABSORBERS
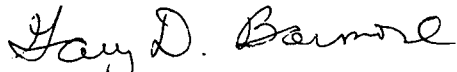
Michael J. Hayduk

19980422 104

DTIC QUALITY INSPECTED 4

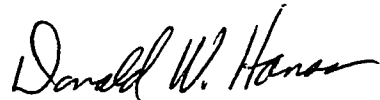**AIR FORCE RESEARCH LABORATORY
ROME RESEARCH SITE
ROME, NEW YORK**

This report has been reviewed by the Air Force Research Laboratory, Information Directorate, Public Affairs Office (IFOIPA) and is releasable to the National Technical Information Service (NTIS). At NTIS it will be releasable to the general public, including foreign nations.

RL-TR-97-198 has been reviewed and is approved for publication.

APPROVED:

GARY D. BARMORE, Maj., USAF
Chief, Photonics Division

FOR THE DIRECTOR:

DONALD W. HANSON, Director
Surveillance & Photonics Directorate

If your address has changed or if you wish to be removed from the Air Force Research Laboratory mailing list, or if the addressee is no longer employed by your organization, please notify AFRL/SNDR, 25 Electronic Pky, Rome, NY 13441-4514. This will assist us in maintaining a current mailing list.

Do not return copies of this report unless contractual obligations or notices on a specific document require that it be returned.

ALTHOUGH THIS REPORT IS BEING PUBLISHED BY AFRL, THE RESEARCH WAS ACCOMPLISHED BY THE FORMER ROME LABORATORY AND, AS SUCH, APPROVAL SIGNATURES/TITLES REFLECT APPROPRIATE AUTHORITY FOR PUBLICATION AT THAT TIME.

REPORT DOCUMENTATION PAGE

Public reporting burden for this collection of information is estimated to average 1 hour per response, including the time for reviewing instructions, searching existing data sources, gathering and maintaining the data needed, and completing and reviewing the collection of information. Send comments regarding this burden estimate or any other aspect of this collection of information, including suggestions for reducing this burden, to Washington Headquarters Services, Directorate for information Operations and Reports, 1215 Jefferson Davis Highway, Suite 1204, Arlington, VA 22202-4302, and to the Office of Management and Budget, Paperwork Reduction Project (0704-0188), Washington, DC 20503.

1. AGENCY USE ONLY *(Leave blank)*	2. REPORT DATE March 1998	3. REPORT TYPE AND DATES COVERED **FINAL, Oct 95 - Aug 97** (In-House)

4. TITLE AND SUBTITLE **PASSIVELY MODE-LOCKED ERBIUM-DOPED FIBER LASERS USING MULTIPLE QUANTUM WELL SATURABLE ABSORBERS**	5. FUNDING NUMBERS C - NA PE - 62702F PR - 4600
6. AUTHOR(S) **Michael J. Hayduk**	TA - P1 WU - 19

7. PERFORMING ORGANIZATION NAME(S) AND ADDRESS(ES) **Rome Laboratory/OCPA** **25 Electronic Pky** **Rome NY 13441-4515**	8. PERFORMING ORGANIZATION REPORT NUMBER RL-TR-97-198

9. SPONSORING / MONITORING AGENCY NAME(S) AND ADDRESS(ES) **Rome Laboratory/OCPA** **25 Electronic Pky** **Rome NY 13441-4515**	10. SPONSORING / MONITORING AGENCY REPORT NUMBER RL-TR-97-198

11. SUPPLEMENTARY NOTES

Rome Laboratory Project Engineer: Michael J. Hayduk, OCPA, 315-330-7753

12a. DISTRIBUTION AVAILABILITY STATEMENT **APPROVED FOR PUBLIC RELEASE; DISTRIBUTION UNLIMITED**	12b. DISTRIBUTION CODE

13. ABSTRACT *(Maximum 200 words)*

An experimental study of the mode-locking process in erbium-doped fiber lasers (EDFL's) operating at 1.55 μm using multiple quantum well saturable absorbers is presented. The self-starting passively mode-locked laser was constructed in a Fabry-Perot configuration using the saturable absorber as the back reflector of the cavity. Picosecond pulses that range from 14.2 to 38.8 ps were generated using a series of saturable absorbers. The pulse widths were dependent upon the optical properties of the saturable absorber used as the mode-locking element. The output power of the EDFL varied from 0.2 to 6.7 mW and was also dependent upon the saturable absorber used in the cavity.

Soliton mode-locking using saturable absorbers was the mechanism responsible for the generation of the picosecond pulses by the EDFL. The long-lived carrier lifetime in the quantum wells was the primary optical property of the saturable abosrber that determined the final pulse width. The carrier lifetimes of the eight individual saturable absorbers were investigated using time-resolved pump/probe experimental techniques. The lifetimes ranged from 40 to 1757 ps. The soliton mode-locking process allowed pulse widths of up to 45 times shorter than these carrier lifetimes to be produced.

14. SUBJECT TERMS erbium, fiber laser, passive mode-locking, saturable absorber, multiple quantum well, soliton shaping Cr^{4+}:YAG laser, solid-state laser	15. NUMBER OF PAGES 136
	16. PRICE CODE

17. SECURITY CLASSIFICATION OF REPORT **UNCLASSIFIED**	18. SECURITY CLASSIFICATION OF THIS PAGE **UNCLASSIFIED**	19. SECURITY CLASSIFICATION OF ABSTRACT **UNCLASSIFIED**	20. LIMITATION OF ABSTRACT **UNLIMITED**

NSN 7540-01-280-5500

TABLE OF CONTENTS

LIST OF TABLES

LIST OF FIGURES

Chapter 4

Chapter 5

ABSTRACT

An experimental study of the mode-locking process in erbium-doped fiber lasers (EDFL's) operating at 1.55 µm using multiple quantum well saturable absorbers is presented. The self-starting passively mode-locked laser was constructed in a Fabry-Perot configuration using the saturable absorber as the back reflector of the cavity. Picosecond pulses that ranged from 14.2 to 38.8 ps were generated using a series of saturable absorbers. The pulse widths were dependent upon the optical properties of the saturable absorber used as the mode-locking element. The output power of the EDFL varied from 0.2 to 6.7 mW and was also dependent upon the saturable absorber used in the cavity.

Soliton mode-locking using saturable absorbers was the mechanism responsible for the generation of the picosecond pulses by the EDFL. The long-lived carrier lifetime in the quantum wells was the primary optical property of the saturable absorber that determined the final pulse width. The carrier lifetimes of the eight individual saturable absorbers were investigated using time-resolved pump/probe experimental techniques. The lifetimes ranged from 40 to 1757 ps. The soliton mode-locking process allowed pulse widths of up to 45 times shorter than these carrier lifetimes to be produced.

A self-starting passively mode-locked solid-state Cr^{4+}:YAG laser was also developed using a novel saturable absorber mirror structure. The laser produced femtosecond pulses that were tunable from 1.488 to 1.535 µm. The average output power of the laser ranged from 40 to 80 mW at a repetition rate of 95 MHz. A minimum pulse width of 120 fs was generated at 1.488 µm. The high peak power of these pulses combined with its tunability in the 1.5 µm region made this laser an ideal spectroscopic source for use in the time-resolved pump/probe experiments.

Chapter 1
Introduction

1.1 WHY ULTRASHORT PULSES?

The ever increasing popularity of the internet, specifically the World Wide Web, has lead to an unprecedented demand for more information bandwidth. The user demand is expected to continue to increase by a factor of eight annually.[1] Any typical user of the 'Web' has undoubtedly experienced bottlenecks while trying to access remote sites. The increase in graphic intensive sites and the introduction of the Java language, where application files as well as the object files are downloaded, will certainly lead to further bottlenecks and reduced user access speeds. Current electronic time division multiplexing (TDM) technology is only increasing user bandwidth by a factor of 1.5 per year. The user demand for bandwidth is clearly outpacing the electronic advancements. The questions arise - "Where do we go from here?" and "What can be done to provide the additional bandwidth?". The answers are found in the emerging technologies of fiber optics and optoelectronics. The available bandwidth of a single optical fiber is 25 THz! By comparison, high-speed T1 telecommunication lines currently available operate at only 1.55 megabits per second. One can only imagine the possibilities that will exist with the implementation of all optical networks. User access to this technology is slowly becoming a reality. The installation rate of optical fiber in the United States stands at 4000 strand miles per day with approximately 10 million strand miles already installed.[2] Therefore the actual placement of optical fiber for use as main trunk lines is almost complete. Unfortunately the average user will not be able to fully appreciate this technology until the fiber reaches their home or desktop computer

at work. This final implementation of fiber will not occur until the cost of the necessary optoelectronic components makes it worthwhile.

The key in making this technology cost worthy lies in the development of the optical networking architectures and also the required optoelectronic devices such as lasers, modulators, switches, and detectors. The search for a standard architecture for optical networks has been the subject of intense debate and research over the past decade. TDM schemes assign each user a certain time slot with all of the information sent to each receiver's port. The receiver then selects the time slot of interest and extracts the desired information. TDM bottlenecks can result at each port because all of the data is broadcast to each port. The front-end electronic speed at the receiver is slowed down by this extra data.

Wavelength division multiplexing (WDM) is rapidly becoming the architecture of choice in the telecommunications industry. Each user in WDM is assigned a certain wavelength or color of operation. The receivers then select the specific wavelength containing the desired information. Depending upon the specific network architecture, the user may receive only his/her desired data and not the entire broadcast, thus reducing the electronic bottleneck. The enormous bandwidth of optical fiber is also best accessed in the wavelength domain rather in the time domain. The emergence of the erbium-doped amplifier (EDFA) has also allowed WDM to become a reality. The THz bandwidth of the amplifier around 1.5 μm allows multiple wavelength signals to be amplified in parallel without conversion to an electronic form as was previously required.

TDM technology is however expected to complement WDM networks so that terabit per second speeds can be reached. The idea is to interleave the lower speed WDM signals into a single higher speed TDM channel. These TDM systems require lasers capable of producing ultrashort pulses at high repetition

2

rates. The electronic information that is to be transmitted is encoded onto these pulses using an external electro-optic modulator. Erbium-doped fiber lasers (EDFL's) are one such practical source of picosecond pulses which can support terahertz data rates. The 1.55 μm output of the laser coincides with the minimum loss window of optical fiber The all fiber nature of these lasers also allows them to be easily integrated with the other components in the optical network.

WDM systems typically require an array of lasers each of which is set to a different wavelength. For example, a 16 channel WDM system requires 16 different single frequency lasers. An alternative scheme has recently been proposed which uses a single laser producing pulses with temporal durations of 85 fs.[3] The corresponding spectral bandwidth of 9 nm is then sliced into 16 individual channels each of which is modulated at the repetition rate of the laser. The need for 16 individual lasers has been replaced a single laser. This scheme has also been demonstrated in an EDFL [4] which illustrates the usefulness of this laser in WDM-only type systems.

1.2 OVERVIEW OF THIS WORK

The issue of developing a compact, stable and reliable source of ultrafast pulses for use in all optical networks is explored in this work. Specifically, the process of picosecond pulse generation by an EDFL using a multiple quantum well saturable absorber is investigated. The optical properties of the saturable absorbers that control the pulse width produced by the laser were also examined.

The EDFL was constructed as a linear or Fabry-Perot cavity using the saturable absorber as the back high reflector. The gain medium consisted of approximately 22.5 m of erbium-doped fiber which was pumped by 80 mW from a laser diode operating at 980 nm. The saturable absorber was simply butt-

3

coupled to the erbium-doped fiber. The output coupler was a fiber Bragg grating with 49% reflectance centered at 1556 nm. The FWHM linewidth of the grating was 1 nm. Pulse widths were generated that ranged from 14.2 to 38.8 ps depending upon the saturable absorber that was used at the back of the cavity. The average output power of the laser ranged from 0.2 to 6.7 mW.

The quantum well saturable absorbers consisted of 50 periods of 100 Å $In_{0.53}Ga_{0.47}As$ wells and 100 Å barriers grown on semi-insulating InP substrates. The barriers for seven of the eight absorbers used in this work were $In_{0.52}Al_{0.48}As$. The final sample had InP barriers. The quantum well materials were grown lattice matched to the InP substrates. The pulses shaped by the saturable absorbers were dependent upon the carrier lifetime or recovery time of the quantum wells. The growth temperature of the saturable absorbers were varied to reduce the recovery times of the quantum wells. The carrier lifetimes were determined using time-resolved pump/probe techniques and were found to range from 40 to 1757 ps.

A Cr^{4+}:YAG laser was also developed for use in the pump/probe experiments. The laser generated self-starting and highly stable transform-limited femtosecond pulses that were tunable from 1488 to 1535 nm. The average output power ranged from 40 to 80 mW with a minimum pulse width of 120 fs recorded at 1488 nm. The laser was mode-locked using a saturable absorber mirror (SAM) structure which also served as the back high reflector of the cavity. The SAM consisted of alternating layers of AlAs/GaAs each of which was a quarter-wavelength thick so that a reflectance of over 99% was achieved. Two 70 Å $In_{0.53}Ga_{0.47}As$ quantum wells placed between two $In_{0.52}Al_{0.48}As$ barriers provided the saturable absorption necessary for the startup and stabilization of the

mode-locking process. The high peak powers of the Cr^{4+}:YAG pulses allowed us to simulate the incident EDFL intensity on the saturable absorbers.

This work is organized into seven chapters, including this introduction. Chapter 2 gives a detailed description of erbium-doped fiber amplifiers and lasers. The introduction of the EDFA has revolutionized photonics and helped to make terabit per second data rates possible. The important parameters of EDFA's are discussed along with the various laser cavity configurations that have been previously examined. The principles of mode-locking or ultrashort pulse generation by lasers is presented in Chapter 3. Both active (forced mode-locking) and passive (self mode-locking) techniques are discussed. The EDFL constructed in this work is mode-locked using a form of passive mode-locking known as soliton mode-locking with a slow saturable absorber. This method allows pulses much shorter than the recovery time of the saturable absorber to be generated. Chapter 4 presents the development of the passively mode-locked femtosecond Cr^{4+}:YAG laser. The ultrashort pulses in the 1.5 µm region are critical for the time-resolved pump/probe measurements of the saturable absorbers. The results of the EDFL characterization including the temporal pulse widths generated by the different saturable absorbers are presented in Chapter 5. The optical characterization of the saturable absorbers including the linear absorbance, photoluminescence and time-resolved measurements are also given in this chapter. Chapter 6 provides insight into how the recovery times of the saturable absorbers contribute to the soliton pulse formation process in the EDFL. The parameters of the laser are also analyzed to show that the laser has the ability to be self-starting which is absolutely critical if the laser is to be used in high-speed optical networks. Finally, the results of this work are summarized in Chapter 7.

1.3 REFERENCES

1.   P. E. Green, Jr., IEEE J. Select. Areas in Commun. **14**, 764 (1996).

2.   J. Kraushaar, FCC Common Carrier Bureau, May 13, 1994.

3.   E. A. De Souza, M. C. Nuss, W. H. Knox, and D. A. B. Miller, Opt. Lett. **20**, 1166 (1995).

4.   S. Tsuda, W. H. Knox, J. L. Zyskind, J. E. Cunningham, W. Y. Jan, and R. Pathak, Paper CFD2, Conference on Lasers and Electro-optics, Anaheim, CA. 1996.

Chapter 2
Erbium-doped Fiber Lasers

2.1 INTRODUCTION

The field of lightwave communications has been greatly revolutionized with the advent of the erbium-doped fiber amplifier (EDFA). Signals centered at the 1.55 μm peak transmission point of optical fiber are attenuated at a rate of 0.2 dB/km as they propagate through the fiber. These losses become significant as the transmission distances approach several tens of kilometers. Long-distance communication systems, which may vary in length from several hundred to several thousand kilometers for undersea transmission, therefore require some form of signal amplification. Traditionally, the optical signal was first converted to an electrical signal and then amplified electronically in a process called regeneration. The signal was then converted back to optical form and resent through fiber until it needed to be amplified again. These electro-optical signal regeneration systems have the disadvantage of being quite expensive and the ultimate bandwidth of the communication link was limited to the speed of the electronics, which is much slower than the optical fiber can carry. The use of all optical amplifiers eliminates the need for any electro-optical conversion and thus allows the signal to remain in optical form for the entire transmission distance. This is more cost effective, and also allows utilization of more bandwidth on the fiber.

Many types of all optical amplifiers are available including semiconductor optical amplifiers, Raman amplifiers and Brillouin amplifiers. However, EDFA's have proven to be the current amplifier of choice because of their high gain (G > 40 dB), large gain bandwidth (BW > 4 THz), nearly quantum-limited noise and

compatibility with the 1.55 μm transmission window of traditional silica fiber.[1] These amplifiers consist of silica optical fibers doped with the rare earth ion erbium (Er^{3+}). The core of the amplifier is smaller than in typical fibers so as to increase the available density of erbium ions thus decreasing the pump threshold. However, the insertion loss associated with core mismatch is easily overcome by using specialty arc fusion splice techniques.

EDFA's are easily transformed into fiber lasers with the simple addition of positive feedback mechanisms. The fiber lasers discussed in this work employ erbium-doped fiber as the gain medium. This chapter will discuss the fundamental principles of erbium-doped fiber lasers beginning with erbium amplifiers. The chapter will then conclude with a section on the various types of mode-locked or short pulse fiber laser configurations.

2.2 PROPERTIES OF ERBIUM-DOPED AMPLIFIERS

EDFA's use the process of stimulated emission to amplify optical signals. The key ingredient in obtaining stimulated emission is the creation of a population inversion where Er^{3+} ions are raised from their natural ground state to a higher energy level. For amplification to occur, more ions must be in the higher energy state or excited state than in the ground state. Stimulated emission then occurs when photons of the right energy stimulate a transition of the excited ion. The ion drops to a lower energy state, emitting a photon that is an exact copy of the photon that stimulated the transition. The stimulated photon has the same frequency, polarization, phase and direction as the incident photon. Therefore by creating the population inversion, incident photons can be amplified.

The energy level diagram for an Er^{3+} ion in silica is shown in Figure 2.1.[2] The various energy levels listed correspond to the angular momentum states of the f-shell electrons in erbium. The transition that results in amplification at 1.55 μm corresponds to the $^4I_{13/2}$ to $^4I_{15/2}$ transition. The creation of the population inversion necessary for stimulated inversion requires that the ions be optically pumped to a higher energy level from the $^4I_{15/2}$ ground state.

As shown in Figure 2.1 three primary energy levels may be excited. The dopants pumped to higher energy levels other than the $^4I_{13/2}$ must decay nonradiatively to this state. Radiative transitions by stimulated emission to the ground state then produce the desired amplification. The first pumping scheme involves using 1.48 μm light to pump the $^4I_{13/2}$ to $^4I_{15/2}$ transition. The interested reader will be curious at this point as to how the energy transition can be pumped at 1.48 μm and emit at 1.55 μm. The answer lies in the fact that both the energy states, $^4I_{13/2}$ and $^4I_{15/2}$, are actually split into 8 energy sub-levels due to Stark splitting. Phonon broadening then 'smears' these states into a continuum. The population statistics of each energy state are governed by Boltzmann statistics. The lower lying energy sub-levels are more fully populated than the upper sub-levels so absorption more easily occurs from the lowest lying level of the ground state to the highest level of the excited state which corresponds to 1.48 μm. Similarly, emission occurs from the lowest sub-levels of the excited state to the highest sub-levels of the ground state corresponding to 1.55 μm. High power and highly reliable 1.48 μm InGaAsP/InP laser diodes are readily available as EDFA pump sources.

EDFA's can also be pumped at 980 nm using the $^4I_{11/2}$ to $^4I_{15/2}$ transition. The atoms then decay (on the order of a microsecond) down to the $^4I_{15/2}$ level. Strained-layer InGaAs/GaAs laser diodes are used as the pump sources at this

Energy (cm^{-1})

20000

$^4H_{11/2}$

Relaxation

$^4F_{9/2}$

$^4I_{9/2}$

$^4I_{11/2}$

Excited State
Absorption

10000

$^4I_{13/2}$

Pump
Absorption

Emission

0

$^4I_{15/2}$
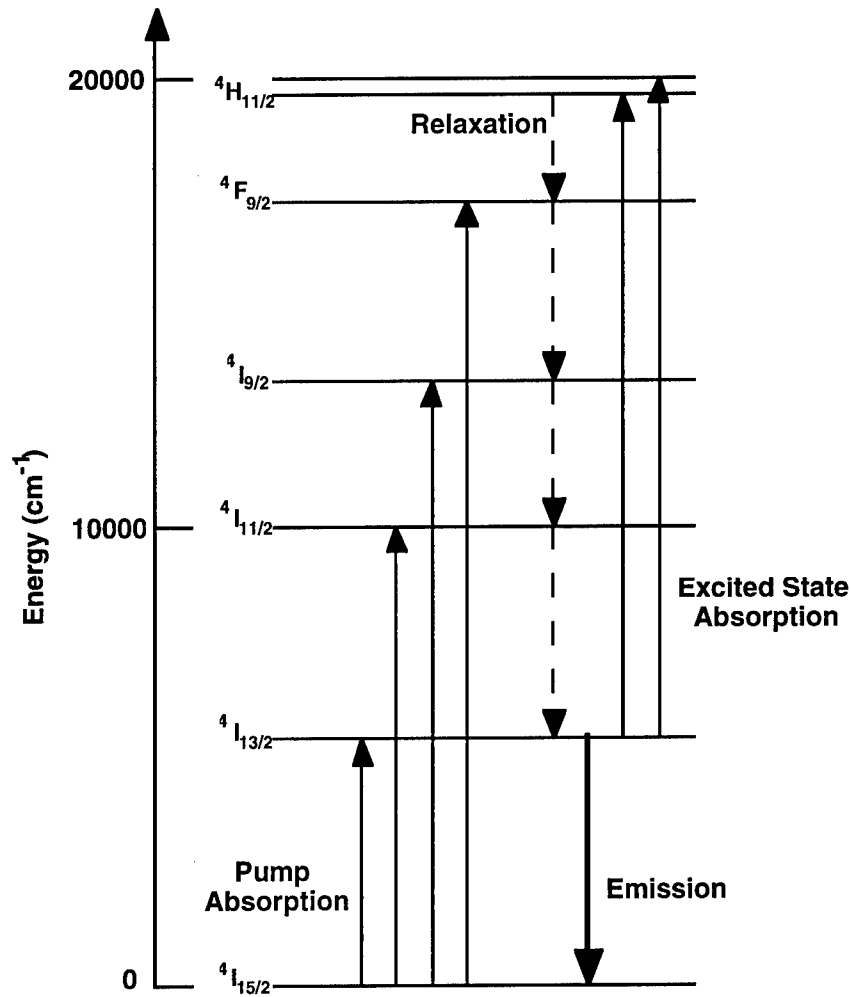
Figure 2.1   Energy level diagram for Er^{3+} ion in silica lattice. (after Ref. 2)

wavelength.   Improvements in long term reliability of these diodes has made them an attractive alternative to the 1.48 μm sources.   The noise figure for EDFA's pumped at 980 nm is typically 1 dB lower than for 1.48 μm diodes.[3] Pumping at 980 nm compared to 1.48 μm results in a higher inversion efficiency thus lowering the noise figures.   Pump power efficiencies of 11 dB/mW at 980 nm has been achieved.[4]   The erbium-doped fiber lasers used in this work are pumped at this wavelength.

Finally, EDFA's can be pumped at approximately 800 nm using the $^4I_{9/2}$ to $^4I_{15/2}$ transition. High power laser diodes using relatively mature GaAs technology are well developed at this wavelength. However, excited state absorption (ESA) plays a significant role in reducing pump efficiency at this wavelength. ESA causes a depletion of the population inversion established by promoting ions from the $^4I_{13/2}$ state up to a higher lying level at the $^4H_{11/2}$ state.

High power amplifiers can be realized using an alternative fiber architecture.[5] The silica based fiber is doped with ytterbium (Yb) as well as with erbium. The Yb ions are pumped at 1.06 μm and transfer their energy directly to the erbium ions creating a population inversion between the $^4I_{13/2}$ and $^4I_{15/2}$ states. Compact, high power Nd:YAG and Nd:YVO$_4$ solid state laser sources are readily available at 1.06 μm.

The gain spectra of erbium is affected by the co-dopants of the silica core which include elements such as germanium, aluminum and phosphorus.[6,7] The emission spectra of EDFA's co-doped with various elemental compositions are shown in Figure 2.2. The gain spectra is narrowest for the erbium-doped silica cores. We see that the aluminum-doped cores provide the flattest gain in the 1545 to 1560 nm range. Flat gain response over a wide range covering the 1550 nm transmission window of optical fiber is important in multi-wavelength communication architectures such as wavelength division multiplexing (WDM). The flat responses ensure that each wavelength or channel sees an approximately equal amount of amplification.

2.3 ERBIUM-DOPED FIBER LASERS

The erbium-doped fiber amplifiers discussed in the previous section are easily transformed into lasers through the use of positive feedback mechanisms.
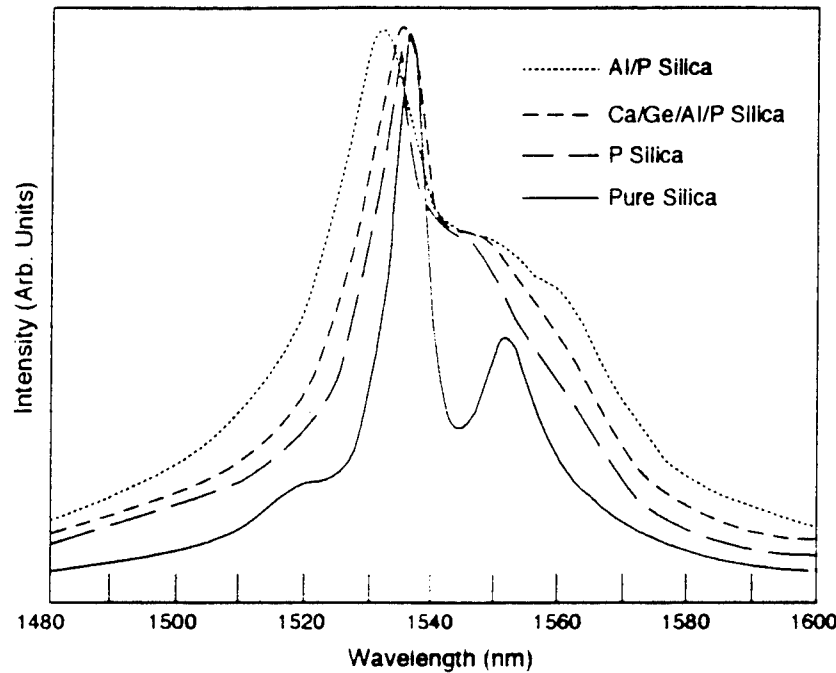
Figure 2.2   Emission spectra of four erbium-doped amplifiers with various co-
dopants. (after Ref. 6)

The simplest of laser cavities is the Fabry-Perot and is formed by placing the gain

medium between two highly reflecting end mirrors.[8]   The erbium-doped fiber

laser (EDFL) used in this work is a Fabry-Perot laser that uses a multiple

quantum well saturable absorber as the mirror at one end of the cavity and a

nearly 50% reflective fiber Bragg grating as the other mirror on the opposite

end.   This laser will be described in great detail in Chapter 5.   This current

section will discuss some of the important general concepts of fiber lasers

including: rate equations, lasing threshold and slope efficiency.

EDFLs operating at 1.55 μm are described by a three level rate equation

model.[9]   The energy level diagram for this model is shown in Figure 2.3.   This

model assumes that the population of level 3 is nearly zero because the photons

pumped into level 3 decay very rapidly to level 2 through non-radiative

transitions.   The rate equation governing the excited state of level 2 is of interest
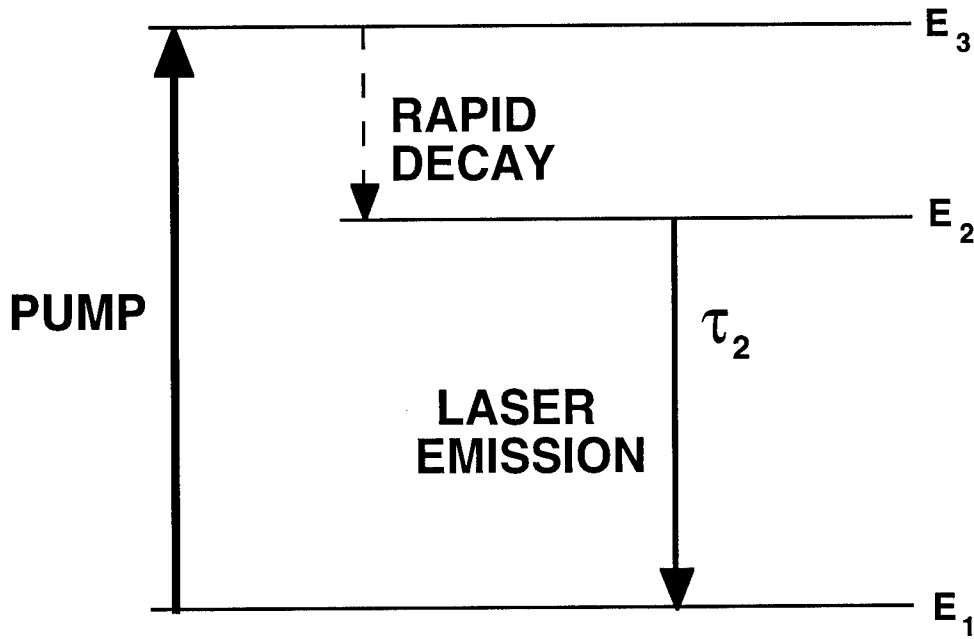
Figure 2.3   Schematic of three level laser system

and the density of ions in this level is $N_2(z,t)$. The rate equation for this level is given by [8]

$$\frac{\partial N_2}{\partial t} = W_p N_1 - W_s (N_2 - N_1) - \frac{N_2}{\tau_2} \qquad (2.1)$$

where N_1 is the ground state ion density, W_p is the transition rate for the pump, W_s is the transition rate for the signal and τ_2 is the lifetime of ions in state 2. The transition rates are defined as

$$W_p = \frac{\sigma_p P_p}{a_p h \nu_p} \qquad (2.2)$$

13

$$W_s = \frac{\sigma_s P_s}{a_s h \nu_s} \qquad (2.3)$$

where σ_p is the transition cross section for the pump, P_p is the pump power, a is the area of the pump mode, and ν_p is the pump frequency. The parameters for W_p are defined in a similar manner. The steady-state solution of Eq. 2.1 for the excited state population is found by setting $\partial N_2/\partial t=0$ and is

$$N_2 = \frac{(P_p{'} + P_s{'})N_t}{1 + 2P_s{'} + P_p{'}} \qquad (2.4)$$

where $P_p{'}=P_p/P_p{}^{sat}$ and $P_s{'}=P_s/P_s{}^{sat}$. $P_p{}^{sat}$ is the saturation pump power given by

$$P_p{}^{sat} = \frac{a_p h \nu_p}{\sigma_p \tau_2}. \qquad (2.5)$$

The signal saturation power, $P_s{}^{sat}$ is defined in the same manner. Therefore the population of the excited state depends upon the pump power as well as parameters of the erbium such as the transition cross section and upper state lifetime.

The threshold condition for lasing is reached when the round trip gain in the cavity is greater than the round trip losses. We can trace this out in a simple Fabry-Perot laser as

$$G^2 R_1 R_2 e^{-2\alpha_{int}L} > 1 \qquad (2.6)$$

where G is the saturated single pass gain of the cavity, $R_{1,2}$ are the mirror reflectivity's, α_{int} is the absorption coefficient of the cavity and L is the length of the gain medium. If this condition is satisfied, the intensity will continue to build in the laser cavity with each round trip until the gain saturates. The single pass gain is related to the gain coefficient, g(z) by

$$G = \exp\left[\int_0^L g(z)dz\right]. \qquad (2.7)$$

The insightful reader will wonder why the gain coefficient is not constant throughout the length of the gain medium. This is quite simply due to local variations in the pump and signal powers as they transverse the erbium-doped fiber. The population inversion $N_2(z)$-$N_1(z)$ is also dependent upon this power variation and is related directly to the gain coefficient by

$$g(z) = \sigma_s\left[N_2(z) - N_1(z)\right]. \qquad (2.8)$$

The value of N_2 was given by Eq. (2.4). Substitution of Eq. (2.7) into Eq. (2.6) gives the threshold lasing condition in terms of the gain coefficient as

$$\frac{1}{L}\int_0^L g(z)dz = \alpha_{cav} \qquad (2.9)$$

where α_{cav} are the losses of the cavity including those due to the gain medium and mirrors.

The evaluation of this integral in Eq. (2.9) often requires numerical methods to determine the necessary parameter values for lasing threshold. This is indeed true for a three level laser system such as erbium. However as shown by Agrawal, this integral is readily solved when a four level laser system is used.[9] The solution proves insightful in terms of the laser parameters necessary for threshold and is indeed applicable to erbium. An EDFL is modeled as a four level system when pumped at a wavelength of 800 nm due to the presence of ESA.[10] The pump absorption varies along the gain medium by

$$P_p(z) = P_p(0)e^{-\alpha_p L} \qquad (2.10)$$

where $P_p(0)$ is the input pump power. The lasing threshold can now be evaluated in terms of $P_p(0)$ and is

$$P_p(0) = \frac{\alpha_{cav} L}{1 - \exp(-\alpha_p L)} \left(\frac{\alpha_p}{\alpha_s}\right) P_p^{sat} \qquad (2.11)$$

where $\alpha_{p,s}$ are the absorption coefficients for the pump and signal respectively. It is important to note that the absorption coefficient is related to the total ion population, N_t, and cross section by

$$\alpha = \sigma N_t. \qquad (2.12)$$

16

The threshold power can be rewritten in terms of absorbed pump power, P_{abs}, which is defined as

$$P_{abs} = P_p(0)\left(1 - e^{-\alpha_p L}\right). \tag{2.13}$$

Substituting Eq. (2.13) into Eq. (2.11) and defining the threshold pump power, P_{th}, as equal to the absorbed pump power results in

$$P_{th} = \alpha_{cav} L P_p^{sat} \frac{\alpha_p}{\alpha_s}. \tag{2.14}$$

Using Eq. (2.5) for P_p^{sat}, P_{th} is given in its final form as

$$P_{th} = \alpha_{cav} L \left(\frac{a_p h \nu_p}{\sigma_s \tau_2} \right). \tag{2.15}$$

We now see that the threshold power is a function of cavity losses, cavity length, emission cross section, and the upper state lifetime.

Now let us turn our attention to the output power that we can obtain from the laser. During lasing, the gain of the laser becomes saturated down to the threshold level. This allows us to again use the thresholding condition given by Eq. (2.9). Once again we will use a four level model in determining the output power. The simplicity of the solution gives us valuable insight into the key

parameters involved in the output power of a laser. The solution of the integral in Eq. (2.9) is very straight forward and the intra-cavity power, P_s, is given by

$$P_s = P_s^{sat}\left(\frac{P_{abs}}{P_{th}} - 1\right).$$
(2.16)

Since radiation must be coupled out of the cavity through one of the mirrors, we define the transmission of mirror 1 as $T_1 = 1 - R_1$. The output power, P_{out}, is given by

$$P_{out} = T_1 P_s.$$
(2.17)

Therefore, the output power depends on the input pump power as would be expected and also on other parameters as given through P_s^{sat} and P_{th}.

Finally, we will conclude this section with a look at the slope efficiency which is a measure of how efficiently a laser coverts pump power into lasing power after threshold has been reached. The slope efficiency of fiber lasers is typically 10%.[9] The slope efficiency, η, is determined from

$$\eta = \frac{T_1}{\alpha_{cav} L} \frac{a_s}{a_p} \frac{v_s}{v_p}.$$
(2.18)

Slope efficiency is best increased by decreasing the intra-cavity losses, α_{cav}, which includes the mirror reflectivity's and also the coupling losses associated with intra-cavity elements such as the saturable absorber.

This section has presented a mathematical description of erbium-doped fiber lasers. Such important parameters as population inversion, gain, laser threshold, output power, and slope efficiency were analyzed. The next section will describe some of the different cavity configurations employed by fiber lasers. Specifically, configurations will be analyzed that produce short pulses. These short pulses are required in digital communication applications.

2.4 MODE-LOCKED FIBER LASERS

Mode-locked fiber lasers are capable of producing ultra-short pulses in both the picosecond and femtosecond regime. One important application of these lasers is in digital optical communication systems where stable and moderate energy pulses are required. The EDFL's are easily spliced with the standard telecommunications grade fiber used as the transmission medium in the long-distance systems. In addition, EDFL's operate at 1.55 µm which coincides with the optimum minimum loss transmission window of optical fiber. Finally, the fiber laser can be easily spliced to an additional section of erbium-doped fiber so as to amplify the available pulse energy.

This section will discuss some of the popular cavity configurations that are used to produce mode-locked or ultra-short pulses. Some of the characteristics associated with the different cavities will also be discussed. A thorough theoretical presentation of the physics behind the mode-locking process will be presented in Chapter 3.

Active or forced mode-locked laser cavities use either an acousto-optic modulator or an electro-optic modulator placed within the laser cavity to produce the ultra-short pulses. Acousto-optic modulators are typically not used in EDFL's because they are very bulky and cannot be easily integrated. However,

fiber pig-tailed electro-optic modulators such as lithium-niobate (LiNbO$_3$) are readily available making them very attractive for use in an EDFL. The schematic of a typical actively mode-locked EDFL employing a ring cavity is shown in Figure 2.4. Ring cavities are made to operate in one direction and do not require end mirrors. Actively mode-locked EDFL's typically produce pulse widths in the picosecond range. This type of laser was originally demonstrated in 1989.[11] Pulses of 50 ps were originally produced but by using soliton pulse formation techniques the pulses were shortened to 4 ps at a repetition rate of 90 MHz. The shortest pulses produced using an all active mode-locking technique were 20 ps in duration.[12] Mode-locked systems have also been demonstrated which integrate the modulator within the actual fiber making for a very compact system. Pulse widths of 200 ps at a repetition rate of 417 MHz have been produced using this type of integration scheme.[13]

Passive or self mode-locking is the second main type of mode-locking. Active mode-locking requires the use of an active element within the cavity that is synchronized electronically to the cavity repetition rate. Passive mode-locking does not require this synchronization but rather uses an all optical nonlinear process to shorten the pulse width. Passive mode-locking is capable of producing much shorter pulses than an actively mode-locked system.

One type of passively mode-locked laser uses a nonlinear fiber loop mirror to generate ultra-short pulses. This laser is shown in Figure 2.5 and is referred to as a figure-8 laser because of its general shape. The coupler at the center part of the laser is vital to the operation of the laser. It splits the incident radiation from the top left branch of the laser into counter propagating parts. The erbium-doped gain medium is placed off center in the right loop of the laser. The counter propagating radiation sees the gain at different times as it travels through

20
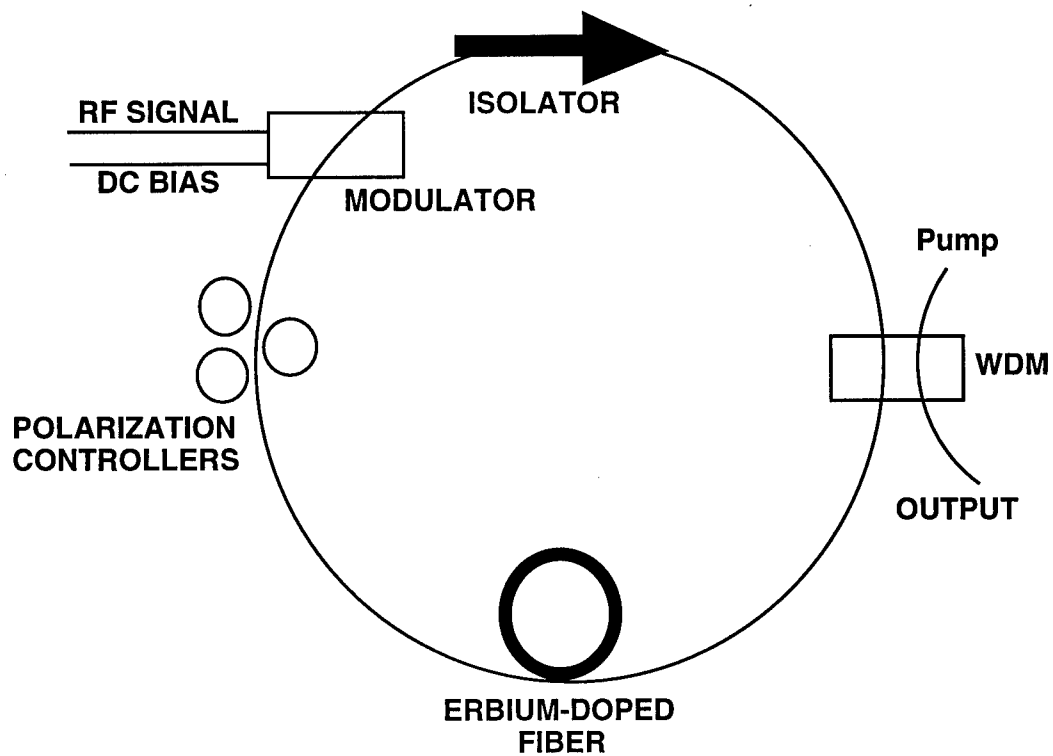
Figure 2.4   Schematic of actively mode-locked fiber ring laser
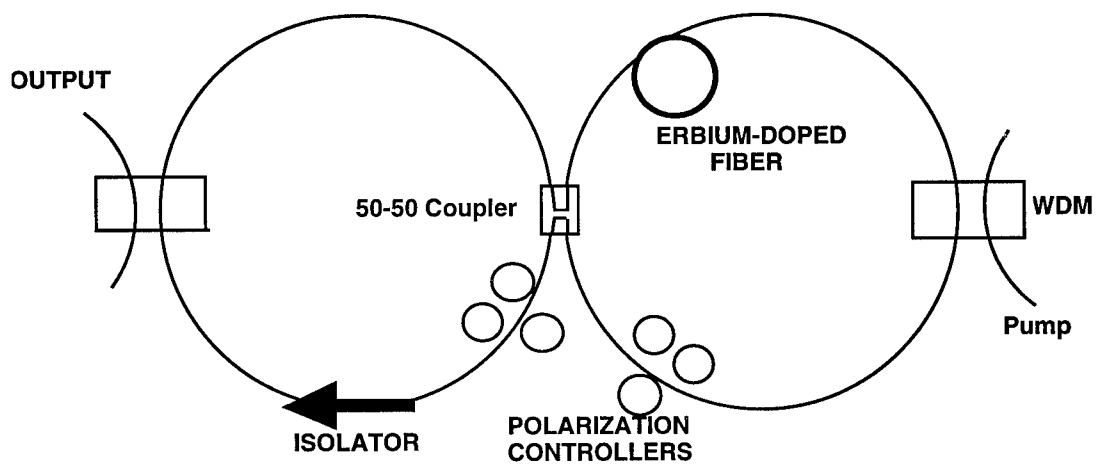
Figure 2.5   Schematic of figure-8 mode-locked fiber laser

this fiber loop. One part immediately sees gain while the other part must travel nearly the entire loop before it sees gain. The two different waves see a different amount of nonlinear phase shift due to the offset of the gain. The radiation is then recombined in the coupler but instead of returning along its original path to the top left port (reflected) the light can actually be switched (transmitted) to the bottom left port. The transmission is determined by the amount of phase shift acquired by thewaves. As the pulses are shaped in the cavity, the intensity of the peak will eventually become intense enough and acquire enough shift so that it is transmitted. However at the same point in time the wings of the pulse will be less intense and they do not acquire enough phase shift to be transmitted and they are simply absorbed by the isolator. Therefore the pulse is effectively shortened because the peak is transmitted while the wings are attenuated. This process will continue until a final steady-state pulse width is reached.

Figure-8 lasers were first introduced in 1991, with initial pulse widths of 314 fs.[14,15] Since then pulses as short as 98 fs have been reported.[16] Unfortunately, figure-8 lasers are severely limited in their usefulness in communication systems because of widely varying repetition rates. Actively mode-locked lasers have their repetition rates controlled by the synchronized operation of the active element. Figure-8 lasers contain no such element capable of controlling the repetition rate. Stabilization of the repetition rate has been demonstrated in different ways including the placement of a mirror near the output port so that a Fabry-Perot cavity is formed with a known repetition rate.[17]

A second type of passive mode-locking uses intensity dependent changes in the state of polarization when orthogonally polarized components propagate in a fiber. Figure 2.6 illustrates the nonlinear polarization rotation technique. The
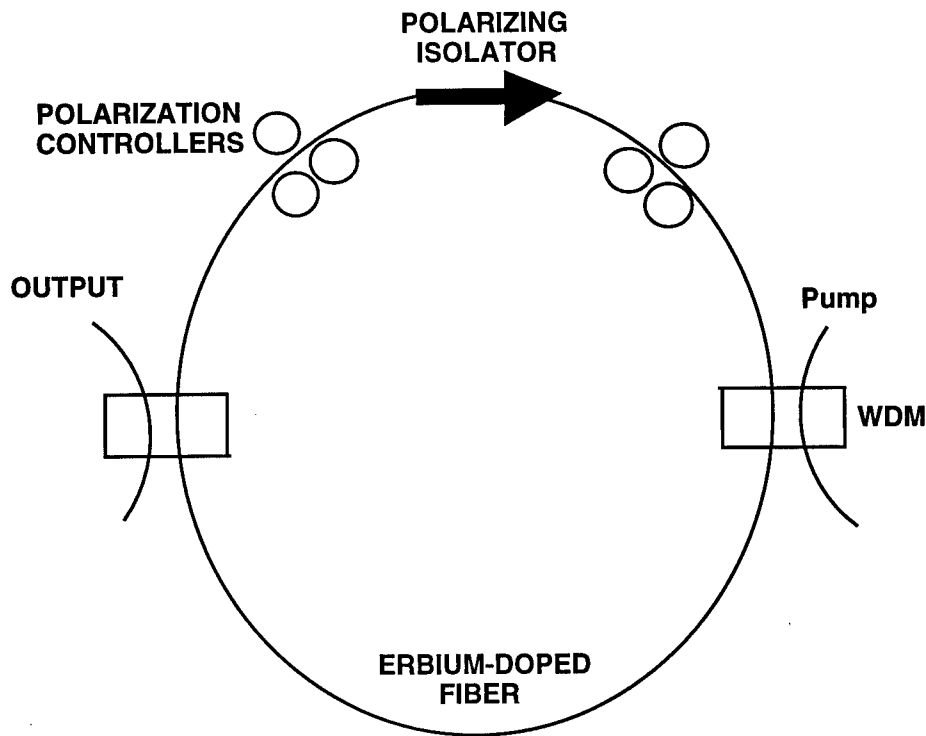
Figure 2.6   Schematic of passively mode-locked fiber laser using the non-linear polarization rotation technique

polarizing isolator that is placed between two polarization controllers is the key element in shaping the pulses. Radiation exiting the isolator is linearly polarized. The first polarization controller that the light sees after the isolator changes the state of polarization to elliptical.   As the light travels through the fiber it experiences various nonlinearities which induce phase shifts on the orthogonally polarized components of the light.   The second polarization controller is then adjusted so that the central peak of the pulse is passed by the isolator and the less intense wings are attenuated.   The pulse is shortened in this manner after a single pass through the ring cavity.   As with the figure-8 laser, this process continues until a final steady-state pulse width is reached.   This technique is capable of generating high energy (> 0.5 nJ) sub 100 fs pulses in EDFL's.[18]

Finally, we will briefly discuss passive mode-locking using saturable absorbers in EDFL's. This is the technique used to mode-lock the EDFL used in this work and is described in great detail in the next chapter. Pulse shortening in saturable absorbers is best understood by looking at the specialized case of a fast saturable absorber. If the central peak of the pulse is intense enough to saturate the absorption of the saturable absorber it will be transmitted. However the wings of the pulse will be attenuated by the absorption of the fast saturable absorber. This is similar to the pulse shortening mechanism used by nonlinear polarization rotation technique discussed previously. Previous uses of semiconductor saturable absorbers in erbium-doped fiber lasers have resulted in pulse widths as short as 0.84 ps with pulse energies of 0.85 nJ at repetition rates of 22 MHz.[19] Tsuda et al., more recently demonstrated 235 fs pulses at a repetition rate of 50 MHz.[20]

2.5 CONCLUSIONS

This chapter has discussed the operation of erbium-doped fiber amplifiers and their use as the gain medium in fiber lasers. The required population inversion necessary for gain in an EDFA was derived using basic laser rate equations. The gain of the amplifier was then used to determine other important parameters including threshold, output power and slope efficiency.

The second part of the chapter described some of the important laser cavity configurations that are capable of generating ultra-short pulses. The mode-locking process will be described in great detail in the following chapter. It should be pointed out that there is great deal of continuing research in the area of mode-locked EDFL's. The pulse widths produced by these lasers are certainly capable of supporting multiple gigabit per second communication systems.

However there remains a great deal of work to be done in producing mode-locked systems with stable repetition rates, stable pulse widths, and low timing jitter between the adjacent pulses.

2.6 REFERENCES

1.   C. R. Pollock, *Fundamentals of Optoelectronics* (Irwin, Chicago, 1995).

2.   R. I. Laming, S. B. Poole, and E. J. Tarbox, Opt. Lett. **13**, 1084 (1988).

3.   M. Yamada, M. Shimizu, M. Okayasu, T. Takeshita, M. Horiguchi, Y. Tachikawa, and E. Sugita, IEEE Photon. Tech. Lett. **2**, 205 (1990).

4.   M. Shimizu, M. Yamada, M. Horiguchi, T. Takeshita, and M. Okayasu, Electron. Lett. **26**, 1641 (1990).

5.   S. G. Grubb, W. F. Humer, R. S. Cannon, S. W. Vendetta, K. L. Sweeney, P. A. Leilabady, M. R. Keur, J. G. Kwasegroch, T. C. Munks, and D. W. Anthon, Electron. Lett. **28**, 1275 (1992).

6.   W. J. Miniscalco, IEEE J. Lightwave Tech. **9**, 234 (1991).

7.   J. L. Zyskind, E. Desurvire, J. W. Sulhoff, and D. J. DiGiovanni, IEEE Photon. Tech. Lett. **2**, 869 (1990).

8.   A. E. Siegman, *Lasers* (University Science Books, Mill Valley, CA, 1986).

9.   G. P. Agrawal, *Nonlinear Fiber Optics* (Academic Press, San Diego, CA, 1995).

10.   P. R. Morkel and R. I. Laming, Opt. Lett. **14**, 1062 (1989).

11.   K. Rottwitt, J. H. Povlsen, A. Bjarklev, O. Lumholt, B. Pedersen, and T. Rasmussen, Electron. Lett. **28**, 287 (1992).

12.   M. W. Phillips, A. I. Ferguson, and D. C. Hanna, Opt. Lett. **14**, 219 (1989).

13.   M. W. Phillips, A. I. Ferguson, G. S. Kino and D. B. Patterson, Opt. Lett. **14**, 680 (1989).

14.   I. N. Duling, III, Electron. Lett. **27**, 544 (1991).

15.   D. J. Richardson, R. I. Laming, D. N. Payne, M. W. Phillips, and V. Matsas, Electron. Lett. **27**, 730 (1991).

16.   M. Nakazawa, E. Yoshida, and Y. Kimura, Electron. Lett. **29**, 63 (1993).

17.   M. L. Dennis and I. N. Duling, III, Electron. Lett. **28**, 1894 (1992).

18.   K. Tamura, C. R. Doerr, L. E. Nelson, H. A. Haus, and E. P. Ippen, Opt. Lett. **19**, 46 (1994).

19.   W. H. Loh, D. Atkinson, P. R. Morkel, M. Hopkinson, A. Rivers, A. J. Seeds, and D. N. Payne, Appl. Phys. Lett. **63**, 4 (1993).

20.   S. Tsuda, W. H. Knox, J. L. Zyskind, J. E. Cunningham, W. Y. Jan, and R. Pathak, Paper CFD2, Conference on Lasers and Electro-optics, Anaheim, CA. 1996.

Chapter 3
Ultrashort Pulse Generation

3.1 INTRODUCTION

This chapter describes the principles behind the generation of ultrashort pulses by lasers. The term mode-locking is often used to describe the generation of these pulses. Mode-locking of a laser can be achieved by a variety of means, but is broken down into two main categories. The first category is active mode-locking where the loss introduced by an intra-cavity element such as an acousto-optic modulator is synchronized by an external clocking source to the round trip frequency of the laser cavity. Passive mode-locking is the second type of mode-locking and is also referred to as self-mode-locking. This type of pulse production uses a non-linear element within the laser cavity which has its transmission properties altered by the incident radiation. The loss introduced by the non-linear element is modulated by the radiation itself and no external clocking is required as in the former case. Both active and passive mode-locking periodically modulate the intra-cavity loss which serves to shape the ultra-short pulses as they make many passes within the cavity.

This chapter begins with the general theory of ultrashort pulse formation within a simple laser cavity. Active mode-locking is then examined including the minimum pulse width that can be achieved with this technique. Finally the major components of passive mode-locking will be presented including fast saturable absorption, slow saturable absorption with gain saturation and soliton mode-locking. It is this later case that provides the dominant pulse shaping mechanism in the erbium-doped fiber laser discussed in this work.

3.2 LASER MODE-LOCKING THEORY

A simple laser cavity consists of a gain medium positioned between two highly reflecting end mirrors. The cavity is capable of supporting a large number of electromagnetic field distributions. The distributions, or longitudinal modes, satisfy Maxwell's equations and the boundary conditions that are imposed by the end mirrors of the cavity. The spacing of these modes, f, in the frequency domain is related to the overall length of the cavity and is given by

$$f = \frac{c}{2nL} = \frac{1}{T_r} \qquad (3.1)$$

where c is the speed of light, n is the index of refraction of the laser cavity, L is the single pass length of the laser cavity, and T_r is the round-trip time of the cavity. The absolute frequency of these modes is confined to be within the finite gain bandwidth of the laser which is limited by the lasing transition. In a free-running state also known as continuous-wave (cw) operation, the phases of the modes will be uncorrelated and will randomly evolve due to the occasional addition of a spontaneous photon in the mode. In the presence of an appropriate perturbing force or modulating function these modes can be forced to oscillate in phase. The modulating function serves to transfer energy between the modes thus coupling them together. The synchronization of the modes is termed mode-locking and the power of the cavity is now emitted in a series of pulses which are temporally spaced at the round trip time of the cavity.

The temporal profile of the pulse and its corresponding spectral bandwidth are linked by a Fourier transformation. Therefore an increasing number of modes that can be locked together results in an increasingly shorter temporal

pulse width. The actual pulse width depends on the intensity profile of all the modes as well as the number, but certain generalizations can be made. For example, if each mode has the same intensity then the average normalized intensity of the mode-locked laser, I(t) will be given by

$$I(t) \propto \frac{\sin^2(N\omega t / 2)}{\sin^2(\omega t / 2)} \qquad (3.2)$$

where N is the number of locked longitudinal modes and ω is 2π times the mode-spacing, f. Figure 3.1 shows a plot of I(t) for the case of 5 longitudinal modes.

The spacing of these pulses is given by the inverse of the round-trip cavity time, T_r and the temporal pulse width is approximated as

$$\tau \approx \frac{1}{NT_r} \approx \frac{1}{\Omega} \qquad (3.3)$$

where Ω is the gain bandwidth of the laser. As stated previously the temporal pulse width decreases as the number of modes locked together increases. The peak power of the mode-locked laser is N times the average power which shows that the peak power is dramatically increased by locking together a large number of modes. These equations are approximations and the actual pulse widths are more complicated functions of dispersive and nonlinear laser cavity parameters.

The pulse width is always the Fourier transform of its corresponding spectral bandwidth. In the situation where all of the longitudinal modes are oscillating in phase, the pulse shape can be determined from the optical spectrum and the resulting pulse is said to be 'transform-limited'. The resulting description
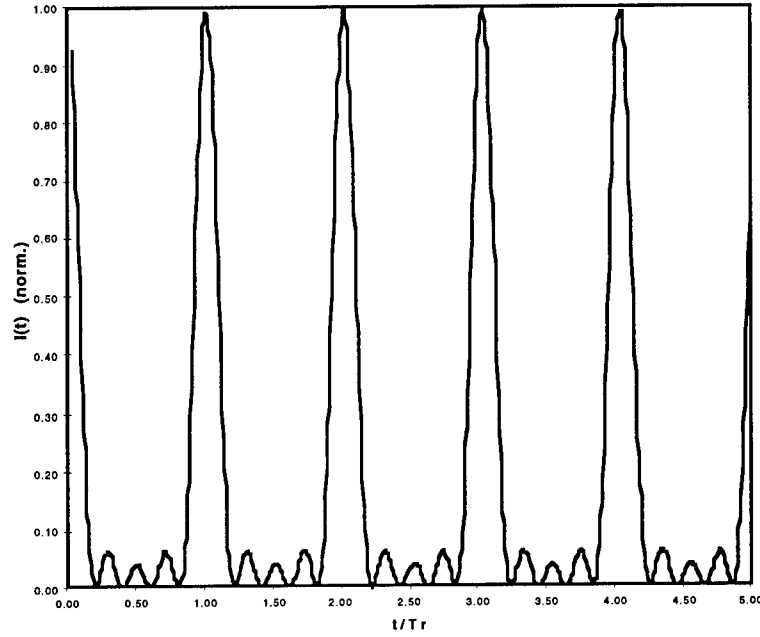
Figure 3.1 Plot of the normalized output intensity of a mode-locked laser with N
= 5 longitudinal modes.

of the transform-limited pulse is given by the time bandwidth product

$$\Delta v \tau = k \qquad\qquad (3.4)$$

where Δv is the spectral bandwidth of the pulse, τ is the transform-limited pulse width and k is a constant that is strictly determined by the pulse shape. For a Gaussian pulse shape, k = 0.44 and for a hyperbolic secant squared pulse shape k = 0.315. The resulting time bandwidth product when all of the oscillating modes are not locked together will be greater than the constant k. Therefore the measurable time-bandwidth product gives us a 'completeness' or efficiency of the mode-locking process.

3.3 ACTIVE MODE-LOCKING

Active mode-locking can be quite easily analyzed in the frequency domain. A simple laser cavity consisting of two end mirrors, a modulator and a gain medium is shown in Figure 3.2. The modulator changes the loss or gain in the cavity so that sidebands are placed on the longitudinal modes corresponding to modulation frequency of the modulator, f_m. By setting the modulation frequency equal to the inverse of the round-trip cavity time, energy is transferred between the adjacent modes and these modes become coupled or locked in phase. Active mode-locking is achieved using either a time varying amplitude modulation (AM) or a time varying phase change known as frequency modulation (FM).
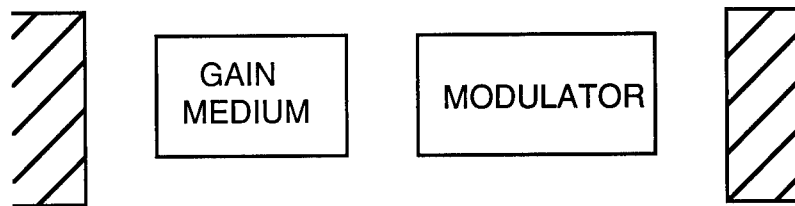
Figure 3.2   Schematic of an actively mode-locked cavity showing the gain medium and modulator

AM mode-locking typically uses an acousto-optic Bragg cell placed within the laser cavity to introduce loss by periodically diffracting the laser radiation. The rf modulation frequency of the Bragg cell is set to one-half the frequency spacing of the cavity so that loss is introduced at all times with the exception of time when there is maximum transmission through the modulator. This is easily viewed in the time domain by envisioning a shutter which is open only once per cavity round trip. At all other times the shutter is closed and the cavity experiences high loss. The pulse is synchronized to this open shutter time

window and the peak of the pulse will see a higher net gain than the wings of the pulse. This will serve to temporally compress the pulse after many round-trips through the cavity. Analysis of this process requires a mathematical description of the loss mechanism. One common loss function is the cosinusoidal loss function, t_{AM},

$$t_{AM} = \exp[-\Delta_m(1 - \cos\omega_m t)] \qquad (3.5)$$

where $2\Delta_m$ is the peak to peak sinusoidal modulation depth and ω_m is the modulation frequency.[1] Analysis of the cavity using this loss function under steady-state conditions, showed that a self-consistent Gaussian shaped pulse will be generated. The minimum achievable pulse width, τ_p for the Gaussian pulse is then derived as

$$\tau_p = 0.45 \left(\frac{\alpha}{\Delta_m}\right)^{\frac{1}{4}} \left(\frac{1}{f_m \Omega}\right)^{\frac{1}{2}} \qquad (3.6)$$

where α is the saturated gain coefficient, f_m is the modulation frequency and Ω is the gain bandwidth. Therefore, the pulse width is dependent on the 1/2 power of $1/f_m$ and $1/\Omega$ but only the 1/4 power of α and $1/\Delta_m$.

FM mode-locking typically employs an electro-optic modulator using the Pockels effect to provide the necessary modulation. The modulator provides a time-varying sinusoidal phase change, $\phi(t)$ for the laser radiation. The phase change adds a frequency chirp to the radiation and after many round trips the center frequency of the intracavity radiation is shifted outside of the gain bandwidth. Once outside of the gain bandwidth, the radiation will not oscillate.

Only the radiation that arrives when $d\phi(t)/dt$ is zero will remain unchirped. Once again we see that there is a time window that is formed at the turning points of the sinusoidal modulation function. The pulses in this window see a large net gain while the radiation outside of this window is attenuated. The transmission function of the phase modulator is given by [1]

$$t_m = \exp[-j\Delta_m \cos\omega_m t].\qquad(3.7)$$

The pulse width is still given by Eq. (3.6) except that it is now scaled by the 1/8 power of the RF drive power. The pulses formed by FM mode-locking are generally not transform-limited because of the acquired frequency chirp. Historically, most actively mode-locked lasers use AM and not FM techniques.

3.4 PASSIVE MODE-LOCKING

As discussed in the previous section, both AM and FM active mode-locking require an external synchronization signal. Passive mode-locking on the other hand does not require such an external signal. Rather, a nonlinear element that is placed within the cavity provides the necessary synchronization signal through its interaction with the pulse. The term self-mode-locking is often used to describe passive mode-locking. Figure 3.3 shows a simple laser cavity consisting of two end mirrors, the gain medium, and the nonlinear element.

There are different types of nonlinear effects that can be exploited to passively mode-lock a laser including the Kerr effect, self-phase modulation, and saturable absorption. Specifically, we will discuss passive mode-locking using a saturable absorber as the nonlinear element. The key property of the saturable
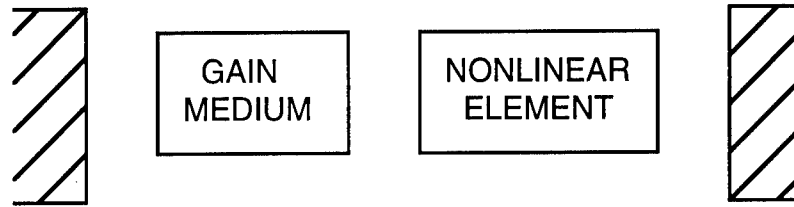
Figure 3.3   Schematic of a passively mode-locked cavity showing the gain medium and nonlinear element

absorber that determines its usefulness for mode-locking is that its transmission must be modified by the incident intensity.   In this situation, the saturable absorber can be described by a two level energy system.   The atoms are all initially considered to be in the ground state and the saturable absorber exhibits absorption.   Absorption of a certain amount of radiation can result in the promotion of a significant number of atoms from the ground state to the excited state which reduces the net absorption.   Such an absorber is said to be saturated. The time that the atoms remain in the excited state is the upper state lifetime of the absorber which is also denoted as the absorber recovery time.   The amount of saturation of the saturable absorber is dependent upon the amount of incident radiation over the time frame dictated by the absorber's recovery time.   Three types of passive mode-locking will be discussed in the following sections.   Fast saturable absorption occurs when the laser pulse width is on the order of the absorber recovery time.   Slow saturable absorption with gain saturation and saturable absorber soliton mode-locking result in pulse widths much shorter than the absorber recovery time.

3.4.1 FAST SATURABLE ABSORBER MODE-LOCKING

Fast saturable absorbers are characterized by the initial incident pulse width being much longer than the recovery time of the absorber. The pulse shaping is then done entirely by the absorption modulation of the saturable absorber by the instantaneous intensity of the incident pulse. The peak of the pulse which has the highest intensity will saturate through the absorber and be preferentially amplified by the gain medium. The less intense leading and trailing edges of the pulse will not be able to saturate the loss and will experience a large amount of attenuation in the absorber. After many passes through the cavity with the leading and trailing edges being trimmed off, the pulse shortens until the pulse width is on the order of the absorber recovery time. Figure 3.4 shows the gain and loss mechanisms of a fast saturable absorber. For most times the loss of the cavity exceeds the gain, so no light oscillates. When the loss is saturated, there is a net gain window that is open for the peak of the pulse and closed for both the leading and trailing edges of the pulse. This open time window corresponds to the pulse width. We will begin this section with a look at the evolution of the pulse in a cavity containing a fast saturable absorber.

The buildup or 'seeding' of the initial pulse begins with a fluctuation of the cw laser. As discussed in the first section of this chapter there are a large number of longitudinal modes oscillating in the cavity with random phases. There are noise spikes in the cavity that are now generated due to a few random modes being locked together in phase. The initial intensity of these noise spikes will continue to increase after many trips through the gain medium, but at the same time will be spectrally narrowed due to the finite gain bandwidth of the gain medium. This process continues until one of the noise spikes becomes intense enough to saturate the absorber and be preferentially amplified. The less intense
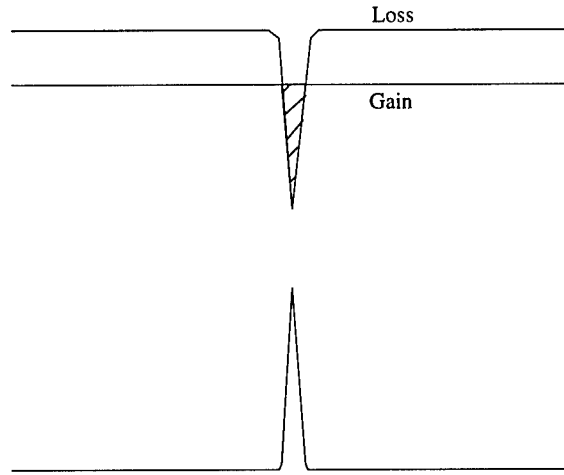
Figure 3.4   Schematic showing pulse shaping mechanism in a laser containing a
fast saturable absorber

noise spikes will end up being attenuated by the absorber.   The preferred noise
spike will continue to be shaped by the absorber as its leading and trailing edges
are attenuated and the peak is amplified.   The trimming, or compression, of the
pulse will continue for many passes through the cavity until its temporal width is
on the order of the absorber recovery time.   At this point, the transmission of the
absorber is no longer intensity dependent and further compression does not
continue.   As expected from general mode-locking theory, the pulses are spaced
at the round-trip cavity time.

The pulse shortening done by the saturable absorber can be evaluated using
the input intensity, $I_1(t)$, the saturation intensity, I_{sat}, and the small signal or non-
saturated transmission, T_o, of the absorber.   This relation is derived as

$$\ln\frac{I_2(t)}{I_1(t)} + \frac{I_2(t) - I_1(t)}{I_{sat}} = \ln(T_o) \qquad (3.8)$$

where T_o is defined as

$$T_o = e^{-2\alpha L} \qquad (3.9)$$

with α being the unsaturated absorption coefficient of the saturable absorber and L the length of the absorber.[2] I_{sat} is defined as

$$I_{sat} = \frac{h\nu}{\sigma_a T_a} \qquad (3.10)$$

where $h\nu$ is the energy of the incident radiation, σ_a is the absorber cross section and T_a is the saturable absorber recovery time. The absorber cross section is related to the unsaturated absorption coefficient by

$$\sigma_a = \frac{\alpha}{N_d} \qquad (3.11)$$

where N_d is the density of absorber atoms or the density of states if the absorber is a semiconductor. Therefore for any given input pulse shape on the absorber with intensity $I_1(t)$, the output intensity $I_2(t)$ can be calculated. The resulting temporal reduction in pulse width for a given input pulse shape can also be calculated from this output intensity.

The final pulse width, τ_p will ideally be on the order of the saturable absorber recovery time. However as shown by Haus, τ_p, is a more complicated function of both the laser and saturable absorber parameters.[3] The output pulse shape, $\xi(t)$, is derived as

$$\xi(t) = \xi_o \operatorname{sech}\left(\frac{t}{\tau_p}\right) \qquad (3.12)$$

where ξ_o is the initial electric field amplitude. The resulting pulse width is given by

$$\tau_p = \left(\frac{2g}{\alpha L}\right)^{\frac{1}{2}} \left(\frac{I_{sat}}{I}\right)^{\frac{1}{2}} \frac{1}{\Omega} \qquad (3.13)$$

where g is the saturated gain of the laser, I is the intensity on the absorber and Ω is the gain bandwidth of the laser. We see that the final pulse width is inversely proportional to the gain bandwidth. This is consistent with the earlier theory which showed that the pulse width is limited by available spectral bandwidth. The pulse width is also limited by how deep the absorber can be modulated. This is given by the 1/2 power of I_{sat}/I and is analogous to the modulation depth found in actively mode-locked systems.

Passively mode-locked lasers using fast saturable absorbers initially used dye cells as the pulse shaping element. The recovery times of certain dyes are as short as a few ps and pulses on this order were generated.[4,5] However, these dyes are rather impractical and have large insertion losses and are difficult to saturate. Fortunately, semiconductor multiple quantum well structures are well suited for passive mode-locking in the near infrared region. These structures exhibit relatively low saturation intensities and are easily integrated into compact laser systems. The absorption recovery times of the quantum wells can also be tailored using low temperature molecular beam epitaxial growth of group III-V compounds or post-growth ion implantation. Pulses on the order of a picosecond

have been readily generated using fast saturable absorption in a variety of laser systems.[6,7]

3.4.2 SLOW SATURABLE ABSORPTION WITH GAIN SATURATION

The use of slow saturable absorbers in conjunction with gain saturation of the lasing medium can result in pulse widths that are much shorter than the recovery time of the saturable absorber. Unlike fast saturable absorbers which do all of the pulse shaping, this type of mode-locking uses a combination of saturable absorption and gain saturation to shape the pulses. Figure 3.5 shows a simple laser cavity consisting of two end mirrors, a saturable absorber and a saturable gain medium. The intracavity pulse must be able to sufficiently deplete the gain as it makes a single pass through the cavity. Gain saturation is most commonly observed in dye lasers and semiconductor diode lasers. Solid-state and erbium-doped fiber lasers are not able to use this type of mode-locking because of their very long upper state lifetimes which makes them hard to saturate. First we will begin with a look at how a pulse is actually shortened using a saturable absorber and gain saturation.
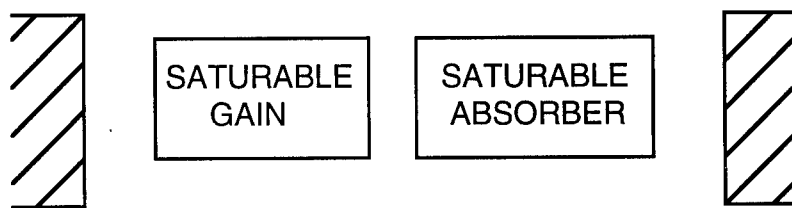
Figure 3.5 Schematic of a mode-locked cavity showing the saturable gain medium and saturable absorber

The saturable absorber attenuates the leading edge of the pulse as it passes through the saturable absorber. The peak of the pulse travels through the absorber with minimum loss and is then amplified as it passes through the gain medium, where it sufficiently depletes the gain. The remaining gain is now below the cavity loss, so the trailing edge of the pulse sees more loss than gain and is attenuated. The pulse is effectively compressed by the attenuation of the leading edge, amplification of the peak and attenuation of the trailing edge. The pulse compression continues for many round trips until a minimum pulse width is reached as determined by laser parameters such as dispersion and gain bandwidth. Figure 3.6 shows the gain and loss dynamics that govern the shaping of the pulse. We see that the loss saturates before the gain but it recovers quicker than the gain. This ensures that there is net loss before and after the pulse and net gain during the peak of the pulse.

Passive mode-locking with a slow saturable absorber and gain saturation can only be achieved if there is appreciable change in the gain and loss of the laser cavity during the round trip transit time of the pulse. The following two criteria that satisfy these requirements are:

$$\frac{\sigma_a}{A_a} > \frac{\sigma_g}{A_g} \qquad (3.14)$$

and

$$T_a < T_g \qquad (3.15)$$

42
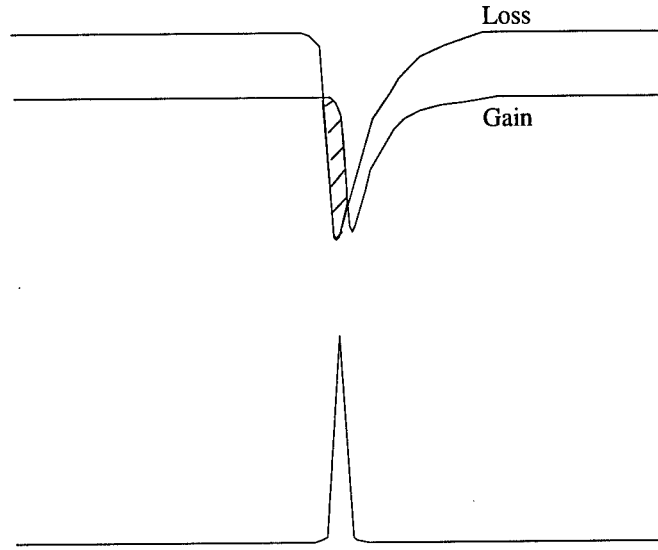
Figure 3.6 Pulse shaping mechanism for a laser containing both a slow saturable absorber and saturable gain medium. The cross hatch region illustrates where a net gain is available in the cavity.

where σ_a and σ_g are the saturable absorber and gain medium cross-sections respectively, A_a and A_g are the physical geometrical cross sections of the laser beam in the saturable absorber and gain medium, T_a is the slow saturable absorber lifetime and T_g is the upper state lifetime of the gain medium. Eq. 3.14 states that the absorber loss must saturate faster than the laser gain, while Eq. 3.15 states that the absorber recovery time must be shorter than the gain recovery time. However, stable mode-locking will also only be achieved if the round trip pulse transit time is on the order of the upper state lifetime of the gain medium. The upper state lifetime of erbium is 10 ms while a typical round trip transit time for a pulse in a typical erbium-doped fiber laser cavity is 200 ns [8,9]. Therefore this type of passive mode-locking cannot be achieved in the Fabry-Perot erbium fiber laser discussed in this work. As a final note, Haus has shown that the pulse width for such a system is inversely proportional to the inverse pulse energy in

the laser cavity.[10] This technique has been used in a passively mode-locked dye laser to generate sub 100 fs pulses[11]. In this laser system different types of dyes were used as both the gain medium and the saturable absorber. Fork, *et al.,* subsequently produced 6 fs pulses with a dye laser which until recently were the shortest optical pulses ever generated.[12]

3.4.3   SATURABLE ABSORBER SOLITON MODE-LOCKING

The final type of passive mode-locking that we will discuss in this chapter is soliton mode-locking using a slow saturable absorber. The Fabry-Perot fiber laser discussed in this work uses soliton mode-locking as the principle pulse shaping mechanism. A primary feature of this type of mode-locking is that pulses much shorter than the recovery time of the saturable absorber can be formed and the pulse width is independent of the upper state lifetime of the gain medium. Therefore, solid-state lasers as well as erbium-doped fiber lasers which have long upper state lifetimes can be mode-locked in this manner.

The formation of solitons requires that the group velocity dispersion (GVD) in the laser cavity is balanced by the self-phase modulation (SPM). The saturable absorber is used to initiate and stabilize the mode-locking process. It will be shown later in this section that the recovery of the saturable absorber also contributes to the final pulse width. Figure 3.7 shows the elements that must be present in a passively mode-locked soliton laser cavity.

Optical solitons are a solution to the wave equation that propagate without distortion even over very long distances.[13] This very basic property of solitons makes them ideally suited for long-haul telecommunication systems. Under normal conditions, a pulse will become temporally broadened as it travels through a dispersive medium. The distortion eventually results in intersymbol

44
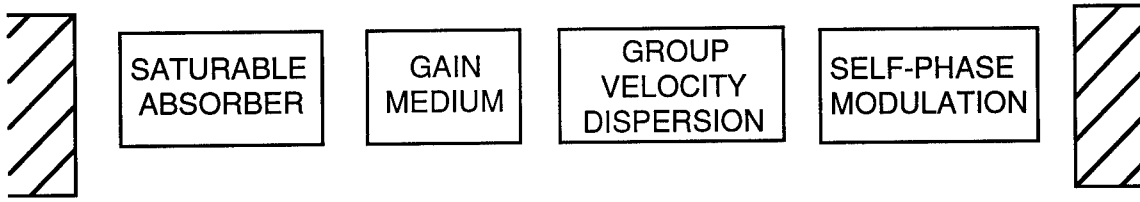
Figure 3.7　Schematic showing the four key components in a passively mode-locked laser using soliton formation

interference errors between adjacent time slots in communication channels. The temporal broadening of the pulse is due to the interaction of a finite spectral bandwidth of the pulse with the group velocity dispersion of the fiber. The different wavelengths travel at different group velocities and reach the receiver at different times, effectively stretching out the pulse in time. The group velocity dispersion, GVD, is stated as

$$GVD = -\frac{\lambda}{c}\frac{d^2n}{d\lambda^2} \qquad (3.16)$$

where λ is the wavelength, c is the speed of light, and n is the index of refraction of the transmission medium. The region termed negative GVD is of the most interest for soliton formation. In this regime, longer wavelengths travel slower than the shorter wavelengths.

Negative GVD can actually temporally compress a pulse when it is balanced with the proper amount of nonlinearity due to self-phase modulation (SPM). The essential component in SPM is the index of refraction of a dielectric, given by

$$n(I) = n_o + n_2 I \qquad (3.17)$$

where n_o is the commonly used index of refraction, n_2 is the nonlinear index of refraction and I is the intensity of the light in the given medium. Typical values for n_2 are 3.2 x 10^{-16} cm^2/W for fused silica and 3. x 10^{-16} cm^2/W for sapphire. The contribution of n_2 to the index of refraction is negligible except for very high intensities. However the small diameter of an optical fiber (on the order of 10 μm) coupled with the long interaction lengths, leads to the high intensities needed to generate significant index nonlinearities.

The electric field, E(z), description of a plane wave traveling in a dielectric medium is given by

$$E(z) = E_o e^{j\phi} = E_o e^{j(\omega_o t - k_o n(I) z)} \qquad (3.18)$$

where E_o is the electric field amplitude, ϕ is the phase of the plane wave, ω_o is the angular frequency, k_o is the wavevector given by ω_o/c, and z is the direction of propagation. The phase of the plane wave can be rewritten as

$$\phi = \omega_o t - \frac{\omega_o z}{c}[n_o + n_2 I(t)]. \qquad (3.19)$$

We see that the phase of the wave can be varied by changing its own intensity. This is referred to as self-phase modulation. The instantaneous frequency, $\omega(t)$, is the phase derivative with respect to time,

46

$$\omega(t) = \frac{d\phi}{dt} = \omega_o \left[1 - \frac{z}{c} n_2 \frac{dI(t)}{dz} \right]. \qquad (3.20)$$

The instantaneous frequency is therefore a function of the intensity of the incident light, $I(t)$. If $I(t)$ varies in time, the pulse frequency can become 'chirped'. As $I(t)$ changes with time, $\omega(t)$ is modulated. In this manner, the time dependent index of refraction acts like a phase modulator. $I(t)$ is lower at the leading edge of the pulse than in the peak resulting in a lower index of refraction. The phase velocity of the leading edge, given by $v = c/n$, is therefore slightly faster relative to the velocity at the peak of the pulse. The phase fronts pull away from the center of the pulse and are shifted to lower frequencies. The phase fronts of the trailing edge undergo a similar process and advance toward the peak of the pulse. The pulse is compressed in this region which leads to shorter wavelengths or higher frequencies. In this manner, phase modulation creates additional frequency components in a pulse. The total accumulated variation in the phase of the pulse is given by

$$\Delta\phi = \frac{2\pi L}{\lambda} n_2 I_{max} \qquad (3.21)$$

where I_{max} is the peak intensity of the pulse.

At certain intensities, the GVD and SPM will exactly balance so that the pulses can propagate without distortion. In other words, the chirping or temporal narrowing effect caused by the SPM compensates for the temporal broadening introduced by the GVD. Soliton formation is of course much more complicated when viewed mathematically and the solitons are modes or solutions

of the nonlinear wave equation.[13] Let us now return to a description of soliton formation within a laser and how it differs from the passive mode-locking techniques described in previous sections.

In both fast saturable absorption and slow saturable absorption with gain saturation, there is a net gain window that is open only long enough for the pulse to see gain. However as shown in Figure 3.8, the net gain window stays open for much longer after the pulse has passed. Since the gain window is open for a time frame much longer than the actual pulse, background noise will be amplified during this time frame. However, this noise does not have enough intensity to experience the nonlinearity required for soliton formation. Dispersion dominates the propagation of the background noise and it is spread in time. Since this noise cannot effectively buildup within the cavity, it is easily attenuated by the saturable absorber. In this manner the saturable absorber provides the intensity discrimination for both mode-locking startup and stabilization from intracavity noise.

The saturable absorber also affects the minimum temporal soliton pulsewidth generated by the laser system. Kärtner derives this pulsewidth, τ_p as

$$\tau_p = \left(\frac{1}{\sqrt{6}\Omega}\right)^{\frac{3}{4}} \left(\frac{T_a g^{\frac{3}{2}}}{q_o}\right)^{\frac{1}{4}} (\Delta\phi)^{-\frac{1}{8}} \qquad (3.22)$$

where Ω is the gain bandwidth of the laser, T_a is the saturable absorber recovery, g is the saturated laser gain, q_o is the unsaturated losses of the saturable absorber, and $\Delta\phi$ is the nonlinear phase shift per round trip due to SPM.[14] We see that

48
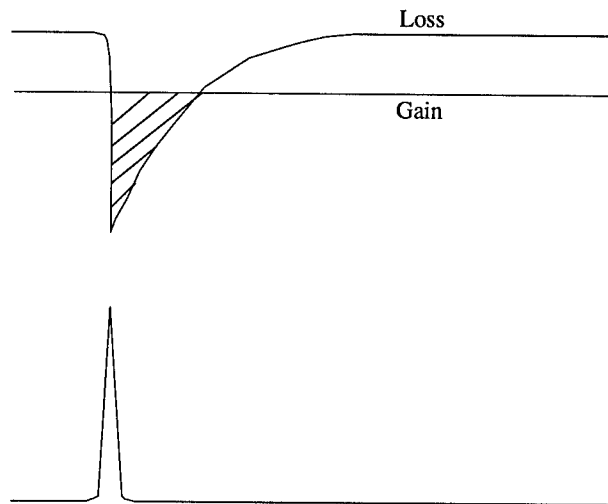
Figure 3.8   Pulse shaping mechanism in soliton laser using a slow saturable absorber.   The resulting pulse width is much narrower than the open time window of the gain.

the pulse width is proportional the 1/4 power of the saturable absorber recovery time.   This equation will be applied in detail in Chapter 6 to show the relation between the measured recovery for a number of individual saturable absorbers and the pulse widths obtained from the Fabry-Perot erbium-doped fiber laser mode-locked by the saturable absorbers.

3.5   CONCLUSIONS

This chapter has provided an overview of ultra-short pulse generation in lasers. Both active and passive mode-locking techniques were described. Active mode-locking requires the synchronization of an intracavity modulator to the round trip laser frequency by an external clocking source. This involves the use of both a bulky modulator and expensive rf drive electronics. Passive mode-

locking eliminates the need for synchronization electronics. The bulky modulator is also replaced in this method by a very small piece of semiconductor containing the multiple quantum wells responsible for the saturable absorption required for pulse formation. The size of the semiconductor only has to be as large as the incident beam. Passive mode-locking can also produce pulses which are shorter than those produced by an actively mode-locked system.

Passive mode-locking therefore offers many advantages over active mode-locking. The use of semiconductor multiple quantum wells as the passive element requires the careful design and analysis of these structures. The carrier recombination time or lifetime of the multiple quantum wells is one key property that must be analyzed because of its influence on the mode-locking process in the fiber laser discussed in this work. Experimental measurements of the lifetimes require the use of an ultrafast mode-locked laser source whose wavelength corresponds to the bandedge of the quantum wells. The pulse widths generated by the laser must also be much less than the lifetimes of the quantum wells. The next chapter describes the development of a tunable femtosecond mode-locked chromium-doped:YAG laser which operates in the 1.5 μm region. This laser is an ideal spectroscopic tool for the analysis of the picosecond carrier lifetimes of the multiple quantum well saturable absorbers which are designed to operate at 1.5 μm.

3.6 REFERENCES

1.   D. J. Kuizenga and A. E. Siegman, IEEE J. Quantum. Electron. **QE-6**, 694 (1970).

2.   A. E. Siegman, *Lasers* (University Science Books, Mill Valley, CA, 1986).

3.   H. A. Haus, in *Compact Sources of Ultrashort Pulses*, edited by I. Duling, III (Cambridge University Press, Cambridge, 1995).

4.   A. J. DeMaria, D. A. Stetser, and H. Heynan, Appl. Phys. Lett. **8**, 174 (1966).

5.   D. J. Bradley, A. J. F. Durrant, F. O'Neill, and B. Sutherland, Phys. Lett. **30A**, 535 (1969).

6.   U. Keller, D. A. B. Miller, G. D. Boyd, T. H. Chiu, J. F. Ferguson, and M. T. Asom, Opt. Lett. **17**, 505 (1992).

7.   U. Keller, Appl. Phys. B **58**, 347 (1994).

8.   B. E. A. Saleh and M. C. Teich, *Fundamentals of Photonics* (John Wiley & Sons, New York, 1991).

9.   M. F. Krol, M. J. Hayduk, S. T. Johns, K. Teegarden, and G. Wicks, SPIE Proceedings **2749**, 47 (1996).

10   H. A. Haus, IEEE J. Quantum. Electron. **QE-11**, 736 (1975).

11.   E. P. Ippen, C. V. Shank, and A. Dienes, Appl. Phys. Lett. **21**, 348 (1972).

12.   R. L. Fork, C. H. Brito Cruz, P. C. Becker, and C. V. Shank, Opt. Lett. **12**, 483 (1987).

13.   A. Hasegawa and F. Tappert, Appl. Phys. Lett. **23**, 142 (1973).

14.   F. X. Kärtner and U. Keller, Opt. Lett. **20**, 16 (1995).

Chapter 4
Passively mode-locked femtosecond
chromium-doped:YAG laser

4.1 INTRODUCTION

The use of solid-state lasers for ultrashort pulse generation covering many wavelength regimes has been the center of much recent attention.[1] This work continues to be motivated by new applications of the ultrafast sciences including time-resolved spectroscopy, biomedical diagnostics and imaging, surveillance, counter-terrorism measures, and metrology. This chapter will concentrate on the generation of femtosecond pulses in the 1.5 μm region for use in time-resolved spectroscopic studies of the saturable absorbers used to passively mode-lock the erbium-doped fiber lasers.

The titanium-doped sapphire (Ti:Al$_2$O$_3$) laser is a popular and widespread ultrafast solid-state laser that has been extensively studied and is now commercially available from a variety of vendors. The Ti:sapphire is widely tunable from 0.7 to 1.1 μm with its peak emission wavelength centered at 735 nm.[2] Unfortunately, optical communication systems typically operate in the 1.3 - 1.5 μm transmission window of optical fiber. The erbium-doped fiber laser that is the focus of this thesis operates at 1.5 μm, making the Ti:sapphire laser incompatible as a spectroscopic test source for the saturable absorber used in these systems. The color center (NaCl:OH⁻) laser operates in the desired wavelength range of 1.5 μm but it must be operated at cryogenic temperatures making it impractical for many test environments.[3]

Therefore there is a particular need for a compact, turn-key, room-temperature mode-locked source that is tunable throughout the 1.5 μm region.

Chromium-doped:YAG (Cr^{4+}:YAG) has become a particularly attractive option because of its broad tunability from 1.34 to 1.6 µm.[4] In this solid-state crystal, the tetravalent chromium ion (Cr^{4+}) serves as the lasing center. The use of Cr^{4+}:YAG as a lasing medium at room temperature was first demonstrated by Shestakov *et al.*.[5] The absorption band of Cr^{4+}:YAG is between 0.9 and 1.1 µm making a neodymium-doped:yttrium aluminum garnet (Nd:YAG) laser operating at 1.064 µm a convenient pump laser source.

One might ask the question, "Why do we need to develop a <u>tunable</u> solid-state mode-locked source around 1.5 µm when many <u>fixed</u> wavelength mode-locked sources are already available at 1.5 µm?". This is certainly a fair and pertinent question. The answer lies in our need to use the femtosecond pulses for time-resolved spectroscopy of devices with potentially wide ranging spectral characteristics. The saturable absorbers used to passively mode-lock the fiber laser in this work contain quantum well structures which have layer thickness' on the order of 100 Å. These saturable absorbers are fabricated by advanced growth techniques such as molecular beam epitaxy. The thickness and composition of the quantum wells must be tightly controlled to place the bandedge or heavy-hole exciton absorption resonance at a specific wavelength. However the desired thickness and composition are often found empirically, requiring multiple growth runs in the device development process. The use of a tunable laser source operating either in the continuous-wave (cw) or pulsed mode greatly aids in the device characterization and development process. The tunability of the laser allows specific properties of the device to analyzed at multiple wavelengths. Using this data the growth of the device could then be optimized so that it performs according to its design specifications. The use of a

tunable laser eliminates the need for expensive and time consuming multiple growth runs of the devices.

This chapter will describe the development of a mode-locked Cr^{4+}:YAG laser that is tunable from 1.488 to 1.53 µm with average output powers of 40 to 80 mW. Nearly transform limited pulses were generated over the entire tuning range with a minimum pulse width of 120 fs at 1.488 µm. The laser is mode-locked using a novel saturable absorber incorporated with a highly reflective distributed Bragg reflector. The pulses are shaped using the soliton mode-locking technique discussed in Chapter 3. This chapter will first begin with a discussion of the cw properties of the Cr^{4+}:YAG laser including its tuning range. The remainder of the chapter will discuss the mode-locked operation of the laser including the design of the saturable absorber mirror and the actual performance characteristics of the laser.

4.2   CONTINUOUS-WAVE OPERATION

The Brewster-angled cylindrical Cr^{4+}:YAG crystal used in our laser system was obtained from the IRE-POLUS Institute (Moscow, Russia). Figure 4.1 shows the emission spectra of the Cr^{4+}:YAG crystal taken at 7°C. This emission spectra was taken using a cw Quantronix116 Nd:YAG laser operating at 1.064 µm as the excitation source and a 0.275 meter ARC monchromater in conjunction with a germanium detector to collect the spectral data. The large spectral emission bandwidth of over 500 nm shows that the Cr^{4+}:YAG crystal can be used as a lasing medium with wide tunability extending throughout the 1.5 µm region.

Using this spectral emission data, we can determine the emission cross section, σ, of the Cr^{4+}:YAG crystal. The cross section is an important parameter that is directly proportional to the gain coefficient of the laser. First we assume

55
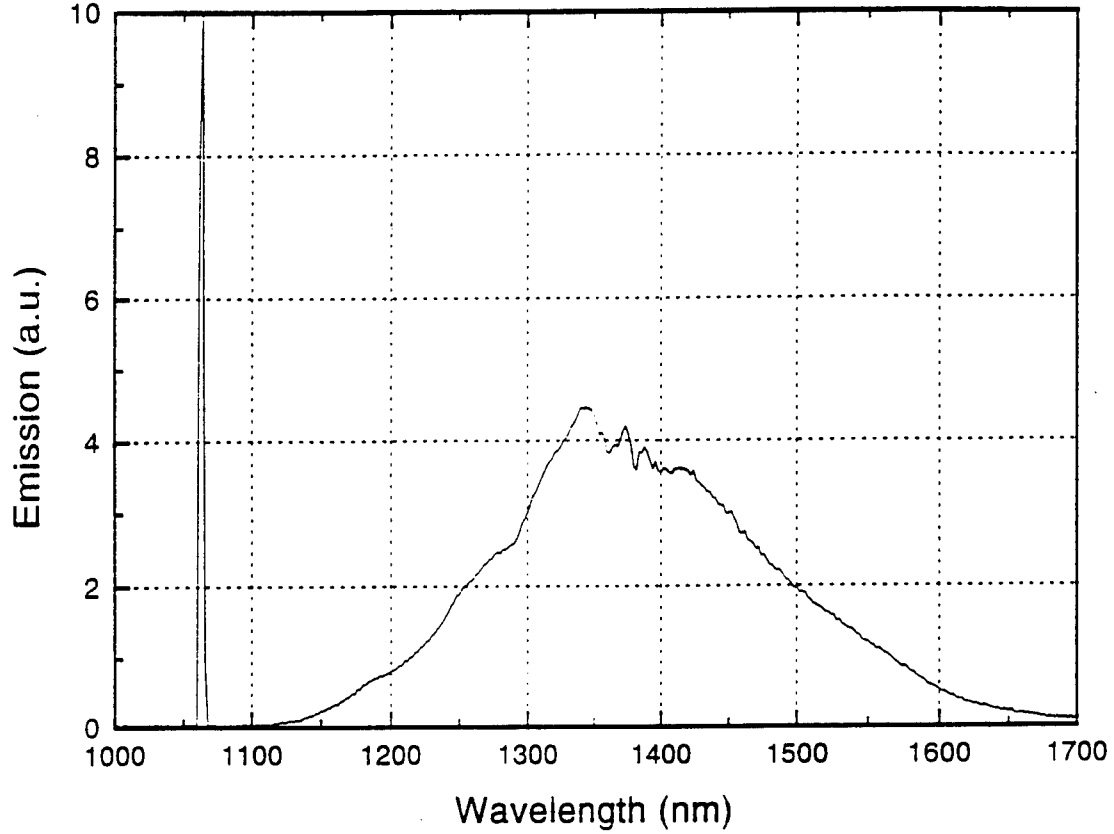
Figure 4.1 Emission spectrum of the Cr^{4+}:YAG crystal at 7°C pumped with 1.064 μm Nd:YAG laser. The sharp spike at 1.06 μm is due to the pump laser light.

that each Cr^{4+} atom of the gain medium has an area of σ. As photons pass through this cross section, they will interact with the atom either through stimulated emission or stimulated absorption. A larger cross section enhances a photon's chance of striking the cross section as it travels through the gain medium. The emission cross section is defined as

$$\sigma = \frac{\lambda^2}{8\pi n^2 \tau} g(\nu)$$
(4.1)

where λ is center emission wavelength, n is the refractive index, τ is the upper state lifetime, and g(v) is the lineshape function which is a probability density function that an atom will emit or absorb a photon at a frequency, v.[6] The value of the lineshape function at the center frequency, v_o, is given by

$$g(v_o) = \frac{2}{\pi \Delta v} \qquad (4.2)$$

where the frequency spread, Δv, is approximately 41 THz as determined from the emission spectrum of Cr^{4+}:YAG. The refractive index for YAG is 1.86 [6] and the upper state lifetime for Cr^{4+}:YAG is 48 μs [7]. Using this data, σ is calculated as 7.1 x 10^{-20} cm^2. For comparison, $\sigma = 3$ x 10^{-19} cm^2 for Ti:sapphire and $\sigma = 6$ x 10^{-21} cm^2 for erbium-doped silica.[8]

The cw Cr^{4+}:YAG laser system consists of a nearly symmetric X-fold cavity as shown in Figure 4.2. The cavity layout is very similar to that of a standard Ti:sapphire laser. The Cr^{4+}:YAG rod which is 5 mm in diameter and 20 mm long was wrapped in indium foil and clamped in a brass housing to provide efficient heat removal. Using a thermo-electric cooler under the brass housing, the temperature of the crystal was maintained at 15°C. The laser rod was placed slightly off center between two highly reflecting focusing mirrors (R > 99.9% from 1.35 to 1.550 μm) each of 10 cm radius of curvature. The angle of each focusing mirror was set to approximately 15° to compensate for the astigmatism introduced by the 20 mm Cr^{4+}:YAG rod. A plane wedged output coupler having 2% transmission was used. The overall cavity length is 1.58 m corresponding to an overall cavity repetition rate of 95 MHz. The laser was pumped by a cw Quantronix 416 Nd:YAG laser at 1.064 μm that is focused into the gain medium
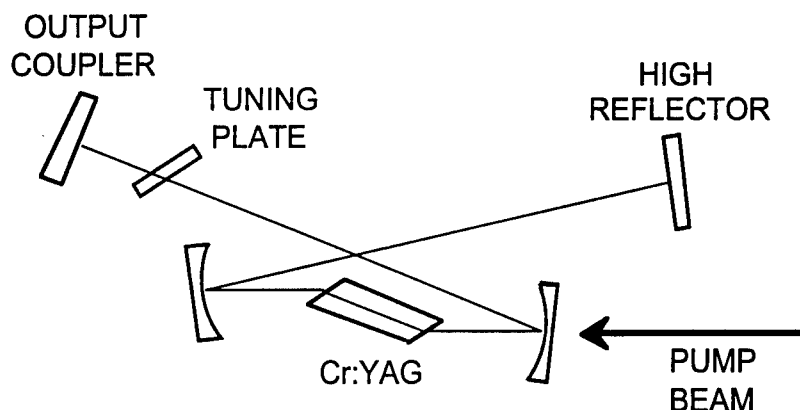
Figure 4.2   Schematic of continuous-wave Cr^{4+}:YAG laser X-cavity

by a 17.5 cm focal length, anti-reflection coated mode-matching lens. The lens
was chosen so as to maximize the overlap between the pump and lasing volumes
in the Cr^{4+}:YAG rod. Optimization of the mode-matching is critical in obtaining
the most efficient cw operation of the laser.

The initial lasing of the Cr^{4+}:YAG system was achieved by 'chopping' the
pump beam at a 50% duty cycle. The fluorescence signal was monitored at the
back of the output coupler by a Newport 818-IR germanium p-i-n detector
attached to an analog oscilloscope set to a long time scale. The focusing mirrors
and position of the crystal were then adjusted to maximize the fluorescence.
Upon optimization of the retro-reflected fluorescence beams from the output
coupler and high reflector,lasing was achieved. Once the lasing signal was
maximized, 'chopping' of the pump beam was no longer necessary and the optical
chopper was removed.

In cw operation approximately 600 mW of TEM_{00} power was obtained at
1.487 μm. Tuning of the cavity could be achieved using one of two different
intracavity elements. The first configuration is to place a fused silica prism

before the high reflector. Using the prism we were able to tune the laser from 1.446 to 1.536 μm. The second configuration used a 0.6 mm thick quartz birefringent tuning plate placed before the output coupler. The tuning plate allowed us to continuously tune from 1.450 to 1.574 μm as shown in Figure 4.3. Further optimization of the laser cavity at the longer wavelengths allowed the tuning range to extend to approximately 1.59 μm. The quartz tuning plate appears to be the tuning element of choice especially on the long wavelength side and easily covers the 1.55 μm transmission window of optical fiber.

4.3 PASSIVE MODE-LOCKING OF THE Cr^{4+}:YAG LASER

Generation of ultrashort optical pulses with the Cr^{4+}:YAG laser has been achieved by many research groups in variety of ways. These methods include active mode-locking using an acousto-optic modulator (AOM)[9], self-starting Kerr lens mode-locking (KLM)[10], and regenerative mode-locking whereby a feedback control circuit drives an AOM[11]. Initiation of mode-locking using an intra-cavity AOM is not easily achieved because the low gain of the Cr^{4+}:YAG rod renders the system intolerant to excess loss mechanisms. The self-starting KLM technique does not require an AOM and pulses as short as 43 fs have been generated.[10] This method of mode-locking solid-state lasers utilizes the intensity dependent refractive index of the lasing medium to modify the transverse beam parameters of the cavity resulting in intensity dependent gain modulation. The gain modulation is provided by either a soft aperture generated by the pump-beam defined gain profile in the lasing medium or an actual intracavity hard aperture. As a result, the KLM process is highly sensitive to cavity alignment and is easily perturbed by mechanical vibrations and pump power fluctuations. A more reliable process of mode-locking solid-state lasers
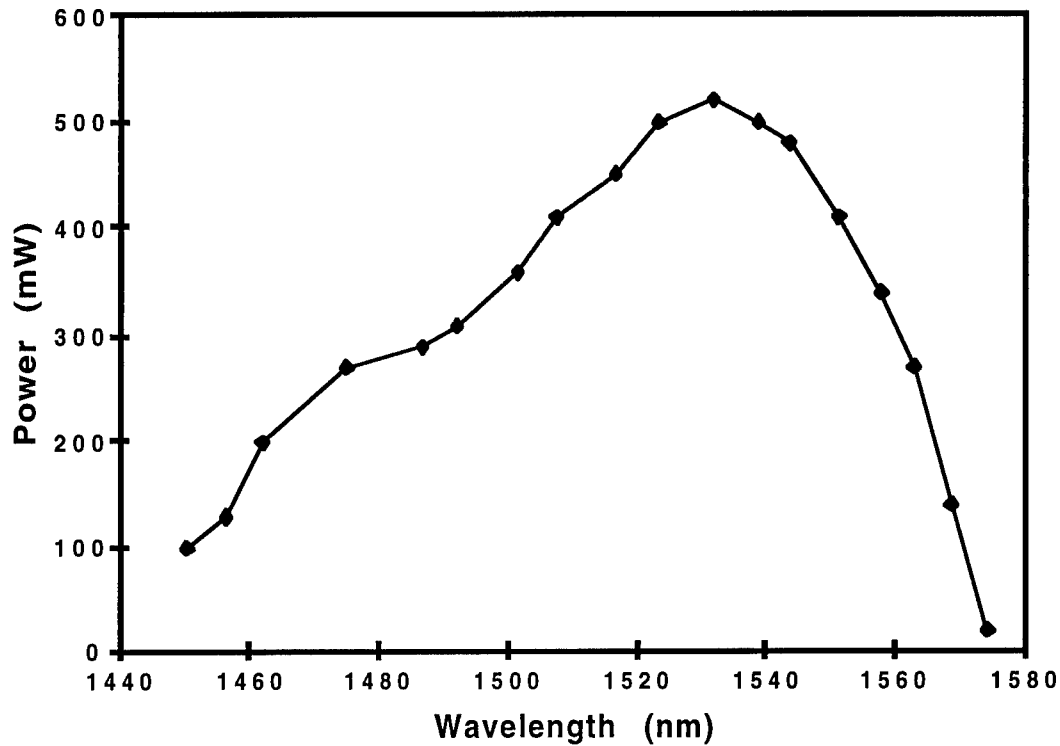
Figure 4.3 CW tuning range of the Cr^{4+}:YAG laser, using a single plate birefringent tuner.

has been recently demonstrated which relies upon the use of a saturable absorber to start and stabilize the soliton formation process.[12,13] This process was described in detail in Chapter 3. The saturable absorber eliminates the need for critical cavity alignment and renders mode-locked operation more tolerant to external perturbations.

Soliton mode-locking using a slow saturable absorber is dependent upon an intracavity balance of group velocity dispersion and the nonlinearity generated through self phase modulation. The nonlinearity in this laser is produced by the

intensity dependent index of refraction in the Cr^{4+}:YAG rod. The negative group velocity dispersion is controlled by the combination of two fused silica prisms placed within the cavity. The slow time constant of the saturable absorber, which is the result of interband trapping or recombination, provides a convenient starting mechanism for the soliton formation process. The pulse train is then stabilized by either this slow time constant or the fast time constant of the saturable absorber.[12] The fast time constant for typical semiconductor structures is on the order of 100 to 300 fs and is due to intraband scattering and thermalization processes. Soliton mode-locking using a slow saturable absorber allows very stable pulse trains to be generated whose pulse widths are much shorter than the temporal response of the absorber. This effect has certainly been exploited in our Cr^{4+}:YAG laser where pulse widths on the order of 100 fs are readily produced.

A schematic of the saturable absorber mirror (SAM) structure used to mode-lock the Cr^{4+}:YAG laser is shown in Figure 4.4. The SAM was grown by molecular beam epitaxy (MBE) on an undoped (100) GaAs substrate using a Varian Gen-II solid-source MBE system by Dr. Rich Leavitt of the Army Research Laboratory, Adelphi, MD. The SAM consists of a distributed Bragg reflector with 24.5 periods of 132.1 nm AlAs low index/ 113.3 nm GaAs high index quarter-wave layers. A 20 nm $Al_{0.48}In_{0.52}As$ buffer layer was grown on top of the partial Bragg stack. The saturable absorber region followed the buffer layer and is composed of the following double quantum well structure: 7 nm $Ga_{0.47}In_{0.53}As$ well / 8 nm $Al_{0.48}In_{0.52}As$ barrier / 7 nm $Ga_{0.47}In_{0.53}As$ well. The entire structure is capped by a 74.1 nm $Al_{0.48}In_{0.52}As$ layer. The total thickness of the buffer layer, the saturable absorber region and the cap layer were chosen so that a high index quarter-wave layer is formed, thus completing the Bragg
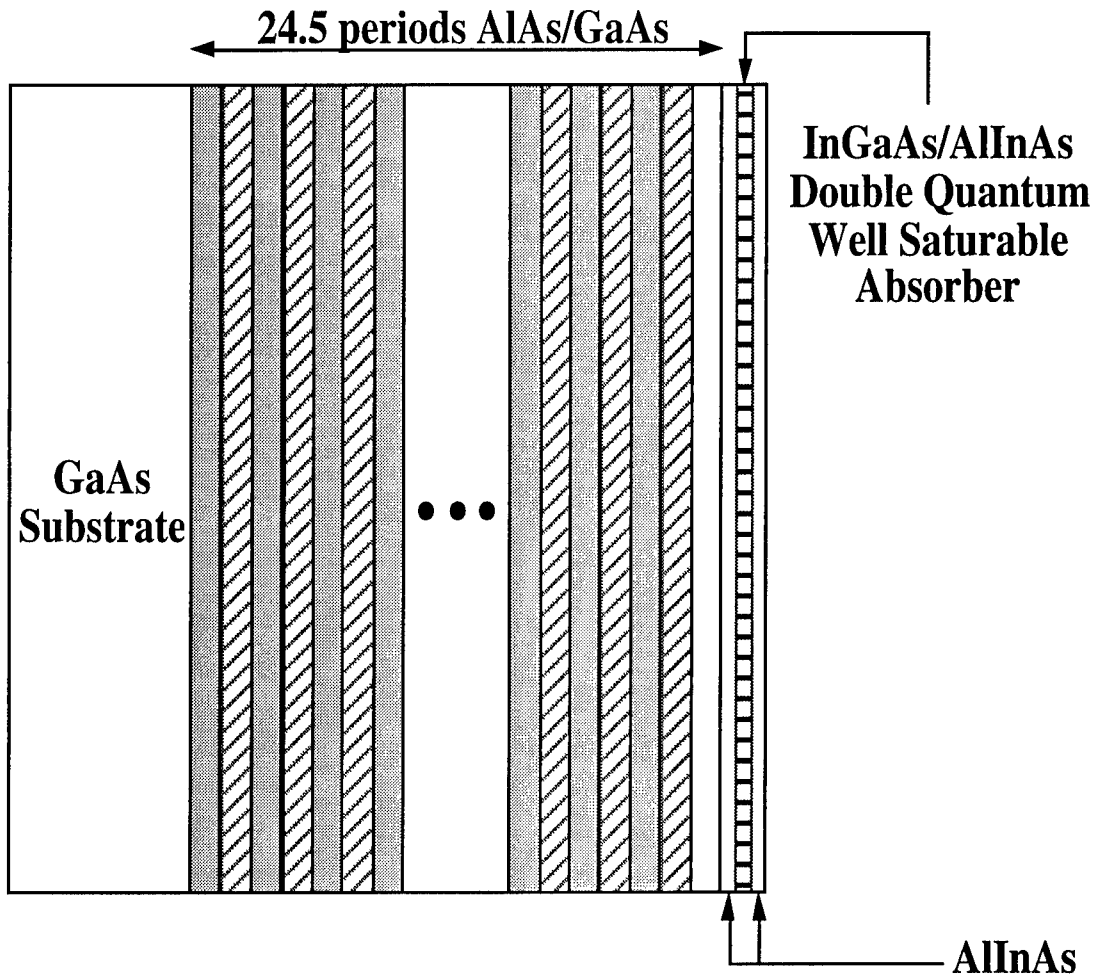
Figure 4.4   Schematic of the saturable absorber mirror structure

reflector. The width of the $Ga_{0.47}In_{0.53}As$ wells were chosen to place the bandedge,

i.e. the heavy hole exciton absorption resonance, at a wavelength of 1.50 μm.

Two quantum wells were used to increase the nonlinear reflectance of the SAM.

The quantum wells were placed near the peak of the electric field distribution in

the first layer of the reflector resulting in a low quantum well saturation

intensity. The measured reflectance spectrum of the SAM is shown in Figure 4.5.

The peak reflectance is 99.9% centered at a wavelength of 1.530 μm. The high

reflectance region of the SAM extends from 1.480 to 1.575 μm. It should be

Figure 4.5   Reflectance spectrum of the saturable absorber mirror

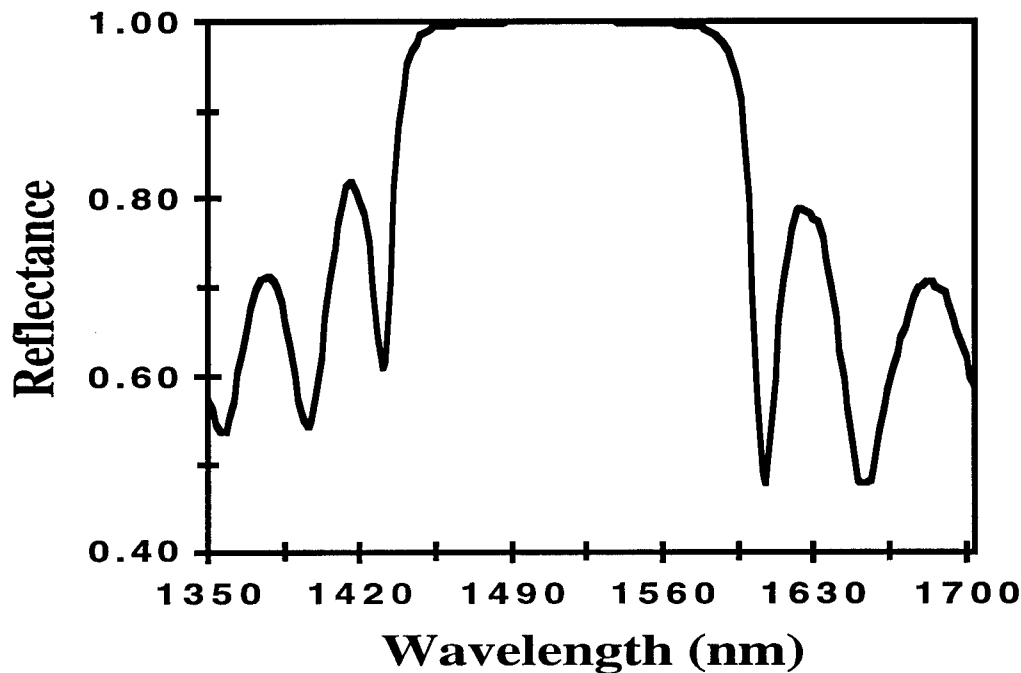noted that a considerable lattice-mismatch exists between the ternary quarter-wave layer (lattice constant, d=0.587 nm) and the remaining GaAs/AlAs layers (d=0.565 nm). X-ray diffraction measurements suggest that the strain at the ternary/binary interface is being partially accommodated by dislocations some of which are deep within the mirror structure as indicated by splitting of the diffracted orders resulting from the periodicity of the distributed Bragg reflector. Various attempts to characterize the linear optical properties of the intra-mirror quantum wells were made using room- and low-temperature photoluminescence spectroscopy and photo- and piezo-reflectance spectroscopy. Unfortunately, we were unable to obtain any quantitative information concerning the spectral position and shape of the actual quantum well bandedge. The lack of a well defined bandedge and excitonic features indicates there is some degradation

of the quality of the quantum well region of the ternary quarter-wave layer resulting in poor linear optical properties. However, the poor lattice structure may result in a faster recovery of the SAM nonlinear response and improve its performance at the high intracavity intensity levels and repetition rates typical of femtosecond solid-state laser systems.

The mode-locked cavity is shown in Figure 4.6 and is similar to the cw cavity discussed previously. The SAM was placed at the focus of a 10 cm ROC high reflector in the high reflector arm of the cavity. Two fused silica Brewster-cut prisms set at minimum deviation (295 mm tip-to-tip separation) were used in the output arm of the cavity to compensate excess positive group-velocity dispersion introduced by the crystal and mirror coatings. A plane-wedged 1% output coupler was used in this configuration. The overall cavity length remained approximately 1.58 m corresponding to a repetition rate of 95 MHz. Mode-matching between the Nd:YAG pump beam and the laser beam was achieved using a 17.5 cm focal length , AR coated lens.

Self-starting mode-locking was readily achieved upon alignment of the laser cavity containing the SAM. The pulse width, optical spectrum and pulse train were simultaneously monitored to ensure the presence of stable mode-locking. An Inrad 5-14B, non-collinear autocorrelator was used to determine the pulse width, and a calibrated spectrometer/InGaAs diode array was used in conjunction with an optical multichannel analyzer to monitor the mode-locked spectrum. The mode-locked pulse train was monitored using a high speed InGaAs detector. Without the dispersion compensating prisms and tuning plate in the cavity, pulse widths on the order of 1 ps centered at 1514 nm were observed. The tuning plate could not be used in conjunction with the SAM because it appears to limit the spectral bandwidth of the Cr^{4+}:YAG laser resulting in very
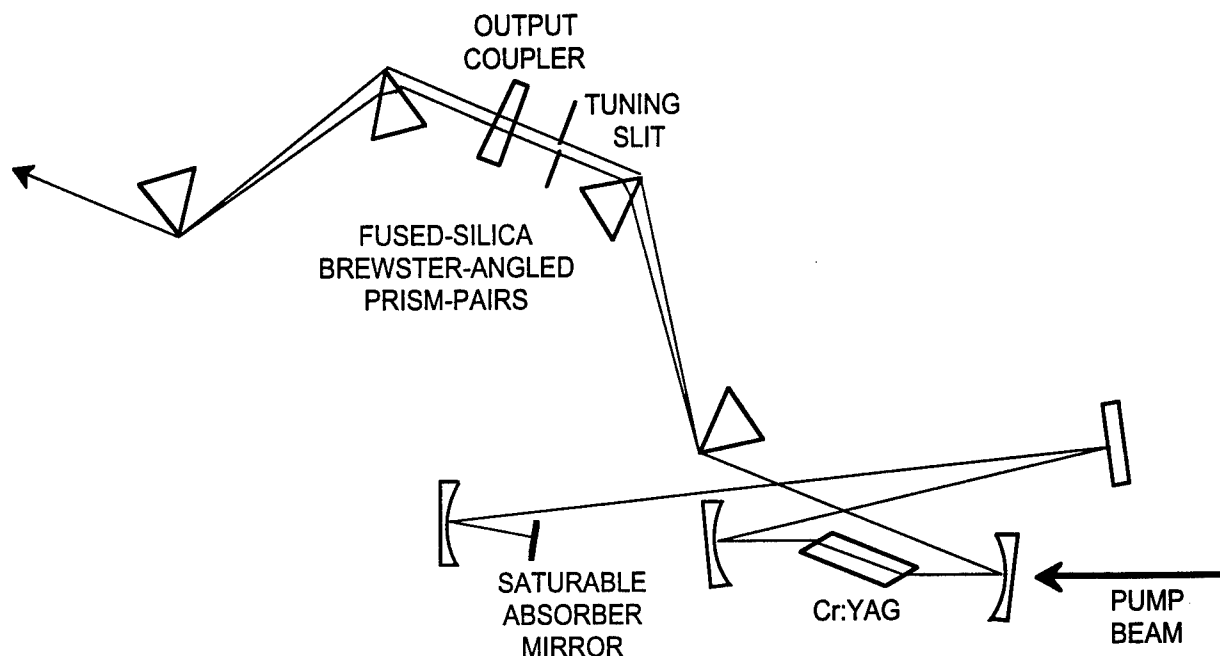
Figure 4.6   Schematic of the mode-locked Cr^{4+}:YAG laser X-cavity

unstable operation.   The insertion of the fused silica prisms provided the necessary dispersion compensation and femtosecond pulses were readily generated.   The absorbed pump power threshold for lasing and self-starting modelocking was 2.7 W.   The position of the SAM relative to the 10 cm ROC focusing mirror was optimized to produce a stable, single pulse per cavity round trip pulse train. Optimum stability was achieved when the average output power was between 40 and 80 mW corresponding to an absorbed pump power of approximately 3.0 W. It should be noted that mode-locking was stable over long periods of time and even remained mode-locked during fluctuations in the Nd:YAG pump power.   Pulse train instability and multi-pulsing were present when the average output power of the Cr^{4+}:YAG laser exceeded 90 mW.   Figure 4.7 shows a typical intensity autocorrelation and mode-locked spectrum at a

center wavelength of 1498 nm and an average output power of 45 mW. Assuming a sech^2 intensity profile, the FWHM pulse width was determined to be 122 fs. The corresponding FWHM spectral width was determined to be 20 nm. As discussed in Chapter 3, the measureable time-bandwidth product provides a 'completeness' of the mode-locking process and is 0.315 for a transform-limited hyperbolic secant squared pulse shape. The time-bandwidth product is 0.33 for this measured pulse, indicating that the pulses are nearly bandwidth limited.

By inserting a vertical slit into the cavity between the second prism and the output coupler we were able to widely tune the laser while maintaining femtosecond mode-locked operation. The laser was tunable between 1.488 and 1.535 μm. Figure 4.8 shows the FWHM pulse width and spectral width of the Cr^{4+}:YAG laser as a function of center wavelength. The wide tunability of the laser was readily achieved by careful optimization of the cavity (including pump lens position, folding mirror separation and separation between the focusing mirror and SAM) as it was tuned away from the free-running wavelength of 1.510 μm. The Nd:YAG pump power was also increased as required so that the optimal average output power of 40 to 80 mW was maintained. The time-bandwidth product varied from a high of 0.33 to a low of 0.28 indicating nearly transform limited pulses over the entire tuning range. It should be noted that stable mode-locking was achieved over the entire tuning range except at the very extreme wavelengths of both the short and long wavelength regions. At these wavelengths, mode-locking was achieved for only brief time intervals. The tuning range on the short-wavelength side is limited by the widely scattered vibrational and rotational H$_2$O absorption lines that are present from 1.2 to 1.7 μm.[14] These absorption lines limit the available spectral bandwidth that is required to support femtosecond pulses. There is a sharp increase in pulse width
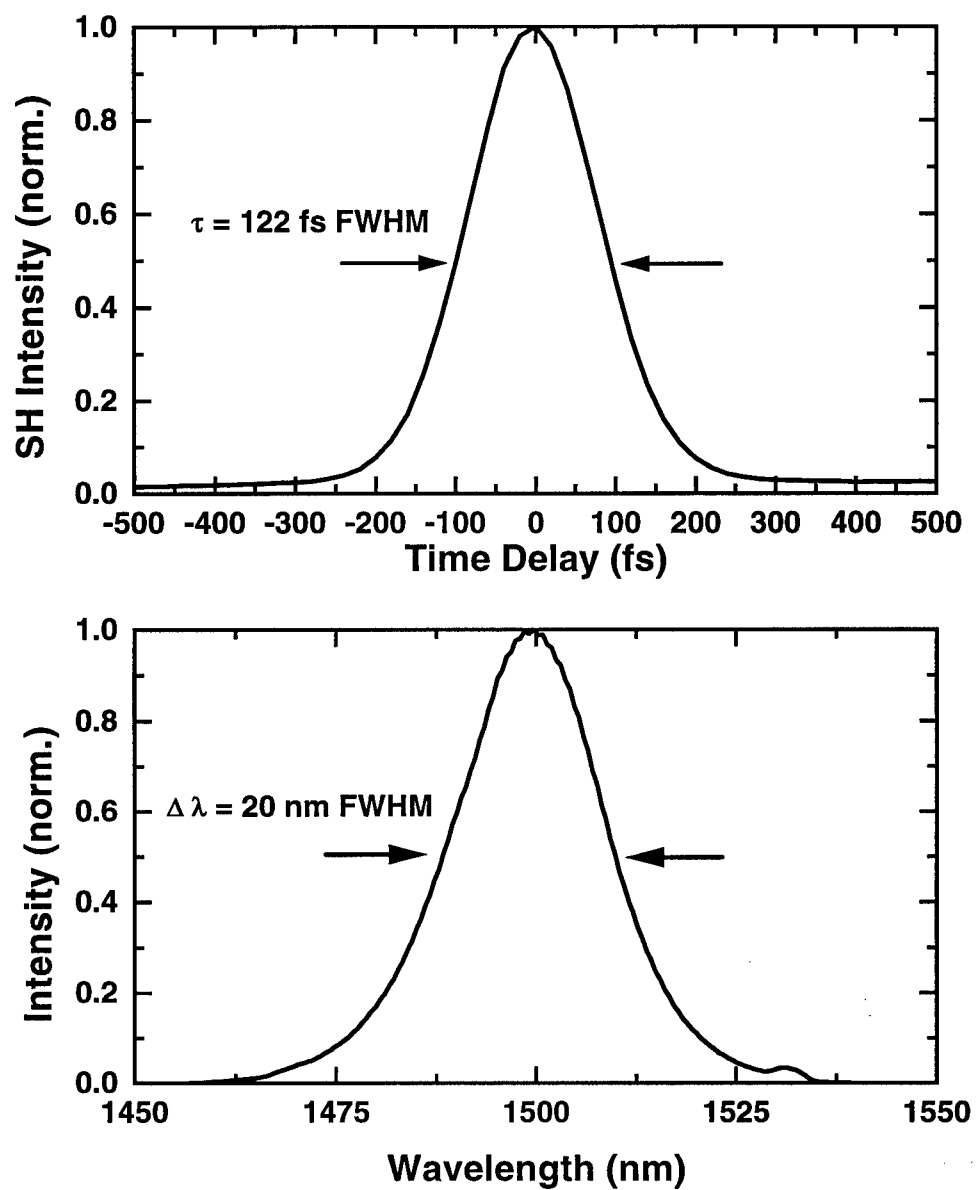
Figure 4.7   Intensity autocorrelation   and   mode-locked   optical   spectrum   of
            femtosecond pulse at a   center   wavelength   of   1498   nm   with   an
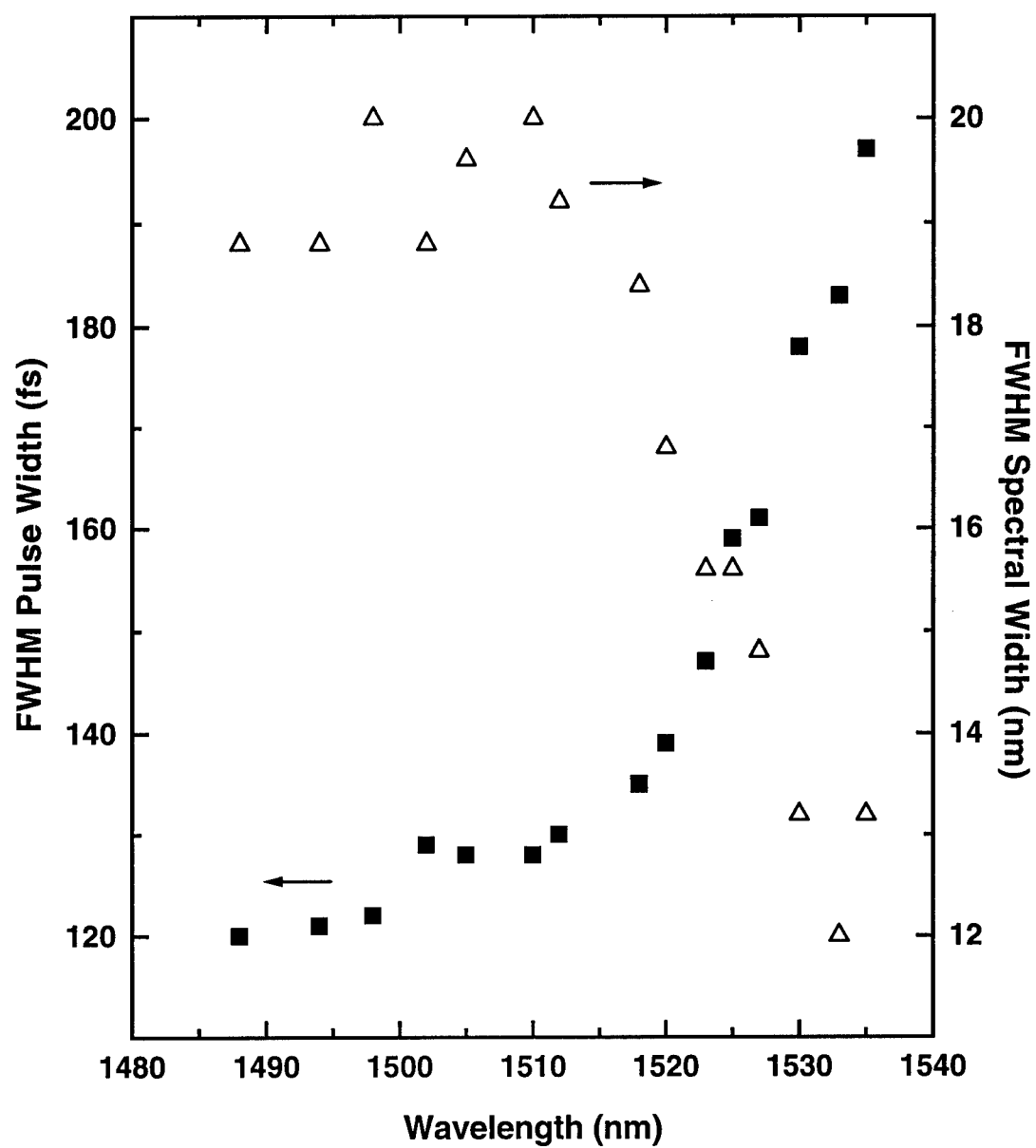   average output power of 45 mW

Figure 4.8 Femtosecond tuning curve of Cr^{4+}:YAG mode-locked laser

as the Cr^{4+}:YAG laser is tuned past 1.515 μm. The calculated round-trip group delay dispersion (GDD) of the laser cavity ranged from -1,700 fs^2 at 1.470 μm to -2,700 fs^2 at 1.550 μm.[15,16] The round-trip third order dispersion (TOD) was also calculated and estimated to be approximately +13,500 fs^3 throughout the tuning range of the laser. These values are in good agreement with previously reported results.[17] However, as shown by Brabec *et al.*, the pulse widths are such that the presence of TOD does not limit the formation of femtosecond pulses at these longer wavelengths.[18] Therefore another mechanism is responsible for the increase in pulse width. The efficiency of the saturable absorber 'falls off' at longer wavelengths as we tune past the heavy-hole excitonic absorption resonance of the quantum wells which is located at approximately 1.50 μm. Theimer *et al.*, have recently shown that a decrease in the efficiency of the saturable absorber will limit femtosecond pulse formation at these longer wavelengths.[19]

4.4 CONCLUSIONS

We have demonstrated both continuous wave and mode-locked operation of a solid-state Cr^{4+}:YAG laser. The cw laser was tunable from 1.450 to 1.574 μm with output powers exceeding 600 mW. The use of a saturable absorber mirror structure provides a very novel and efficient way to effectively mode-lock the Cr^{4+}:YAG laser. Tunable femtosecond pulses were generated from 1.488 to 1.535 μm. Average TEM_{00} output powers ranged from 40 to 80 mW. A minimum pulse width of 120 fs was measured at 1.488 μm. The femtosecond pulse train is highly stable and is not critically dependent upon cavity alignment. The use of the SAM should prove to be an attractive alternative to KLM techniques in terms of its ease of alignment and long term stability.

The development of the tunable, femtosecond Cr^{4+}:YAG laser has proven to be an extremely useful spectroscopic research tool. The following chapter will illustrate the use of the Cr^{4+}:YAG laser in a time-resolved pump/probe experiment. The narrow pulses widths allow us to analyze the dynamics of the carriers in the quantum wells used to mode-lock the erbium-doped fiber laser. The lifetimes of the carriers as determined by interband trapping and carrier recombination in the quantum wells will be shown to be the key component in determining the pulse widths produced by the fiber laser.

4.5 REFERENCES

1.   F. E. Krausz, M. E. Fermann, T. Brabec, P. F. Curley, M. Hofer, M. H. Ober, C. Spielmann, E. Wintner, and A. J. Schmidt, IEEE J. Quantum Electron. **QE-28**, 2097 (1992).

2.   W. Koechner, *Solid-State Laser Engineering*, 2d ed. (Springer-Verlag, Berlin, 1988).

3.   C. P. Yakymyshyn, J. F. Pinto, and C. R. Pollock, Opt. Lett. **14**, 621 (1989).

4.   N. B. Angeert, N. I. Borodin, V. M. Garmash, V. A. Zhitnyuk, A. G. Okhrimchuk, O. G. Siyuchenko, and A. V. Shestakov, Sov. J. Quantum Electron. **18**, 73 (1988).

5.   A. V. Shestakov, N. I. Borodin, V. A. Zhitnyuk, A. G. Ohrimtchyuk, and V. P. Gaponstev, in *Conference on Lasers and Electro-Optics*, Vol. 10 of 1991 OSA Technical Digest Series (Optical Society of America, Washington, D. C., 1991), paper CPDP11.

6.   J. T. Verdeyen, *Laser Electronics*, 2d ed. (Prentice Hall, Englewood Cliffs, N. J., 1989).

7.   G. M. Zverev and A. V. Shestakov, in *OSA Proceedings on Tunable Solid-State Lasers*, (Optical Society of America, Washington, D. C., 1989), **5**, p. 66.

8. B. E. A. Saleh and M. C. Teich, *Fundamentals of Photonics* (John Wiley & Sons, New York, 1991).

9. P. M. W. French, N. H. Rizvi, J. R. Taylor, and A. V. Shestakov, Opt. Lett. **18**, 39 (1993).

10. Y. P. Tong, P. M. W. French, J. R. Taylor, and J. O. Fujimoto, Opt. Commun. **136**, 235 (1997).

11. A. Sennaroglu, C. R. Pollock, and H. Nathel, Opt. Lett. **19,** 390 (1993).

12. D. Kopf, G. Zhang, R. Fluck, M. Mosser, and U. Keller, Opt. Lett. **21**, 486 (1996).

13. B. C. Collings, J. B. Stark, S. Tsuda, W. H. Knox, J. E. Cunningham. W. Y. Jan, R. Pathak and K. Bergman, Opt. Lett. **21,** 1171 (1996).

14. D. A. Gilmore, P. Vujkovic Cvijin, and G. H. Atkinson, Opt. Commun. **103**, 370 (1993).

15. R. L. Fork, O. E. Martinez, and J. P. Gordon, Opt. Lett. **9,** 150 (1984).

16. W. L. Bond, J. Appl. Phys. **36,** 1674 (1964).

17. Y. P. Tong, J. M. Sutherland, P. M. W. French, J. R. Taylor, A. V. Shestakov, and B. H. T. Chai, Opt. Lett. **21,** 644 (1996).

18. T. Brabec, Ch. Spielmann, and F. Krausz, Opt. Lett. **17,** 748 (1992).

19. J. Theimer, M. Hayduk , M. F. Krol, and J. W. Haus, "Mode-locked Cr^{4+}:YAG Laser: Model and Experiment", accepted for publication in Opt. Commun., 1997.

Chapter 5
Mode-locked Erbium-doped Fiber Laser and
Saturable Absorber Characterization

5.1 INTRODUCTION

Fabry-Perot (FP) laser cavities are the most common type of cavity configuration. The simple cavity consists of the gain medium placed between two highly reflecting mirrors. As discussed in Chapter 2, erbium-doped fiber lasers (EDFL's) configured in this manner provide a very compact and simple means of generating ultrashort optical pulses. The EDFL is mode-locked using a saturable absorber (SA) as the back end mirror of the cavity. It will be shown that the temporal pulse widths are controlled by the optical properties of the saturable absorbers.

This chapter will discuss the setup and characterization of an EDFL using a FP cavity configuration. Eight individual saturable absorbers were tested as the back mirror of the cavity, resulting in a wide range of generated temporal pulse widths. The second part of this chapter will discuss the optical characterization of these saturable absorbers. The linear absorbance and photoluminescence properties of each saturable absorber was examined. Finally, a pump/probe experiment will be described which allowed us to determine the carrier lifetimes in the quantum wells of the saturable absorbers. These carrier lifetimes are the key predictor in determining the pulse widths that the EDFL generates.

5.2 ERBIUM-DOPED FIBER LASER CONFIGURATION AND PERFORMANCE

The setup of the Fabry-Perot EDFL used in this work is shown in Figure 5.1. The gain medium consists of 22.5 m of erbium-doped fiber that is simply butt-coupled to the multiple quantum well (MQW) saturable absorber (SA) that serves as the high reflector at the back end of the cavity. The distance from the erbium-doped fiber to the SA is critical in achieving optimum mode-locked performance. This distance was controlled by placing the fiber in a Newport Ultra-align 561D XYZ stage. The other two adjustments on the stage allowed different positions on the SA to be examined. As will be discussed later in this chapter, the temporal pulse width was very dependent upon the lateral position of the fiber on the SA.

The other end of the erbium-doped fiber was fusion spliced to a fiber Bragg grating which served as the output coupler of the laser. The transmission spectrum of the fiber grating used in this laser is shown in Figure 5.2. The 49% peak reflectance of this grating is centered at 1556 nm with a FWHM spectral bandwidth of 1.0 nm. The grating was obtained from the Communications Research Center, Ottawa, Canada. It will be shown in Chapter 6 that the narrow line width of the fiber grating significantly limits the pulse widths generated by the laser.

The EDFL was pumped with a laser diode operating at 980 nm that was obtained from SDL Optics, Saanichton, British Columbia, CA (model number BFSWA0980SDL1180AB). The optical spectrum of the laser diode when driven at a drive current of 190 mA is shown in Figure 5.3. From this plot we see that the peak optical power is obtained at 975 nm. The current versus output optical power performance of the laser diode was also evaluated and is shown in Figure
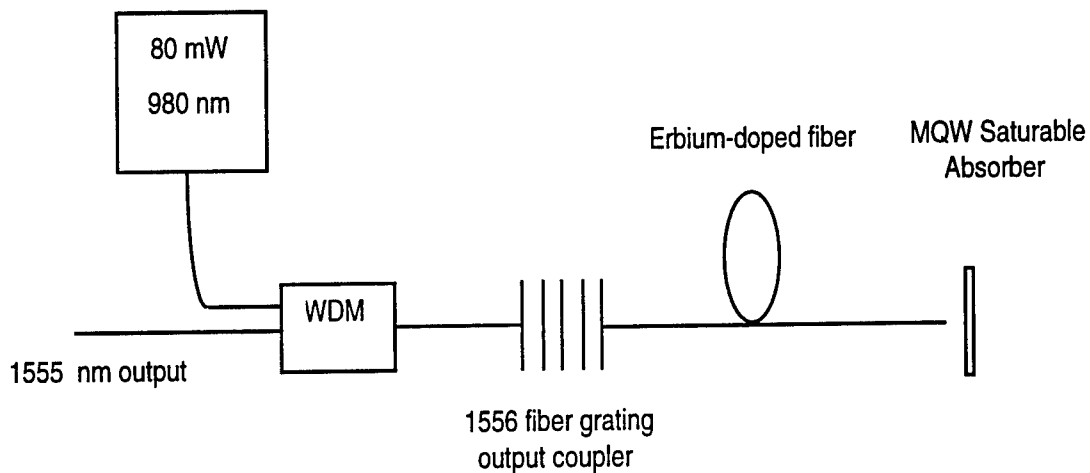
Figure 5.1   Schematic diagram of the passively mode-locked Fabry-Perot fiber laser
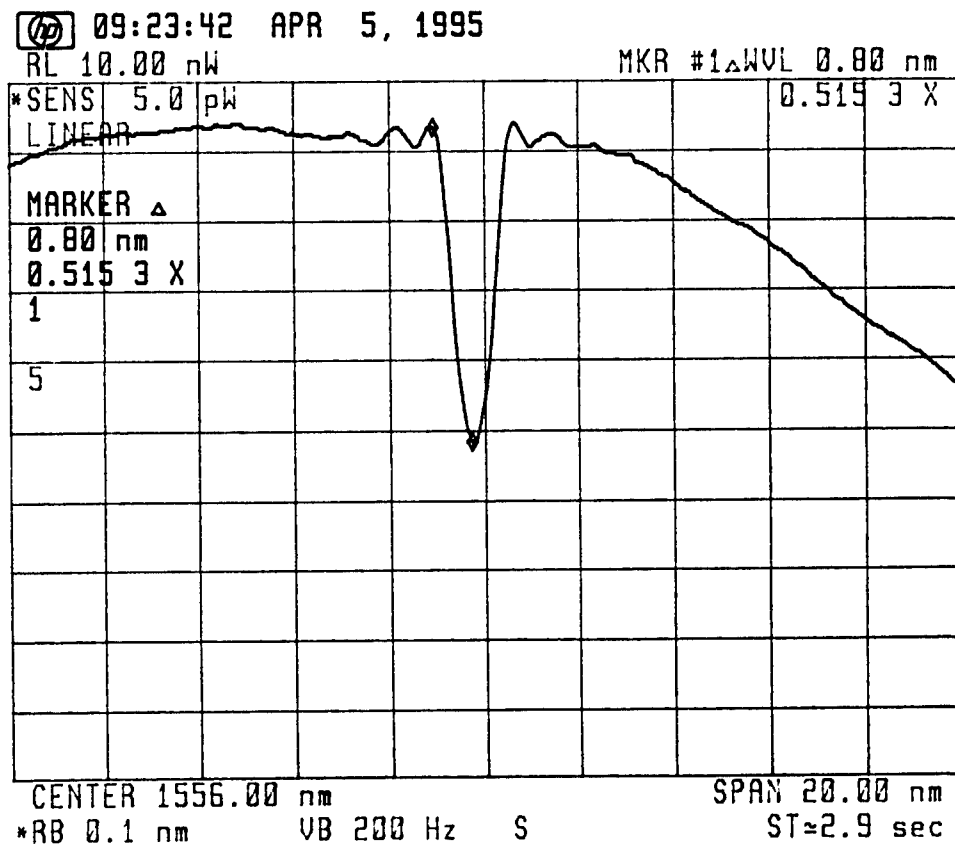

Figure 5.2   Transmission spectrum of the fiber grating centered at 1556 nm used in the EDFL

```
SPECTRUM                          97.02.27 11:49
        10dB/div                          AVR    1
   10
dBm
  -30
8.94



  -70
    0.95         μm        0.975              1
    RES 0.5nm         Wp 0.9753         5nm/div
```
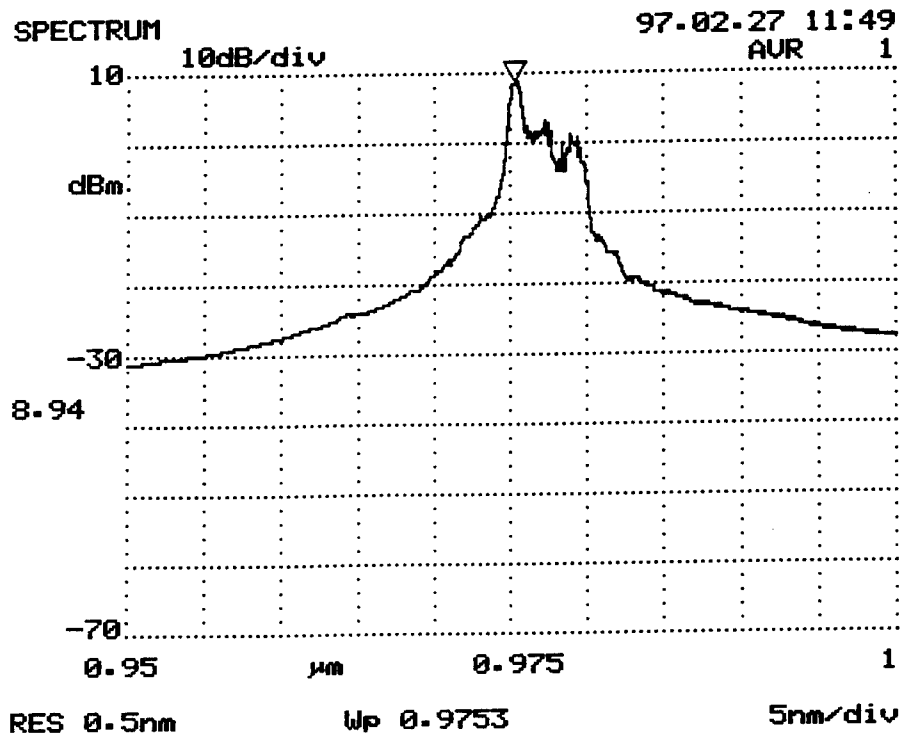
Figure 5.3   Optical spectrum of the laser diode pump laser

5.4. The peak optical power available is 80 mW at a drive current of 200 mA. The specified damage drive current occurs at 210 mA. It is important to note that this power was measured after transmission through the fiber grating just before it enters the erbium-doped fiber. This provides an accurate measure of the power available to pump the gain medium. The pump radiation was coupled into the erbium-doped fiber laser using a wavelength division multiplexor (WDM). The output of the EDFL from the fiber grating was taken through the other available port of the WDM. An isolator was placed after the WDM to eliminate the possibility of any stray reflections coupling back into the cavity and causing lasing instabilities. Finally, a standard FC/PC connector was fusion spliced after the isolator to allow convenient interchange of the EDFL between
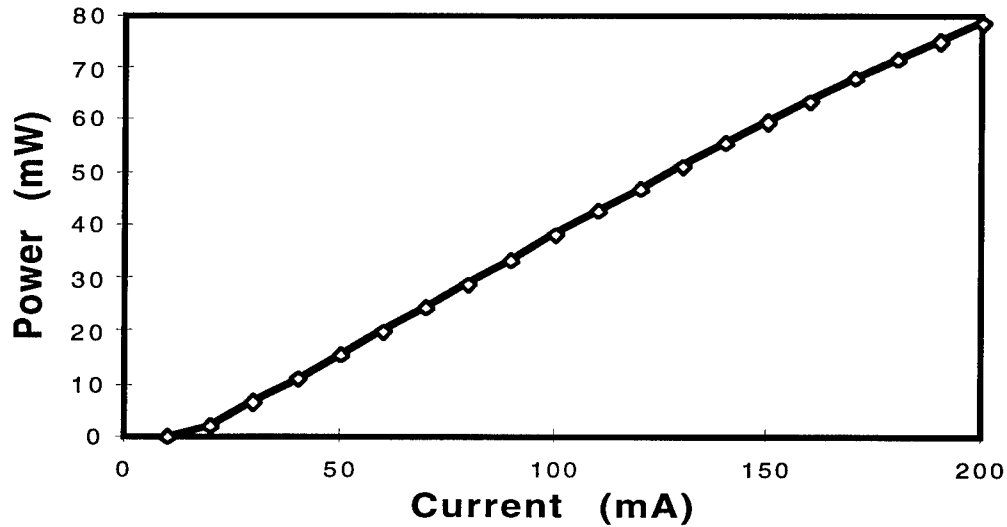
Figure 5.4 Optical output power versus pump current for laser diode used to pump EDFL

the various diagnostic instruments including the power meter, optical spectrum analyzer and autocorrelator.

The semiconductor saturable absorbers were used as both the mode-locking element and the back mirror in the laser cavity. The saturable absorber portion of the devices consisted of 50 periods of multiple quantum well layers grown on top of a semi-insulating InP substrate. The quantum well region in sample 1442 consisted of 100 Å $In_{0.53}Ga_{0.47}As$ wells and 100 Å InP barriers. The seven other samples had quantum well regions that consisted of 100 Å $In_{0.53}Ga_{0.47}As$ wells and 100 Å $In_{0.52}Al_{0.48}As$ barriers. The differences in these samples is the result of different growth temperatures and also post-growth processing such as ion implantation. These differences will be fully detailed in the next section of this chapter.

The mirror action of the device arose from Fresnel reflections at the front and back surfaces of the substrate. The erbium-doped fiber was typically separated from the SA by approximately 11 μm. The incident radiation was partially reflected off of the air/quantum well front interface and partially transmitted into the SA, where the transmitted light was partially absorbed by the quantum well region. The transmitted light was partially reflected by the back substrate/air interface, where it was again partially absorbed, on transit through the quantum well, and partially transmitted and partially reflected when it reached the front air/quantum well front interface. This process continues for an infinite number of round trips and it is best described by basic etalon theory.[1] The reflectance, R, of this etalon at normal incidence is given by

$$R = \frac{\left(\sqrt{R_1} - \sqrt{R_2}\ \exp{(-2\alpha L)}\right)^2 + 4\sqrt{R_1 R_2}\ \exp{(-2\alpha L)}\ \sin^2\frac{\delta_o}{2}}{\left(1 - \sqrt{R_1 R_2}\ \exp{(-2\alpha L)}\right)^2 + 4\sqrt{R_1 R_2}\ \exp{(-2\alpha L)}\ \sin^2\frac{\delta_o}{2}} \quad (5.1)$$

where R_1 is the air/quantum well interface reflectance, R_2 is the air/InP interface reflectance, α is the absorption coefficient of the quantum well region, L is the thickness of the quantum well region, and δ_o is the round-trip phase shift. The reflectance at an air/semiconductor interface at normal incidence is given by

$$R = \left(\frac{1-n}{1+n}\right)^2 \quad (5.2)$$

where n is the refractive index of the semiconductor. The round-trip phase shift is given by

$$\delta_o = \frac{4\pi n L}{\lambda}.$$

(5.3)

The index of refraction for $In_{0.52}Al_{0.48}As$ is n = 3.24 [2] and using Eq. 5.2 the reflectance at the air/$In_{0.52}Al_{0.48}As$ interface is calculated as R_1 = 0.28. Similarly, using n = 3.1 for InP [3], R_2 = 0.26. The absorbance value, αL = 0.5, was determined from linear absorbance measurements of the quantum wells that will be discussed in the next section of this chapter. The maximum reflectance of the saturable absorber using Eq. 5.1 is calculated as R = 0.41.

At a reflection peak, approximately 41% of the incident intensity reflects from the saturable absorber. However, we must now calculate how much of this intensity is actually coupled back into the erbium-doped fiber. A simple ray diagram in Figure 5.5 illustrates this coupling. The light exits the single mode erbium-doped fiber with a nearly Gaussian beam profile characterized by a mode-field diameter of approximately 10 μm. The beam diverges as it travels through both the air and the saturable absorber. The reflected beam continues to diverge before it reaches the erbium-doped fiber again. An overlap integral is used to calculate how much of the return radiation is coupled back into the fiber. Following the analysis of Marcuse, the power coupling coefficient, T, for the light coupled back into the fiber is given by

Erbium-doped fiber

Saturable Absorber
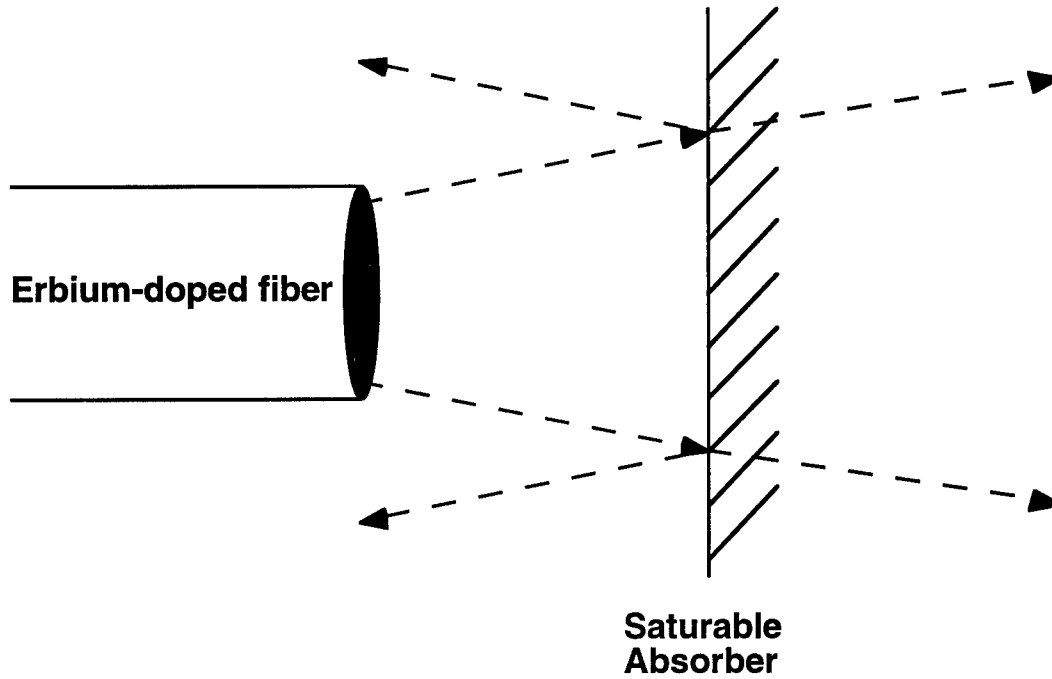
Figure 5.5 Ray diagram showing the coupling loss between the fiber and saturable absorber

$$T = \frac{4\left(4Z^2 + 1\right)}{\left(4Z^2 + 2\right)^2 + 4Z^2} \qquad (5.4)$$

where Z is the normalized fiber separation distance and is defined as

$$Z = \frac{D\lambda}{2\pi n w^2} \qquad (5.5)$$

where D is the separation from the fiber to the back of the saturable absorber and back to the fiber again, n is the index of refraction of the fiber and w is the mode-field radius of the Gaussian beam in the fiber.[4] Using the following

parameters: D = 1022 μm (using approximately 500 μm for the substrate thickness and 11 μm for the fiber/saturable absorber separation, each with a double pass), λ = 1.55 μm, n = 1.5, and w = 5 μm the power coupling coefficient was calculated as T = 0.022. We must also take into account the reflection off of the fiber facets at the air interface, which is also given by Eq. 5.2. This reflection loss is calculated as 4% and so the round-trip transmission is then given by $(1 - 0.04)^2$. The coupling efficiency, η, is then calculated as the product of the etalon reflectance, the fiber coupling coefficient, and the loss due to the fiber/air interface reflection. η is given by

$$\eta = TR(1 - .04)^2. \tag{5.6}$$

The coupling efficiency is approximately η = 0.01. Therefore, we see that the saturable absorber serves as a very low reflectivity mirror at the back of the cavity. Even with a reflectance of approximately 40%, only about 1% of the total energy makes it back to the fiber. Fortunately, the high gain of the erbium-doped fiber compensates for both the extremely high loss at the back of the cavity and the nearly 50% loss at the output coupler.

Eight different saturable absorbers were used as the mode-locking element in the EDFL cavity. Only the saturable absorbers were changed at the back end of the laser cavity. The rest of the laser cavity configuration remained the same. The laser was characterized for each saturable absorber to determine the minimum, maximum and average pulse widths that were generated. These results are summarized in the following table:

Table 5.1 Summary of the pulse widths generated using the different saturable absorbers

Sample	τ_{min} (ps)	τ_{max} (ps)	τ_{ave} (ps)
1305	11.1	19.3	14.2
1442	20.1	49.7	35.2
1590	28.6	52.7	38.8
1590 ii.	17.9	39.3	29.3
1629	26.2	45.5	34.3
1641	29.9	46.2	36.9
1643	20.8	30.0	25.5
1650	18.5	29.6	23.9

The values in Table 5.1 were recorded as the lateral position of the fiber along the saturable absorber was varied. There is much variation as the incident spot is moved on the saturable absorber. Changes in the pulse widths or movement from the pure cw mode-locking to the q-switched mode-locking regime were observed for movements as little as 10 μm. This is most likely attributable, at least in part, to changes in the carrier lifetimes as we change positions on the absorber. This will be discussed in further detail in the next section of this chapter as we analyze the carrier lifetimes of the saturable absorbers.

The output of the mode-locked laser was monitored using a photodetector (New Focus model 1414, 20 GHz) connected to an analog oscilloscope. As the incident spot was moved on the sample, changes in the mode-locking regime were readily observed. The pulse widths were recorded using an Inrad 5-14-LD non-collinear autocorrelator and the optical spectrum was recorded using an Anritsu

MS9001B1 optical spectrum analyzer. Finally, the average optical output power was measured using a Newport 835 - IR power meter.

A typical intensity autocorrelation and mode-locked spectrum centered at 1555 nm are shown in Figure 5.6. These traces were recorded using sample 1305 and correspond to an average output power of 2.2 mW. The repetition rate of the cavity was approximately 4.4 MHz. Assuming a hyperbolic secant pulse shape, the time-bandwidth product in this instance is 0.46 which deviates slightly from the transform limited value of 0.32. It should be noted that the output power of the laser was between 6.7 and 0.2 mW for all of the pulse widths recorded. The FC/PC connector that was used to connect the fiber laser to the various diagnostic instruments often became quite dirty and needed to be cleaned regularly or simply replaced. This resulted in the wide range of recorded output powers. It had been expected that the narrower pulse width recordings would result in higher output powers as a result of soliton pulse shaping within the erbium-doped fiber. Unfortunately, the lossy connector did not allow us to adequately examine this correlation due to the lossy connector.

This section has discussed the experimental fabrication and operation of a mode-locked Fabry-Perot EDFL. The performance characteristics of the laser were also presented including the pulse widths that were generated for each of the eight saturable absorbers. The next section will discuss the optical properties of the saturable absorbers that significantly influence the pulse widths.

5.3 OPTICAL CHARACTERIZATION OF THE MQW SATURABLE ABSORBERS

The previous section discussed the construction of the EDFL and the various pulse widths generated by the different saturable absorbers. The pulse
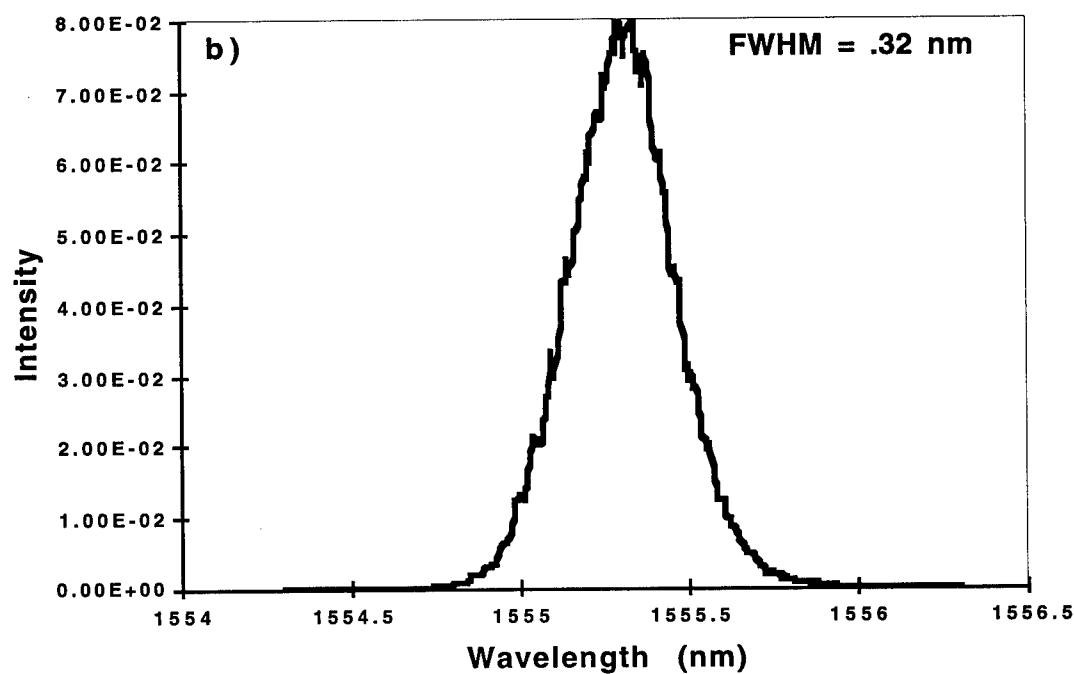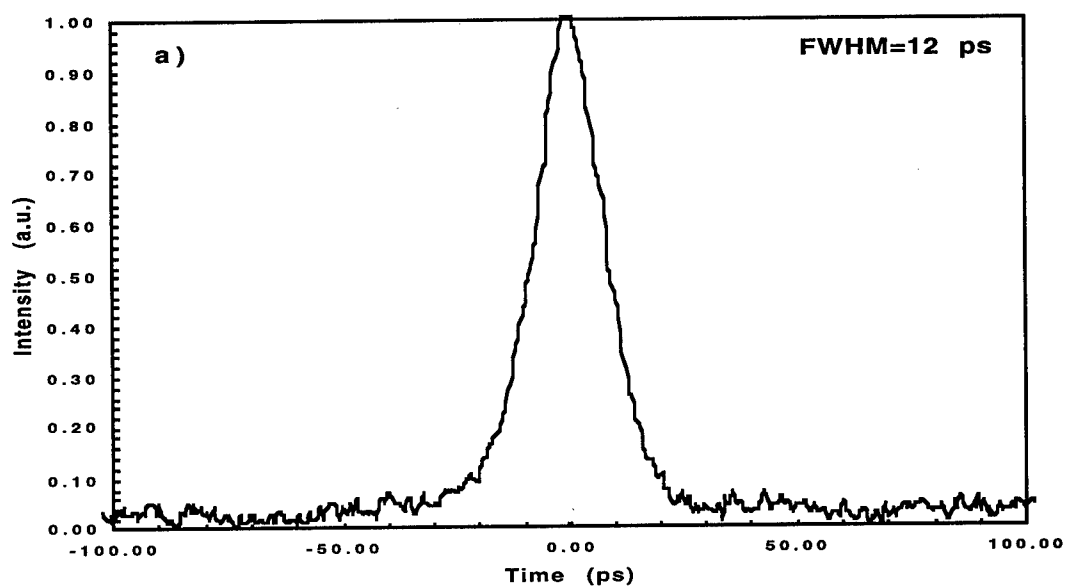
a)

FWHM=12 ps

b)

FWHM = .32 nm

Figure 5.6   a) Measured intensity autocorrelation and b) corresponding optical spectrum of the mode-locked pulses using sample 1305

widths are very dependent upon the saturable absorber used within the cavity. This section explores the optical properties of the saturable absorbers that contribute to the pulse formation in the EDFL. Specifically linear absorbance, time-integrated photoluminescence, and time-resolved pump/probe experiments were performed.

The quantum well region consisted of 50 periods of 100 Å $In_{0.53}Ga_{0.47}As$ wells and 100 Å $In_{0.52}Al_{0.48}As$ barriers for seven of the eight saturable absorbers. Sample 1442 consisted of 100 Å $In_{0.53}Ga_{0.47}As$ wells and 100 Å InP barriers. The total thickness of the absorbing region for all of the saturable absorbers was 1 μm. The quantum well region was grown directly on semi-insulating InP substrates. All of the samples used in this work were grown by Dr. Gary Wicks of The Institute of Optics at the University of Rochester, Rochester, NY.

Table 5.2 lists the growth temperatures of the saturable absorbers. Low-temperature (LT) growth of semiconductors introduces nonradiative recombination centers which effectively shortens the lifetimes of the carriers.[5,6] The recombination centers or traps lie within the bandgap of the semiconductor and capture both the electron and hole thereby destroying the electron-hole pair. This process is much faster than band to band recombination which is the result of an electron decaying from the conduction band to fill a hole in the valance band. Ion implantation is another method of shortening the carrier lifetimes in quantum wells and also introduces recombination centers.[7,8] It was hoped that the enhanced recovery times of the quantum wells would result in the generation of shorter temporal pulse widths. It should be noted that sample 1590 ii. is actually sample 1590 that was ion implanted with He^+. The ions were implanted at three different energies and doses to achieve uniform damage through the 1 μm quantum well region. The samples were implanted at: 40 keV

Table 5.2   MBE growth temperatures of the saturable absorbers

Sample	Growth Temperature (°C)
1305	490
1442	430
1590	405
1590 ii.	405
1629	300
1641	450
1643	425
1650	325

with 8×10^{14} cm^{-2} ions, 80 keV with 6×10^{13} cm^{-2} ions, and 140 keV with 1.5 x 10^{14} cm^{-2} ions. The samples were also annealed at 400 °C for 30 minutes. The ion implantation was performed by Dr. Paul Yu of the University of California at San Diego, La Jolla, CA.

The experimental setup used to measure the linear absorbance spectra is shown in Figure 5.7. A tungsten bulb was used as the white-light illumination source. The intensity of the light was controlled with a variable iris and an RG 850 filter was used to pass only the near-IR portion of the tungsten output. The incident light was focused onto the sample with a 50 mm focal length lens. The transmitted light was collected and collimated with a 50 mm focal length lens. Reflected light off of the surface of the sample passed back through a non-polarizing beam splitter onto a card placed a small distance away from the beam splitter. The focal position of the sample was then adjusted until the best image
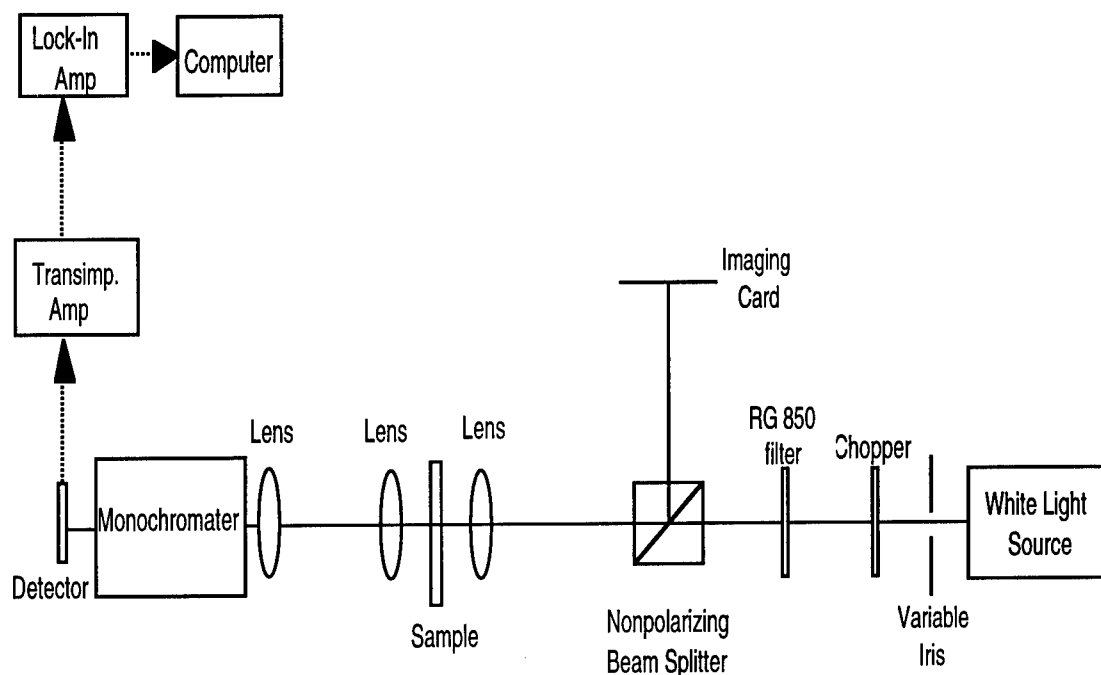
Figure 5.7 White-light linear absorbance experimental setup

was observed on the card. A 38 cm focal length lens focused the collimated light into an 0.275 meter triple grating spectrometer (ARC SpectraPro 275). A germanium detector (Newport 818-IR) collected the dispersed light. A transimpedance amplifier (UDT 101C) and lock-in amplifier (SRS 510) followed the detector. A computer program controlled the spectrometer and collected the lock-in transmission data.

The transmission measurements were performed using the following calibration procedure. First a baseline or sourcemeasurement was performed with no saturable absorber sample present. Next the transmission through the sample was recorded. The absorbance, αL, of the quantum wells is found from Beer's law and is given by

$$\alpha L = -\ln (I / I_o) \qquad\qquad (5.7)$$

where I is the transmission through the MQW sample and I_o is the source transmission. The absorption coefficient is found by simply dividing the absorbance by the total thickness L of quantum well region. The linear absorbance spectra of the eight saturable absorber samples, are plotted in Figure 5.8.

Sample 1590 exhibits room-temperature light- and heavy-hole excitonic features at 1560 and 1580 nm, respectively. The ion implantation of sample 1590 (1590 ii) destroyed its original excitonic features and also resulted in a decrease in the absorbance. The light- and heavy-hole excitonic features of sample 1442 and 1305 are much less resolved and indicate the presence of lattice defects or strain incorporated during the growth process. Sample 1629 shows a very broad bandedge with no excitonic features due to its very low-temperature growth at 300 °C. Very well resolved excitonic features are present in both 1641 and 1643. The growth temperature of 1650 at 325 °C is slightly above that of 1629 and now both heavy and light hole excitons are present. However these features are not as well resolved as those in 1641 and 1643, both of which had higher growth temperatures.

Room temperature time-integrated photoluminescence (PL) experiments were also performed to further analyze the linear optical properties of the saturable absorbers. Photoluminescence occurs when an electron which had been promoted to the conduction band by the absorption of a photon, spontaneously decays back to the valence band, emitting a photon. Specifically in a quantum well, the emitted photon's energy corresponds to the transition between the first allowed energy level in the valance band and the first allowed energy level in the
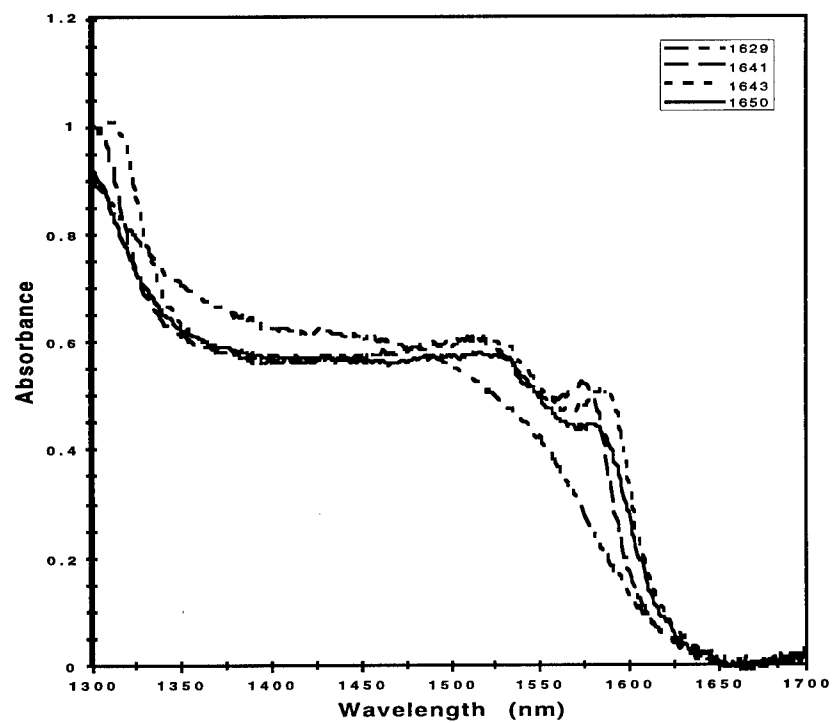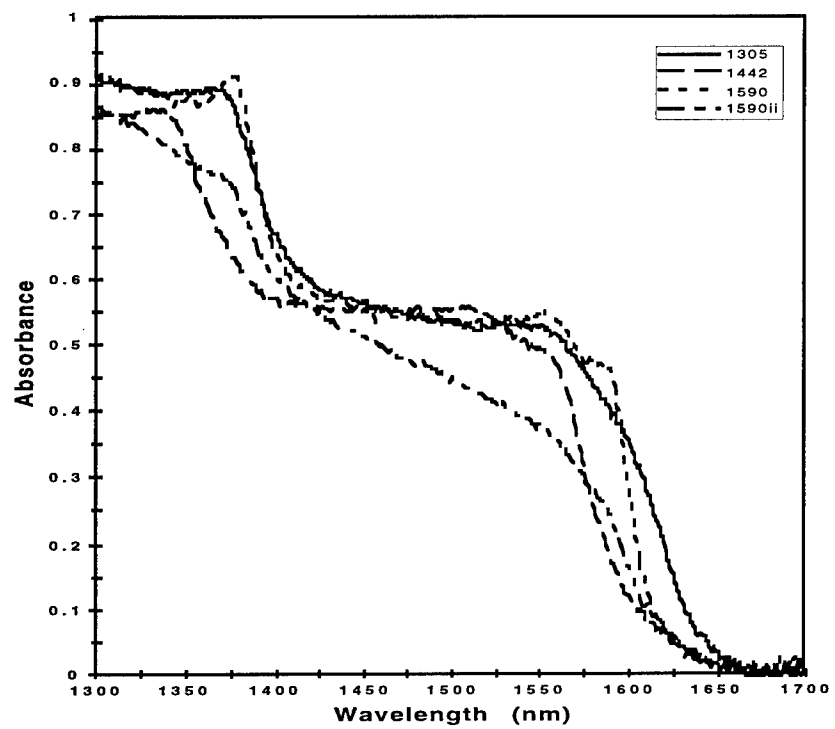
Figure 5.8   Linear absorbance spectra of the MQW saturable absorbers bandgap
of the semiconductor material.

conduction band. The energy used to create the electron-hole pair is usually well above the bandgap of the semiconductor. The electron then decays to the lower energy levels of the conduction band through very fast nonradiative transitions before spontaneously emitting a photon of energy equal to the bandgap as it decays back to the valence band.

The photoluminescence experimental setup is shown in Figure 5.9. The experimental setup is the same as for the linear absorption measurements except that an argon-ion laser (Ion Laser Technology model 5401) producing 68 mW at 515 nm was used as the pump source. The PL results for the eight saturable absorbers are shown in Figure 5.10. The intensity of the PL signal is directly proportional to the carrier lifetime in the sample. The saturable absorber with the highest PL intensity therefore is expected to have the longest lifetimes and correspondingly the saturable absorber with the lowest PL intensity is expected to have the shortest lifetimes. The PL measurements were performed under the exact same experimental conditions which allow us to compare the lifetimes of the saturable absorbers.

Sample 1590 has the largest photoluminescence signal and its peak is centered at 1585 nm. The large signal is most likely the result of the well grown material and is directly correlated with the excitonic features observed in the absorbance measurements. The next largest signal was obtained from sample 1442. The PL peak is centered at approximately 1575 nm. Samples 1641 and 1643 have nearly identical PL intensities and their peaks are centered at approximately 1575 nm. The PL intensity of 1305 is an order of magnitude less than that of 1590. It is therefore expected that the lifetime of 1305 is about ten times less than that of 1590. Samples 1650 and 1629 were grown at very low temperatures and exhibit very small PL intensities due to the added presence of
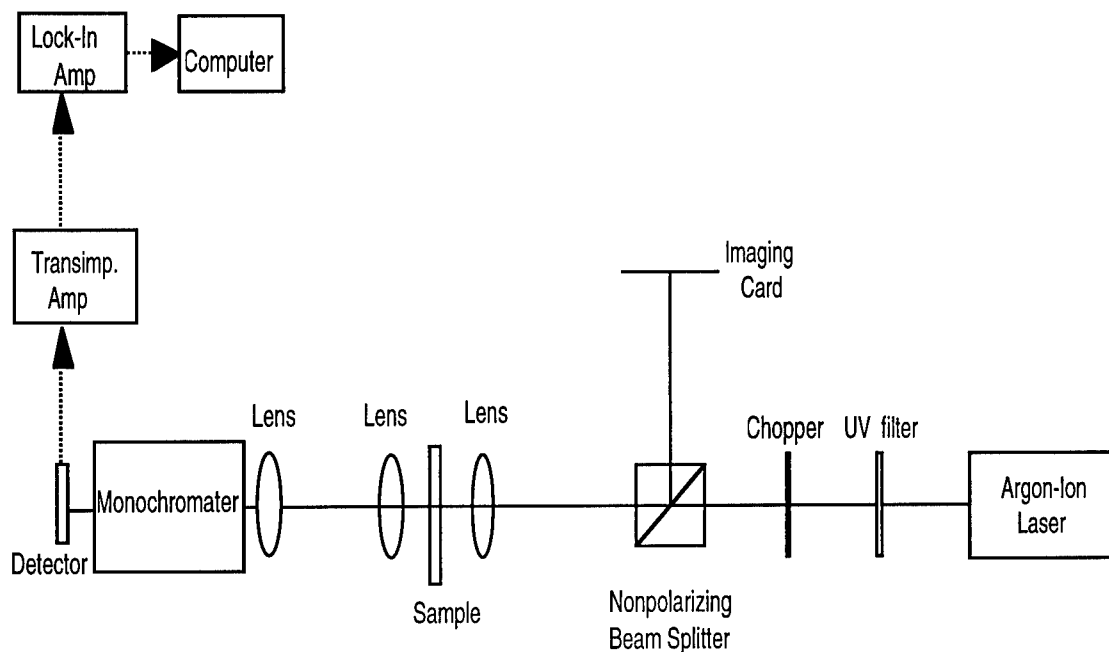
Figure 5.9   Photoluminescence experimental setup

the recombination centers. Finally, it should be noted that a PL signal could not be obtained from the ion implanted sample, 1590 ii. The damage centers caused by the ion implantation severely limits the radiative recombination in the quantum wells of this saturable absorber.

The last section of this chapter will discuss the direct measurement of the carrier lifetimes in the quantum wells of the saturable absorbers. The carrier dynamics were examined using standard pump/probe spectroscopic techniques.[9,10] In this type of experiment, electron-hole pairs are first created by the absorption of an intense pump pulse. The corresponding transmission change is then monitored in time by a weaker probe pulse which is temporally delayed with respect to the pump pulse. The resulting transmission change taken at different points in time allows us to temporally monitor the carrier lifetimes in
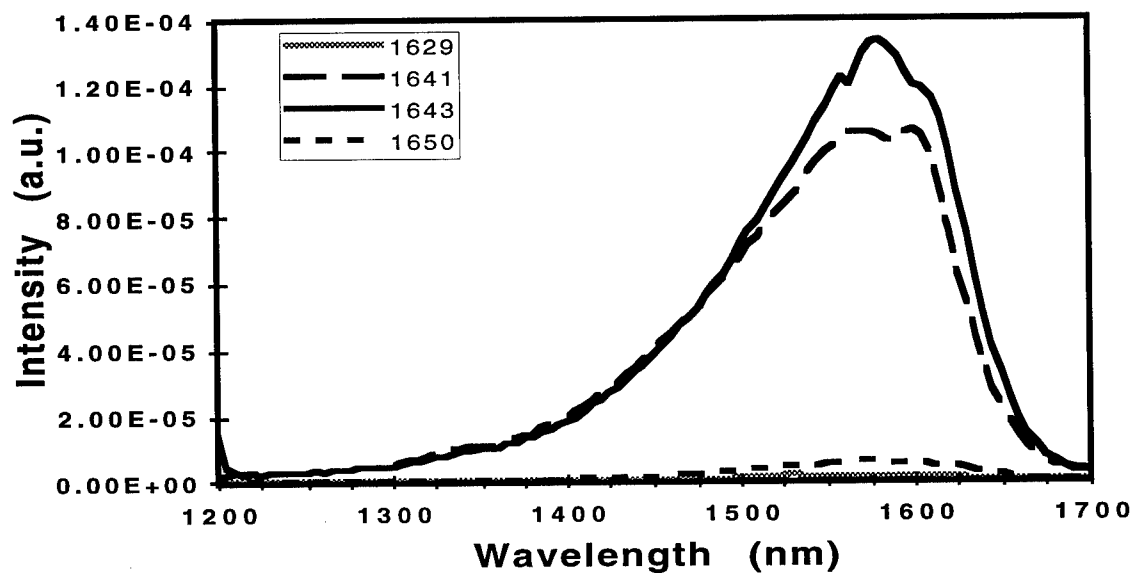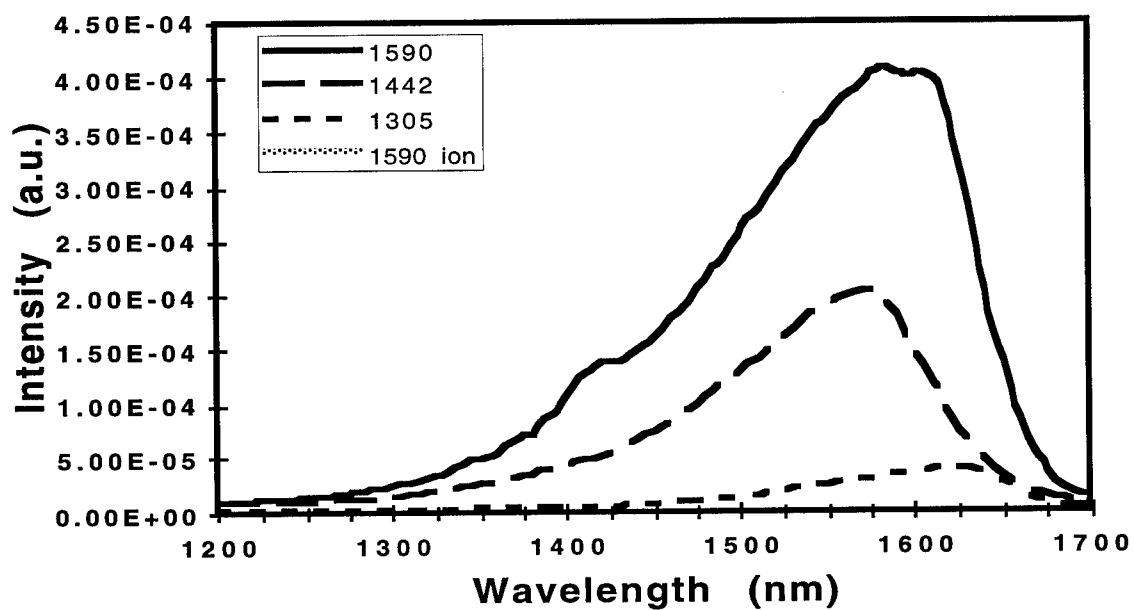
Figure 5.10 Photoluminescence spectra of the MQW saturable absorbers

the quantum wells.

The absorption coefficient, α, of the quantum wells in the saturable absorber after excitation is given as a function of the probe delay, t, by

$$\alpha(t) = \alpha_o + \Delta\alpha e^{-\frac{t}{\tau}} \qquad (5.8)$$

where α_o is the linear absorption coefficient, $\Delta\alpha$ is the change in absorption induced by the pump pulse, and τ is carrier recombination time. The recombination time of the absorption recovery in Eq. 5.8 is related to the transmission data by

$$S(t) = A \int_{-\infty}^{\infty} I(t' - t)e^{\alpha(t')d}dt' \qquad (5.9)$$

where S(t) is the energy of the transmitted probe versus delay, A is the area of the probe beam, I is the intensity of the transmitted signal and d is the thickness of the quantum well region of the saturable absorber. Using the energy density, $W = \int Idt$, of the probe beam, Eq. 5.9 can be rewritten as

$$S(t) \approx AWe^{\alpha(t)d} \approx AW[1 + \alpha(t)d] \qquad (5.10)$$

where the assumption that the temporal change in the absorption coefficient is small compared to the pulse duration has been made. Finally, substituting Eq. 5.8 into Eq. 5.10 gives

$$S(t) = AW \left[1 + \alpha_o d + \Delta \alpha d e^{-\frac{t}{\tau}} \right] \approx S' + AW \, \Delta \alpha d e^{-\frac{t}{\tau}} \qquad (5.11)$$

where S' is the probe transmission before the arrival of the pump pulse. Therefore, we see that the exponential decay time of the change in the probe transmission gives a direct measurement of the carrier recombination time.

The degenerate, co-linear, pump/probe experimental setup used to measure the carrier dynamics in the quantum wells is shown in Figure 5.11. The Cr^{4+}:YAG laser discussed in Chapter 4 was used as the pulsed source in this experiment. The pump and probe beams were separated into orthogonal polarizations by a 50/50 polarizing beam splitter. The probe beam was delayed with respect to the pump beam using a linear stage (Klinger UT 100.100 PP) controlled with a stepper motor (Klinger CC1). The stage provided up to 10 cm of travel. The beams were then recombined co-linearly using a nonpolarizing beam splitter and focused onto the sample using a 10X microscope objective. The transmitted light was re-collimated with a 10X microscope objective. The spot size on the sample was calculated to be approximately 16 μm. A Glan-Thompson polarizer was then used to reject the pump beam ensuring that only the transmitted probe beam reached the detector. The probe beam was focused onto a Ge detector (Newport 818-IR) using a 5 cm focal length lens. The detector was connected to a transimpedance amplifier (UDT 101C) and then to a lock-in amplifier (SRS 510). The data was then collected by a computer which also controlled the movement of the linear stage. An optical chopper provided the reference signal to the lock-in amplifier and cut both the pump and probe beams
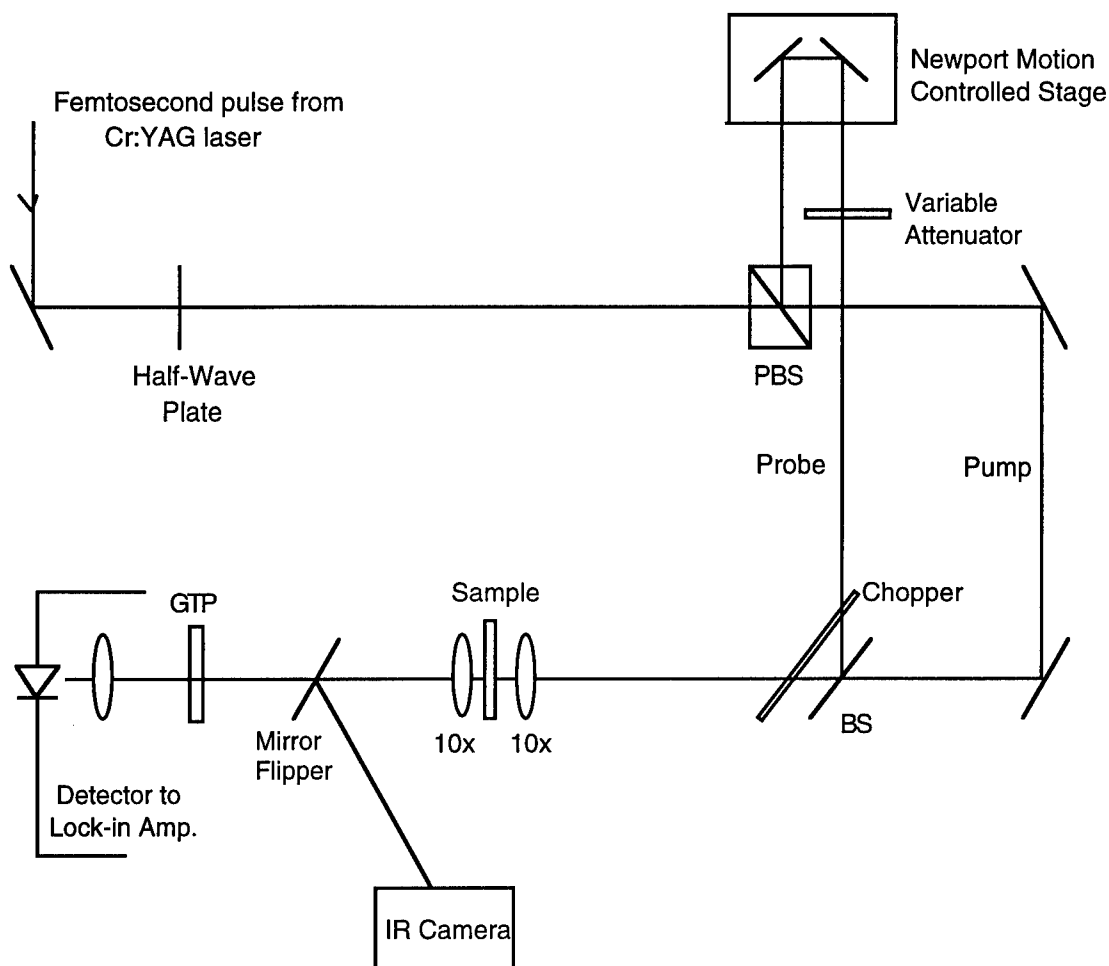
Figure 5.11 The experimental setup for pump/probe measurements using Cr^{4+}:YAG laser

but at different frequencies. This allowed a differential lock-in technique to be used so that only the pump induced change in the probe transmission was detected.

The pump and probe beams must be temporally and spatially overlapped at the sample. Initial spatial alignment was achieved using a IR camera placed at the far end of the experiment with the objectives, sample, polarizer, and detector removed. The position of the pump beam was then adjusted to maximize the

overlap with the probe beam. The linear stage was also scanned over its entire range to ensure that the probe beam did not walk off of the pump beam. Careful and even tightening of the clamps holding the linear stage was needed to prevent unnecessary tension on the stage and subsequent walking of the beam. Final spatial alignment was accomplished using a 50 μm pinhole placed at the focus of the 10X microscope objective. First the pinhole was adjusted to maximize only the probe transmission. The pump beam was then adjusted to maximize its transmission through the pinhole.

The temporal overlap of the pump and probe beams at zero-delay was initially achieved using a fast InGaAs p-i-n detector (Antel D28) in conjunction with a digital sampling oscilloscope. The position of both beams was displayed on the screen and the position of the probe beam was adjusted using the delay line provided by the linear stage. The detector limited the temporal overlap resolution to approximately 50 ps. Interferometric techniques were then used to achieve finer resolution. First a half-wave plate was placed in the pump arm and rotated so that the polarizations of both arms were the same. A Ge detector was then connected to an analog oscilloscope. Interference fringes occur when there is temporal overlap between the two beams. The fringes were observed on the oscilloscope as variations in the dc level with the peak signal corresponding to zero delay between the two signals. The linear stage was slowly scanned to find this peak signal.

The spatial position of the output of the Cr^{4+}:YAG laser was observed to vary in time. It was determined that this variation was caused by pointing variations of the Nd:YAG pump laser. This movement greatly affects the alignment of the pump/probe system. To avoid constant re-alignment of the pump/probe system, the output of the Cr^{4+}:YAG laser was coupled into a very

short, 40 cm piece of dispersion shifted optical fiber. The output of the fiber was collimated and sent to the pump/probe system. The autocorrelation and spectrum of the pulse after propagation through the fiber were analyzed and it was determined that this short piece of fiber did not detectably affect the polarization or temporal properties of the pulse. The pulse width was 110 fs with a corresponding spectral bandwidth of 24 nm centered at 1507 nm. The pulse was nearly transform limited with a time-bandwidth product of 0.35. As the Cr^{4+}:YAG laser moves in time, only the coupling of the laser into the fiber needs to be adjusted. The alignment of the pump/probe remains unchanged.

The ratio of the pump to probe beams was controlled using a variable neutral density filter in the probe arm of the system and a half-wave plate before the polarizing beam splitter. The ratio was set at either 100:1 or 50:1 depending upon the particular sample under test. In both situations the power of the probe beam was small enough so as to not introduce any nonlinear absorption effects. The average pump power varied between 8 and 9 mW depending upon the coupling into the dispersion shifted fiber. Care was taken to ensure that the pump power remained constant during the course of the actual experiment.

Table 5.3 summarizes the results of the pump/probe experiments for all eight of the multiple quantum well saturable absorbers. The average lifetime of each sample is recorded along with its minimum and maximum values. The lifetime of the carriers was once again found to be a function of position on the saturable absorber. A minimum of five different positions on each saturable absorber was examined. Figure 5.12 shows the differential transmission for samples 1629 and 1641. Sample 1629 at this measured spot recovers with an exponential time constant of 42 ps. This very fast recovery is consistent with its low-temperature growth of 300 °C. Sample 1641 is shown to have a slower

Table 5.3   Summary of the measured carrier lifetime dynamics in the different saturable absorbers

Sample	τ_{min} (ps)	τ_{max} (ps)	τ_{ave} (ps)
1305	239	325	271
1442	---	---	885
1590	---	---	1757
1590 ii.	199	352	277
1629	37	44	40
1641	611	1200	799
1643	455	634	533
1650	102	113	109

measured recovery of 622 ps which corresponds to its high growth temperature of 450 °C. It should be noted that the ion implanted sample, 1590 ii, has a double exponential decay with a fast initial average recovery of 39 ps and a slower second component with an average recovery 277 ps.   The slower decay component is important in the soliton pulse shaping used by the fiber laser.   The ion implantation of sample 1590 therefore resulted in approximately a factor of 10 reduction in the carrier lifetime.

Samples 1590 and 1442 were found to have very long exponential decay times which were much longer than the 400 ps time scale of the pump/probe experiment. It was therefore very difficult to curve fit these traces and we could not obtain verifiable pump/probe experimental data. The lifetimes of these two saturable absorbers were determined using a linear correlation between the PL peak intensities discussed previously and the lifetimes of the remaining samples as
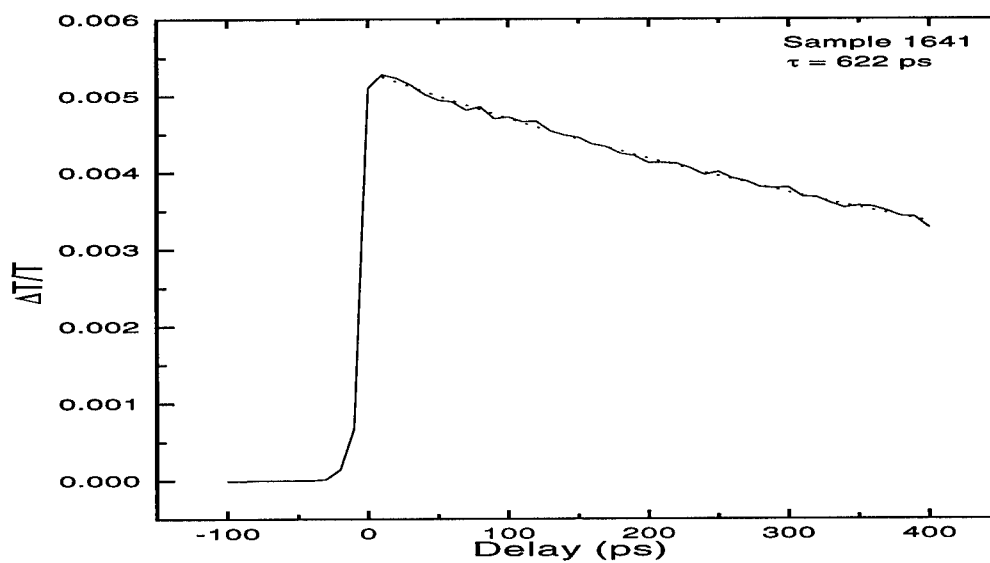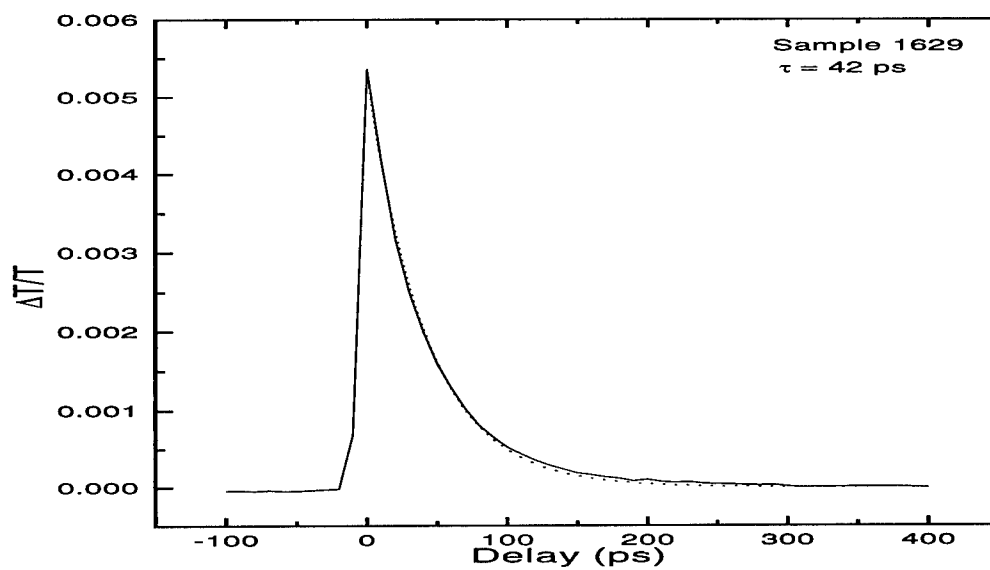
Figure 5.12 Measured recovery of saturable absorbers 1629 and 1641. The
dashed curve is an exponential fit to the measured data indicating a
recovery time of τ = 42 ps for 1629 and τ = 622 ps for 1641.

determined using the pump/probe measurements. Using this method, the lifetimes of samples 1590 and 1442 were determined to be 1757 and 885 ps, respectively.

5.4 CONCLUSIONS

The construction of a mode-locked erbium-doped fiber laser was presented in this chapter. The pulse widths generated by this fiber laser were dependent upon the saturable absorber used as the mode-locking element. The pulse widths were also dependent to a certain extent upon the position of the incident beam upon the saturable absorber.

The linear properties of the saturable absorbers were next examined including the linear absorbance and time-integrated photoluminescence. Finally, time resolved pump/probe measurements were performed to determine the lifetime of the carriers in the quantum wells of the saturable absorbers. Once again there was a wide range of recovery times exhibited by the different saturable absorbers. The next chapter will examine the soliton pulse formation in these fiber lasers and its relation to the recovery times of the carriers in the quantum wells.

5.4 REFERENCES

1.   E. Hecht, *Optics*, 2d ed. (Addison-Wesley, Reading, MA., 1987).

2.   S. Nojima and H. Asahi, J. Appl. Phys. **63**, 479 (1988).

3.   M. Shur, *Physics of Semiconductor Devices* (Prentice-Hall, Englewood Cliffs, NJ., 1990).

4.   D. Marcuse, Bell Syst. Tech. J. **56**, 703 (1977).

5.   S. Gupta, J. F. Whitaker, and G. A. Mourou, IEEE J. Quantum Electron. **QE-28**, 2464 (1992).

6.   R. Takahashi, Y. Kawamura, T. Kagawa, and H. Iwamura, Appl. Phys. Lett. **65**, 1790 (1994).

7.   M. Lambsdorff, J. Kuhl, J. Rosenzweig, A. Axmann, and J. Schneider, Appl. Phys. Lett. **58**, 1881 (1991).

8.   K. F. Lamprecht, S. Juen, L Palmetshofer, and R. A. Höpfel, Appl. Phys. Lett. **59**, 926 (1991).

9.   J. Diels and W. Rudolph, *Ultrashort Laser Pulse Phenomena* (Academic Press, San Diego, CA., 1996).

10.   N. Peyghambarian, S. W. Koch, A. Mysyrowicz, *Introduction to Semiconductor Optics*, (Prentice-Hall, Englewood Cliffs, NJ., 1993).

Chapter 6
Soliton Pulse Shaping in the Erbium-doped Fiber Laser

6.1 INTRODUCTION

Soliton mode-locking with a slow saturable absorber is the dominant pulse formation mechanism in the Fabry-Perot erbium-doped fiber laser (EDFL) discussed in the previous chapter. The temporal duration of the pulse generated by soliton formation is strongly dependent upon the optical properties of the saturable absorbers. These pulse widths were shown to vary from 14.2 to 38.8 ps by simply changing the multiple quantum well saturable absorber at the back end of the cavity. This chapter will show how the optical properties of the multiple quantum well saturable absorbers, specifically the carrier lifetimes, affects the temporal duration of the pulses produced by the EDFL. The soliton pulse formation will also be shown to be dependent upon certain parameters of the EDFL cavity including the gain bandwidth, the saturated gain, the unsaturated loss of the saturable absorber, group velocity dispersion of the erbium fiber, and the length of the erbium-doped fiber. The properties of the saturable absorber and the EDFL that allow for self-starting passive mode-locking using soliton pulse formation will also be briefly discussed. In addition to the properties discussed above, the cavity repetition rate, the saturation power of the absorber, and the saturation power of the laser also contribute to the soliton mode-locking process.

6.2 SOLITON MODE-LOCKING IN THE EDFL

The formation of solitons requires that the group delay dispersion (GDD) and the nonlinearity provided through self-phase modulation (SPM) in the laser

cavity are in balance. The basic model for a laser operating in this regime which is mode-locked using a saturable absorber is described by Haus' master equation [1] for motion of the laser pulse averaged over one round-trip as

$$T_R \frac{\partial A(T,t)}{\partial T} = -iD\frac{\partial^2 A}{\partial t^2} + i\delta|A|^2 A + \left[g - 1 + D_g \frac{\partial^2}{\partial t^2} - q(T,t) \right] A(T,t) \qquad (6.1)$$

where $A(T,t)$ is the slowly varying field envelope, T_R is the cavity round-trip time, D is the GDD, $D_g = g/\Omega_g^2$ is the gain dispersion, Ω_g is the HWHM gain bandwidth, δ is the nonlinear coefficient due to SPM, g is the saturated gain, 1 is the frequency independent loss per round trip, and $q(T,t)$ is the transmission response of the saturable absorber due to the pulse. The master equation describes the gain dynamics on two time scales: T, which is on the order of the round-trip time and t, which is on the order of the pulse width. The saturable absorber dynamics are modeled by the following rate equation as

$$\frac{\partial q(T,t)}{\partial t} = -\frac{q - q_0}{\tau_A} - \frac{|A(T,t)|^2}{E_A} q \qquad (6.2)$$

where q_0 is the unsaturated, but saturable loss of the absorber, τ_A is the recovery time of the saturable absorber, and E_A is the saturation energy of the absorber. The assumption has been made that the absorber completely recovers before the arrival of the next pulse. There are no known analytical solutions to the full master equation in Eq. 6.1. However, the soliton behavior of the laser is approximated by disregarding the second part of the equation which contains the

gain and loss terms. The resulting equation is the nonlinear Schrödinger equation and has the soliton solution,

$$A(T,t) = \sqrt{\frac{W}{2\tau}} \operatorname{sech}\left(\frac{t}{\tau}\right) \exp\left(i\Phi_o \frac{T}{T_R}\right) \qquad (6.3)$$

where W is the pulse energy and Φ_o is the nonlinear phase shift of the soliton per round-trip. Φ_o is given by

$$\Phi_o = \frac{\delta W}{4\tau} = \frac{|D|}{\tau^2}. \qquad (6.4)$$

The actual FWHM pulse width produced by the laser, τ_{FWHM} is related to τ in the above equations as $\tau_{FWHM} = 1.76\tau$.

The pulse shaping mechanism in a soliton laser using a slow saturable absorber was shown in Section 3.4.3 to be approximated by a V-shaped function in time. The resulting pulse width is much narrower than the open time window of the gain. The saturable absorber serves to stabilize the soliton, *i.e.,* keep the continuum energy that is shed from the soliton due to the gain dispersion and losses in the cavity from building up past lasing threshold, during this open time frame. The minimum pulse width that can be stabilized by the saturable absorber is estimated as

106

$$\tau = \left(\frac{1}{\sqrt{6}\,\Omega_g}\right)^{\frac{3}{4}} \left(\frac{\tau_A g^2}{q_o}\right)^{\frac{1}{4}} \Phi_o^{-\frac{1}{8}} \qquad (6.5)$$

where τ_A is the lifetime of the carriers in the quantum wells of the saturable absorber.[2] The soliton pulse width is dependent upon the gain bandwidth, the carrier lifetime, the saturated gain, the unsaturated loss of the absorber, and the nonlinear phase shift.

Eq. 6.5 shows that the soliton pulse width is proportional to the 1/4 power of the saturable absorber lifetime. These recovery times were experimentally determined in Chapter 5. We will now determine the rest of the parameters in Eq. 6.5 so that we can compare the calculated soliton pulse widths to those generated by the EDFL for the different saturable absorbers. The gain bandwidth of the laser is given by $\Omega_g = 2\pi\Delta\nu$ where the spectral bandwidth, $\Delta\nu$ of erbium-doped fiber is approximately 4 THz. However, the gain bandwidth of the laser is actually limited by the narrow bandpass of the fiber grating output coupler. As shown in Figure 5.2, the FWHM linewidth of the grating is only 1 nm. This narrow linewidth cannot support the large spectral bandwidth needed for the formation of sub ps pulses. Using a 1 nm spectral bandwidth, the gain bandwidth is calculated as $\Omega_g = 0.12$ THz. The saturated gain, g, of the cavity is estimated as being equal to the intracavity losses, l, as $g = l = 1 - R_1R_2$ where $R_{1,2}$ are the two mirror reflectance's. Using values of $R_1 = 0.5$ for the fiber grating output coupler and $R_2 = 0.01$ for the reflectance of the back saturable absorber as calculated in Chapter 5, the saturated gain is estimated as $g = 0.9$. The

unsaturated loss of the absorber, q_o, is estimated as 0.02.[2] The final value left to evaluate is the nonlinear phase shift, Φ_o which is defined as

$$\Phi_o = \frac{|D|}{\tau^2} = \frac{|\beta_2 L|}{\tau^2} \tag{6.6}$$

where β_2 is a group velocity dispersion parameter and τ is the soliton pulse width. β_2 is given as

$$\beta_2 = \frac{D_1 \lambda^2}{2\pi c} \tag{6.7}$$

where D_1 is the group velocity dispersion (GVD) given in units ps / nm km and is estimated as $|D_1| = 5$ ps / nm km.[3] Using the actual pulse widths generated by the EDFL, an average value of $\tau_{FWHM} = 30$ ps is used to calculate $\tau = 17$ ps. The nonlinear phase shift is then calculated as $\Phi_o = 0.001$. The values used to calculate the soliton pulse widths of Eq. 6.5 are summarized in Table 6.1.

Table 6.1   Summary of EDFL parameters used in Eq. 6.5 to calculate the soliton pulse width

PARAMETER	VALUE
Ω_g	0.12 THz
g	0.9
q_o	0.02
Φ_o	0.001

Figure 6.1 shows the EDFL pulse widths as a function of carrier lifetime in the saturable absorbers. We see that the calculated values using Eq. 6.5 match rather well with the experimentally measured values. The generated pulse widths are much shorter than the recovery times of the saturable absorbers and agree well with the soliton modelocking results presented by Kärtner, et al..[2,4] The linewidth of the fiber grating output coupler is the primary limiting factor in the EDFL's pulse width. By increasing the bandwidth from 1 nm to the full 35 nm available in erbium, the generated pulse widths predicted by Eq. 6.5 would decrease by approximately a factor of 14 and would be on the order of a few picoseconds. Based on these simulations, shorter pulse widths could be generated by using an output coupler with a larger spectral bandwidth.

It should be noted that sample 1629 which had a measured recovery time of 40 ps was excluded from this fit. This saturable absorber generated multiple pulses per cavity round trip. The multiple pulses were noisy and distributed randomly in time. As the laser tries to form very narrow pulses using this saturable absorber, the corresponding pulse energy increases past a certain stability limit. The laser will now prefer to see extra pulses per cavity round trip each having a much lower energy than the single high energy pulse.[3,5] The pulse widths will now be longer than expected because the decreased pulse energy of the multiple pulses creates less self-phase modulation and directly results in longer pulse durations. Sample 1629 had an average measured pulse width of 34.3 ps which was much larger than the calculated value of 16.5 ps. The pump power of the EDFL was reduced from 80 to 32 mW which was just above lasing threshold in hopes of eliminating the multiple pulses. The multi-pulsing was greatly reduced at this pump level but flashes of extra pulses were occasionally present and the pulses remained very long. Finally, the pump power was set at
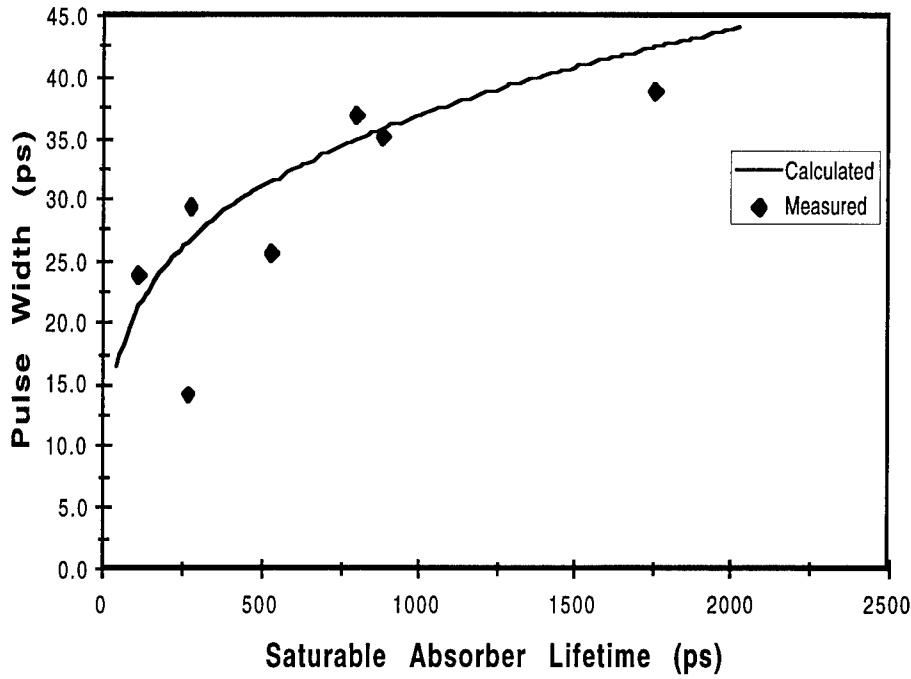
Figure 6.1   Comparison of the calculated and measured EDFL pulse widths as a function of the carrier lifetimes in the saturable absorbers

approximately 40 mW and part of the erbium fiber was intentionally twisted to introduce extra loss into the cavity. This appeared to eliminate all of the extra pulses and a pulse width of 30 ps was measured. However, the optimum pulse width was still not achieved because the low pump powers limited the depth of modulation of the saturable absorber. In this situation soliton pulse formation appears to be superseded by fast saturable absorber mode-locking because the pulse width is now on the order of the recovery time of the absorber (40 ps).

6.3 SELF-STARTING PASSIVE MODE-LOCKING

The final section of this chapter will analyze the self-starting ability of the passively mode-locked EDFL. Self-starting of any mode-locked laser system is essential if the laser is to used in an environment outside of the research laboratory. Self-starting, as the name implies, means that the mode-locking process starts automatically and that no external perturbation has to be applied such as the pushing of a mirror or the use of an intracavity acousto-optic modulator. Practical mode-locked laser systems must have the ability to be 'turn-key' and simply involve the push of a start-up button. Certainly a laser such as described in this chapter will have limited use in applications such as telecommunications if a technician is required to initiate and sustain the mode-locking process.

The self-starting ability of a laser was initially analyzed by Haus [6] and was recently re-stated by Kärtner [7]. As discussed in Chapter 3, the mode-locking process involves locking together the phases of neighboring longitudinal modes all of which are oscillating under the gain bandwidth of the laser. The growth rate of these longitudinal modes that are to be locked together is given by

$$\frac{1}{T_{mode}} = \left[\frac{2q_o}{\left(1+ P\!\!\Big/\!\!P_A\right)^2 + \left(2\pi m T_A\right)^2} \frac{P}{P_A} - \frac{2g_o}{\left(1+ P\!\!\Big/\!\!P_L\right)^2 + \left(2\pi m T_L\right)^2} \frac{P}{P_L} \right] \quad (6.8)$$

where T_{mode} is the growth time of the modes normalized to the cavity round trip time (T_R), T_A is the normalized saturable absorber recovery time (τ_A/T_R), T_L is the normalized upper state laser lifetime (τ_L/T_R), P is the cw laser power, P_A is

the saturation power of the absorber, P_L is the saturation power of the laser, m is the number of longitudinal modes that are locked together, q_o is the unsaturated loss of the absorber, and g_o is the small signal gain of the laser. g_o is defined as

$$g_o = g\left(1 + \frac{W}{T_R P_L}\right) \qquad (6.9)$$

where g is the saturated gain of the laser.[8] The pulse energy W, of the EDFL was calculated as 450 pJ using an average output power of 2 mW, a pulse width of 20 ps and the cavity repetition rate of 4.4 MHz. The intracavity power, P_L, of the EDFL was calculated as 0.04 W. Using these values, g_o is calculated as 0.95.

The number of modes, m, that are locked together was estimated using a 1 nm bandwidth for the EDFL (due to the fiber grating) and a mode spacing of 4.4 MHz to give approximately m = 4340. The upper state lifetime, τ_L, of Er^{3+} is 10 ms. The ratio of P/P_A was estimated as 5 which is the 'rule of thumb' upper limit on this ratio before the onset of multi-pulsing.[9] The ratio of P/P_L was estimated as 10 because we know we are pumping the EDFL well above threshold. The value of q_o = 0.02 was the same value used in the previous soliton pulse width analysis.

The values listed above were used to evaluate Eq. 6.8 as a function of the saturable absorber recovery. If T_{mode} is positive then the laser is not only mode-locked but it is also self-starting. A positive value for T_{mode} indicates that the saturable absorber can be sufficiently bleached to initiate the mode-locking process and that the laser is also stable against self Q-switching. Figure 6.2 shows the mode-locking buildup time as a function of the carrier lifetime in the saturable absorber. This buildup time is positive using all of our EDFL
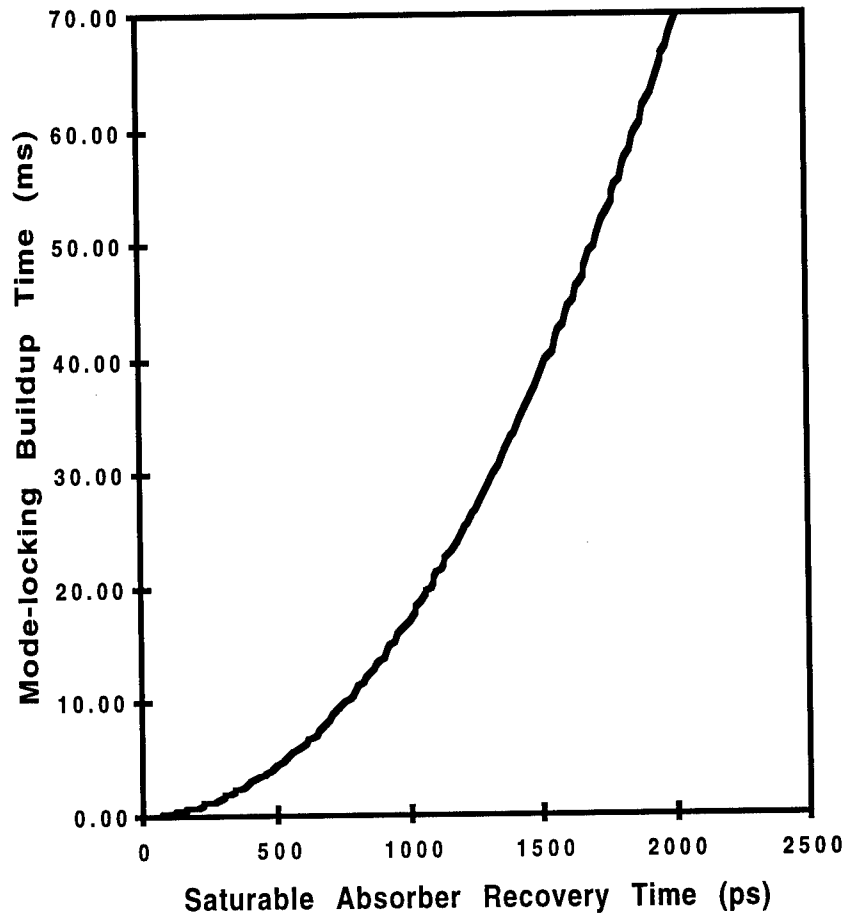
Figure 6.2 Mode-locking buildup time in the EDFL. The positive values indicate that the laser is self-starting over the entire range of absorber recovery times.

parameters indicating that the mode-locked laser is indeed self-starting over the entire range of saturable absorber lifetimes. The millisecond mode-locking buildup times are also consistent with those previously reported for other solid-state lasers.[10]

6.4 CONCLUSIONS

This chapter has discussed the dependence of the soliton mode-locking process in the EDFL upon the optical properties of the multiple quantum well saturable absorbers. The pulse widths generated by the EDFL were shown to be a function of the carrier lifetimes in the saturable absorbers. The soliton mode-locking of the EDFL resulted in pulse durations that are much shorter than the recovery times of the absorbers by up to a factor of 40. It was also shown that the pulses were limited to the tens of picoseconds regime due to the presence of the bandwidth limiting fiber grating output coupler. Finally, the self-starting nature of the EDFL was explored. It was confirmed that the parameters of the laser allow for self-starting of the mode-locking process. The self-starting nature of the laser allows it to be used in a variety of applications outside of the research laboratory.

6.5 REFERENCES

1.   H. A. Haus, J. Appl. Phys. **46**, 3049 (1975).

2.   F. X. Kärtner and U. Keller, Opt. Lett. **20**, 16 (1995).

3.   R. P. Davey, N. Langford, and A. I. Ferguson, Electron. Lett. **27**, 1257 (1991).

4.   I. D. Jung, F. X. Kärtner, L. R. Brovelli, M. Kamp, U. Keller, Opt. Lett. **20**, 1892 (1995).

5.   B. C. Barnett, L. Rahman, M. N. Islam, Y. C. Chen, P. Bhattacharya, W. Riha, K. V. Reddy, A. T. Howe, K. A. Stair, H. Iwamura, S. R. Friberg, and T. Mukai, Opt. Lett. **20**, 471 (1995).

6.   H. A. Haus, IEEE J. Quantum. Electron. **QE-12**, 169 (1976).

7.   F. X. Kärtner, L. R. Brovelli, D. Kopf, M. Kamp, I. Calasso, and U. Keller, Opt. Eng. **34**, 2024 (1995).

8.   F. X. Kärtner, I. D. Jung, and U. Keller, IEEE J. Select. Topics in Quantum. Electron. **2**, 540 (1996).

9. U. Keller, K. J. Weingarten, F. X. Kärtner, D. Kopf, B. Braun, I. D. Jung, R. Fluck, C. Hönninger, J. Aus der Au, IEEE J. Select. Topics in Quantum. Electron. **2**, 435 (1996).

10. U. Keller, T. H. Chiu, and J. F. Ferguson, Opt. Lett. **18**, 217 (1993).

Chapter 7
Summary and Future Directions

7.1 SUMMARY

This research presented in this work is divided into the following three components:

1.   The fabrication of a self-starting, passively mode-locked erbium-doped fiber laser (EDFL) operating at the 1.55 μm minimum loss window of optical fiber.

2.   The construction of a solid-state femtosecond Cr^{4+}:YAG laser tunable from 1.488 to 1.535 μm.[1-4]

3.   The investigation and analysis of the ultrafast carrier dynamics in the multiple quantum well (MQW) saturable absorbers that were used to mode-lock the EDFL.[5]

In the first phase, we demonstrated a Fabry-Perot configuration that used a saturable absorber as the back reflector of the cavity. Picosecond pulses were generated by the EDFL that ranged from 14.2 to 38.8 ps with a repetition rate of 4.4 MHz. The pulse widths were dependent upon the saturable absorber that was used as the mode-locking element. The average output power of the laser varied from 0.2 to 6.7 mW. The compactness of the picosecond laser coupled with its moderate output power makes it an attractive source for ultrafast optical networks and fiber-based interconnects.

The second phase of this research was motivated by the need for a high power tunable femtosecond source in the 1.5 μm region. The use of a novel saturable absorber mirror (SAM) structure to mode-lock the Cr^{4+}:YAG laser resulted in the generation of femtosecond pulses that were very stable over long

periods of time. The ultrashort pulses and high peak power produced by the Cr^{4+}:YAG laser were needed to investigate the carrier lifetimes in the MQW saturable absorbers used to mode-lock the EDFL.

Finally, the third phase of this research investigated the dependence of the pulse durations generated by the EDFL upon the saturable absorber used in the cavity. Time resolved pump/probe experiments were used to determine the carrier lifetimes in each of the eight individual saturable absorbers. It was found that these carrier lifetimes were the primary optical property of the saturable absorber that determined the final pulse width generated by the EDFL. The soliton mode-locking mechanism used by the EDFL allowed pulses of up to 45 times shorter than the recovery time of the MQW saturable absorber to be generated.

7.2 FUTURE DIRECTIONS

There are several issues that need to be addressed before the mode-locked EDFL developed in this work can be used in a practical optical communication system. First, a comprehensive noise analysis of the EDFL needs to be completed. The timing jitter and amplitude fluctuations of the mode-locked pulses are key parameters that will determine the 'real-world' usefulness of this laser.

The coupling between the erbium-doped fiber and the saturable absorber in the EDFL also needs to be increased. Currently only 1% of the light that exits the fiber is coupled back into it following reflection off of the absorber. The coupling will be best increased by integrating a distributed Bragg reflector (DBR) with the saturable absorber. This is very similar to the saturable absorber mirror structure used to mode-lock the Cr^{4+}:YAG laser. The high reflector

serves two purposes. First, the overall reflectance of the saturable absorber can be made very high (> 99%). Second, the distance traveled by the diverging Gaussian beam is greatly reduced. Currently the beam reflects off of the back InP substrate/air interface. Consequently the beam diverges greatly because of the distance that it must travel ($\approx$500 μm) through the substrate before it reaches the interface. By comparison, the total thickness of the high reflector portion of the SAM was only 6 μm. This reduced distance coupled with the large increase in reflectance should dramatically increase the coupling of light back into the erbium-doped fiber.

The minimum pulse width generated by the EDFL in this work was 13.2 ps. It was shown in Chapter 6 that the limiting factor in these pulse widths was the narrow linewidth (1 nm) of the fiber grating output coupler. The generation of transform-limited femtosecond pulses for WDM and various spectroscopic applications require very large spectral bandwidths of over 20 nm. A fiber grating with a larger bandwidth can be used as the output coupler or it can be replaced altogether by a simple rotary splice that is coated with a dielectric, resulting in both a high reflectance and a large spectral bandwidth [6].

Finally, the repetition rate, or spacing between consecutive pulses, of the laser needs to be increased, especially if the laser is to be used in very high bit rate TDM systems. Decreasing the cavity length will increase the repetition rate but at the expense of the population inversion necessary for gain. Optical fiber with a higher density of erbium ions per unit volume needs to be used to compensate for this decrease in gain.

The repetition rate of the EDFL can be increased and the timing jitter decreased by electrical control of the saturable absorber.[7] The quantum-confined Stark and Franz-Keldysh effects effectively shift the bandedge of the

quantum wells to longer wavelengths while decreasing the excitonic oscillator strength.[8] Careful design of the quantum well bandedge relative to the laser wavelength will allow the laser to be switched from a mode-locked to a non-mode-locked state by application of an electronic pulse. The active electrical control of the laser stabilizes the timing jitter. The saturable absorber can also be electrically driven at a higher harmonic of the cavity frequency resulting in an increase in the repetition rate.

7.3 ACKNOWLEDGMENTS

7.4 REFERENCES

1.   M. J. Hayduk, S. T. Johns, M. F. Krol, C. R. Pollock, and R. P. Leavitt, Opt. Commun. **137**, 55 (1997).

2.   M. J. Hayduk, S. T. Johns, and M. F. Krol, Laser Focus World, December 1996.

3.   M. J. Hayduk, S. T. Johns, M. F. Krol, C. R. Pollock, and R. P. Leavitt, Paper MF3, IEEE Lasers and Electro-Optics Society Annual Meeting, Boston, MA., 1996.

4.   J. P. Theimer, M. Hayduk, M. Krol, and J. W. Haus, "Mode-locked Cr^{4+}:YAG laser: Model and Experiment," accepted for publication in Opt. Commun., 1997.

5.   M. J. Hayduk, M. F. Krol, C. R. Pollock, K. J. Teegarden, G. W. Wicks, and W. Kaechele, "Development of passively mode-locked erbium doped fiber lasers using multiple quantum well saturable absorbers," accepted for presentation at IEEE Lasers and Electro-Optics Society Annual Meeting, San Francisco, CA., 1997.

6.   S. Tsuda, W. H. Knox, J. L. Zyskind, J. E. Cunningham, W. Y. Jan, and R. Pathak, Paper CFD2, Conference on Lasers and Electro-optics, Anaheim, CA. 1996.

7.   K. J. Teegarden and W. Kaechele, Private Communication (1997).

8.   D. A. B. Miller, D. S. Chemla, T. C. Damen, A. C. Gossard, W. Wiegmann, T. H. Wood, and C. A. Burrus, Phys. Rev. B **32**, 1043 (1985).